NAVAL POSTGRADUATE SCHOOL

MONTEREY, CALIFORNIA

THESIS

GASDYNAMIC INLET ISOLATION IN ROTATING DETONATION ENGINE

by

Wei Han Eugene Lim

December 2010

Thesis Co-Advisors: Jose O. Sinibaldi
Christopher M. Brophy

Approved for public release; distribution is unlimited

THIS PAGE INTENTIONALLY LEFT BLANK

REPORT DOCUMENTATION PAGE			*Form Approved OMB No. 0704-0188*
Public reporting burden for this collection of information is estimated to average 1 hour per response, including the time for reviewing instruction, searching existing data sources, gathering and maintaining the data needed, and completing and reviewing the collection of information. Send comments regarding this burden estimate or any other aspect of this collection of information, including suggestions for reducing this burden, to Washington headquarters Services, Directorate for Information Operations and Reports, 1215 Jefferson Davis Highway, Suite 1204, Arlington, VA 22202-4302, and to the Office of Management and Budget, Paperwork Reduction Project (0704-0188) Washington DC 20503.			
1. AGENCY USE ONLY ***(Leave blank)***	**2. REPORT DATE** December 2010	**3. REPORT TYPE AND DATES COVERED** Master's Thesis	
4. TITLE AND SUBTITLE Gasdynamic Inlet Isolation in Rotating Detonation Engine		**5. FUNDING NUMBERS** N001410WX20832	
6. AUTHOR(S) Wei Han Eugene Lim			
7. PERFORMING ORGANIZATION NAME(S) AND ADDRESS(ES) Naval Postgraduate School Monterey, CA 93943-5000		**8. PERFORMING ORGANIZATION REPORT NUMBER** N/A	
9. SPONSORING /MONITORING AGENCY NAME(S) AND ADDRESS(ES) Office of Naval Research One Liberty Center 875 N. Randolph Street, Suite 1425 Arlington, VA 22203-1995		**10. SPONSORING/MONITORING AGENCY REPORT NUMBER** N/A	
11. SUPPLEMENTARY NOTES The views expressed in this thesis are those of the author and do not reflect the official policy or position of the Department of Defense or the U.S. Government. IRB Protocol number _____N.A._____.			
12a. DISTRIBUTION / AVAILABILITY STATEMENT Approved for public release; distribution is unlimited		**12b. DISTRIBUTION CODE**	

13. ABSTRACT (maximum 200 words)

The Rotating Detonation Engine (RDE) concept represents the next-generation of detonation-based engines as it provides higher performance and near constant thrust with a simpler overall design. Since RDE systems are in the early stage of development, the physics of engine design is yet to be fully understood and developed. A critical concern of these systems is the practical isolation of the reactant injection manifold and supply system from the combustor pressure oscillations. For this study, the gasdynamic conditions that existed at the combustor inlet are investigated and characterized. Using a shocktube test case for a Hydrogen-Air mixture, various numerical schemes, number of chemical reactions, mesh topology and mesh refinement are first investigated to reliable reproduce the Chapman-Jouguet conditions. It was found that explicit 4^{th} Order Runge-kutta scheme using structured mesh topology, 18 species and 9 reactions with a maximum mesh cell size of 0.05 mm was required to reproduce the Chapman-Jouguet conditions. Once the suitable parameters were identified, a full 2D RDE simulation was carried out to characterize the gasdynamic inlet conditions.

14. SUBJECT TERMS Rotating Detonation Engines, Shock Wave, Detonation Wave			**15. NUMBER OF PAGES** 121
			16. PRICE CODE
17. SECURITY CLASSIFICATION OF REPORT Unclassified	**18. SECURITY CLASSIFICATION OF THIS PAGE** Unclassified	**19. SECURITY CLASSIFICATION OF ABSTRACT** Unclassified	**20. LIMITATION OF ABSTRACT** UU

NSN 7540-01-280-5500 Standard Form 298 (Rev. 2-89)
Prescribed by ANSI Std. 239-18

THIS PAGE INTENTIONALLY LEFT BLANK

Approved for public release; distribution is unlimited

GASDYNAMIC INLET ISOLATION IN ROTATING DETONATION ENGINE

Wei Han Eugene Lim
Captain, Singapore Armed Forces
Bachelor of Engineering (Mechanical), Nanyang Technological University, 2006

Submitted in partial fulfillment of the
requirements for the degree of

MASTER OF SCIENCE IN MECHANICAL ENGINEERING

from the

NAVAL POSTGRADUATE SCHOOL
December 2010

Author: Wei Han Eugene Lim

Approved by: Jose O. Sinibaldi
Thesis Co-Advisor

Christopher M. Brophy
Thesis Co-Advisor

Knox T. Millsaps
Chairman, Department of Mechanical and Aerospace Engineering

THIS PAGE INTENTIONALLY LEFT BLANK

ABSTRACT

The Rotating Detonation Engine (RDE) concept represents the next-generation of detonation-based engines as it provides higher performance and near constant thrust with a simpler overall design. Since RDE systems are in the early stage of development, the physics of engine design is yet to be fully understood and developed. A critical concern of these systems is the practical isolation of the reactant injection manifold and supply system from the combustor pressure oscillations. For this study, the gasdynamic conditions that existed at the combustor inlet are investigated and characterized. Using a shocktube test case for a Hydrogen-Air mixture, various numerical schemes, number of chemical reactions, mesh topology and mesh refinement are first investigated to reliable reproduce the Chapman-Jouguet conditions. It was found that explicit 4^{th} Order Runge-kutta scheme using structured mesh topology, 18 species and 9 reactions with a maximum mesh cell size of 0.05 mm was required to reproduce the Chapman-Jouguet conditions. Once the suitable parameters were identified, a full 2D RDE simulation was carried out to characterize the gasdynamic inlet conditions.

THIS PAGE INTENTIONALLY LEFT BLANK

TABLE OF CONTENTS

LIST OF FIGURES

LIST OF TABLES

THIS PAGE INTENTIONALLY LEFT BLANK

ACKNOWLEDGMENTS

The author would like to thank his wife, Charlene, and his son, Louis, for their patience and understanding for his not being able to spend more family time with them while working on this thesis in school and at home.

The author would also like to express his gratitude to Drs. Jose O. Sinibaldi and Christopher M. Brophy for their mentorship during the course of this research and making this journey a fruitful and memorable one.

Also, special thanks to Office of Naval Research (ONR) for sponsoring this project.

THIS PAGE INTENTIONALLY LEFT BLANK

I. INTRODUCTION

A. MOTIVATION

The Rotating Detonation Engine (RDE) represents the next generation of detonation-based engines in the way that it provides the thermodynamic advantages of detonation-based combustion with nearly constant thrust and a simpler overall design. With the potential to be employed in a wide range of platforms such as missiles, fighter aircraft and unmanned aerial vehicles, the RDE relies on a detonation mode of combustion similar to what is used on the Pulse Detonation Engine (PDE). RDEs can also be used for power generation if implemented in a hybrid engine such as Gas turbine-RDE where the high-pressure compressor spools, the combustion cans and the high-pressure turbine spools are replaced by RDE. This would greatly improve efficiency and motivate the Navy to implement the usage of hybrid Gas turbine-RDE systems onboard ships.

The RDE operates as a pressure-gain combustor with a higher thermodynamic efficiency with a constant energy conversion process to provide high power-to-weight ratio with fewer moving parts [1]. In addition, RDEs can be filled with reactants moving at low subsonic velocities in the axial direction thus drastically lowering the pressure losses encounter in PDE systems. The RDE is also able to internally sustain the detonation once ignited to generate continuous thrust as the combustion wave propagates at its supersonic Chapman Jouguet (CJ) speeds in the azimuthal direction. The fundamentals of RDE design allow the reactants in the detonation chamber flow continuously, reducing the requirement for valves. These advantages give the RDE the potential to surpass the performance of the majority of propulsion systems being fielded today.

With RDEs still in the early stages of development, the physics of the engine design has yet to be fully understood and developed. Presently, no operational RDE has been fielded and theoretical studies on the engine are also limited.

B. BACKGROUND

The basic idea behind the RDE is the generation of a detonation wave that rotates around an annular combustion chamber formed by two concentric cylinders, producing thrust that is nearly continuous as combustion products are expelled out of the RDE. Injecting fuel-oxidizer mixtures axially in the chamber (see Figure 1), produces conditions that allow a detonation wave that propagates in the azimuth direction. A detonation wave initiator which sends a detonation wave into the mixture and the detonation wave will rotate around the combustion chamber. Finally, combustion products expand behind the detonation wave creating weak shockwaves, which flows out along the axial direction.

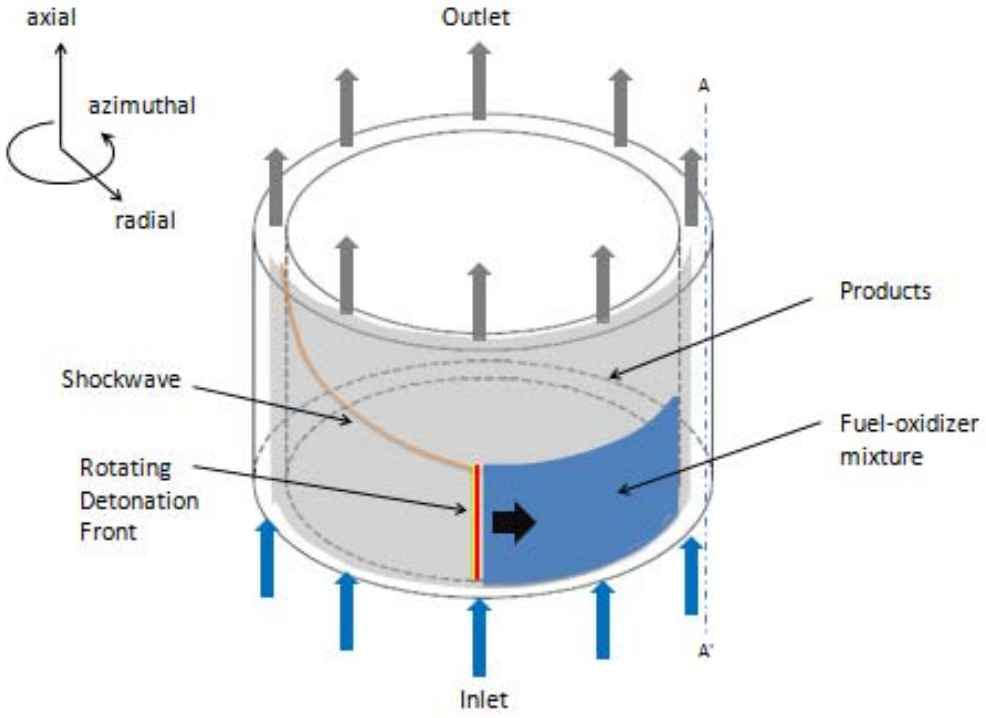

Figure 1. Schematic of a Rotating Detonation Engine

The height and stability of the detonation wave is determined by the inlet conditions and geometry of the RDE. These inlet conditions are in turn affected by inlet

design factors such as the reservoir pressure, dimension of the inlet nozzles and injection velocity. Therefore, careful design of the RDE inlet is required to properly isolate the annular combustion chamber, and this can be achieved only after the gasdynamic effects at the inlet region have been understood.

C. GOALS AND OBJECTIVES

As described in the preceding sections, the design of the engine inlet is crucial to the overall development of the RDE. The goal of this thesis is, therefore, to help engine designers to properly design an RDE inlet that takes the advantage of the existing gasdynamics to help isolate the inlet from the rotating detonation inside the annular combustor.

The objective of this thesis is to understand the gasdynamic conditions namely pressure, temperature, mass flow rate, velocity and density that exist at the combustor inlet. This study conducts numerical computational simulations using the commercial software CFD++ computational platform, which helps us to gain insight into the physical aspects unique to rotating detonations.

Since the focus of this thesis is inlet design, the outlet geometry of the RDE will be simplified. Furthermore, due to complexities that arise from the use of complex hydrocarbon fuels, we restrict our research to the use of a Hydrogen-Air mixture as the RDE fuel.

D. TECHNICAL APPROACH

Numerical computational simulations will be conducted using CFD++ computational software developed by MetaComp Technologies with the methodology as follows:

- The review of detonation theory from previous numerical and experiment studies that have been done on RDE to gain insights into the simulation step up.
- Decomposition of the 3D computational domain into a 2D domain to simplify the computational requirements.

- Use of a shocktube (a subset of the 2D domain), to further reduce the computational requirements to make reliable reproduction of the CJ conditions for rotating detonation.
- Run full 2D cyclic domain simulations with the appropriate initial and boundary conditions.
- Analysis of results.

II. THEORY

A. ROTATING DETONATION ENGINE COMBUSTOR

The RDE represents a propulsion system where thrust is provided by combustion products from a detonation wave rotating azimuthally inside an annular combustion which are accelerated through a nozzle. The process is initiated by injecting a fuel-oxidizer mixture such as Hydrogen-Air mixture via the inlets into the chamber. Once the chamber is sufficiently filled, a detonation wave initiator will send a detonation wave tangentially into the mixture. A high-pressure deflagration wave then propagates for a short distance and forms a rotating detonation wave. The rotating detonation wave will continuously propagate at the CJ velocity. The detonation wave will be continually supplied with freshly injected fuel-oxidizer mixture. The products and oblique shockwaves will exit from the outlet. Thrust is generated by the acceleration of the combustion products. Figures 2 to 4 illustrate the operating mechanism of the RDE.

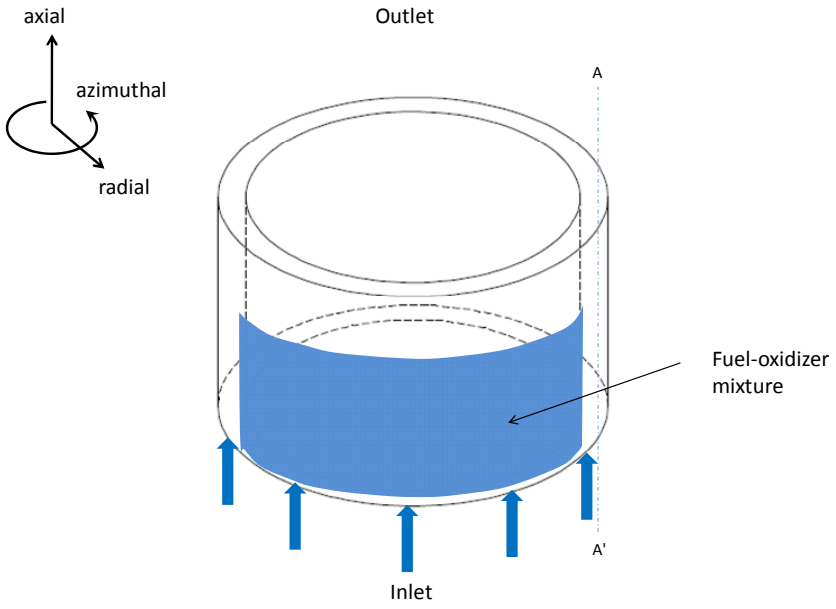

Figure 2. RDE operation mechanism- Fill phase

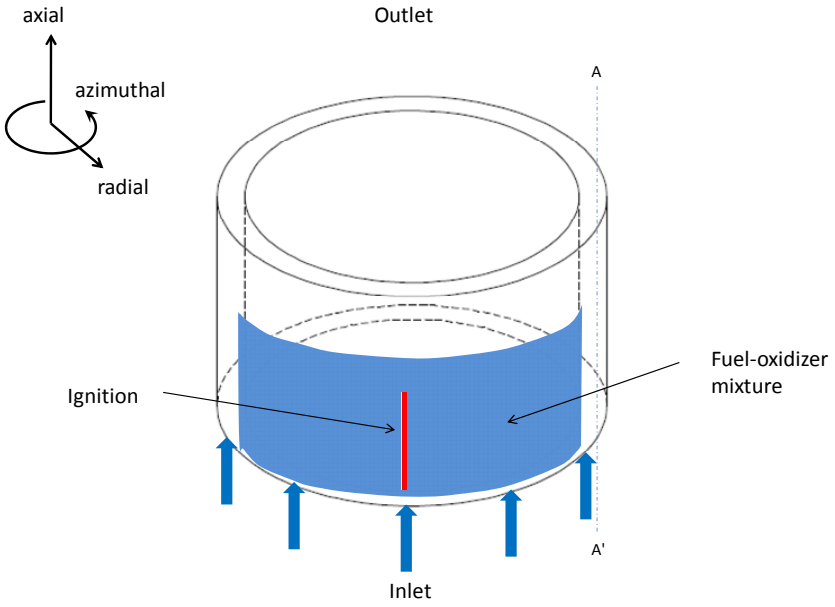

Figure 3. RDE operation mechanism- Ignite phase

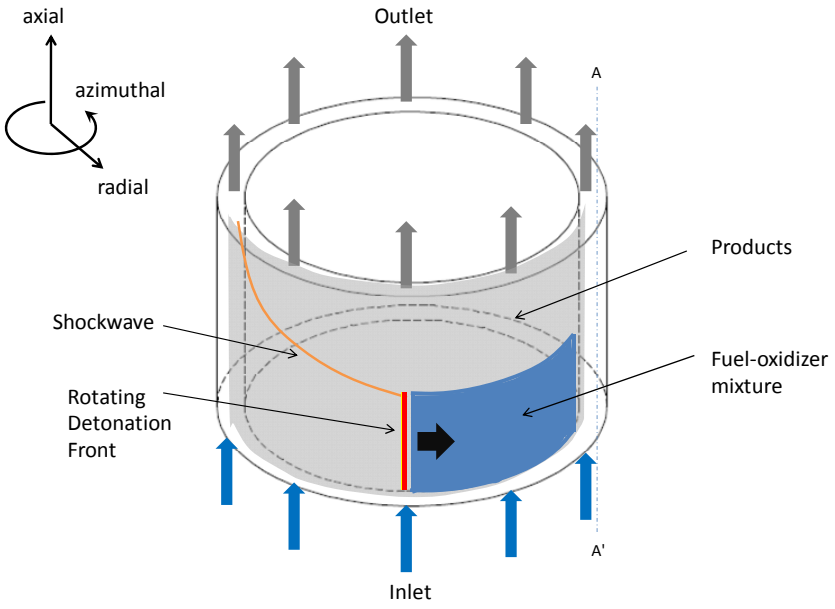

Figure 4. RDE operation mechanism- Continuous operation

B. DETONATION THEORY

There is a need to first understand the basics of detonation physics. A combustion wave which travels at supersonic speed is known as a detonation wave, while a deflagration wave travels at subsonic speeds. A detonation wave shares many features of a shock wave but has the added complexity of chemical reactions occurring.

Figure 5 further illustrates the detonation wave using a simplified 1D wave profile. When the detonation wave moves through the reactant, chemical reactions occur. The "von Neumann" spike is controlled by the timescale of the chemical reactions, with the rate of chemical reaction determined by the width of the reaction zone. At the end of the reactions, the products reach a sonic condition known as the Chapman-Jouguet point, after which the products are released as an expansion wave.

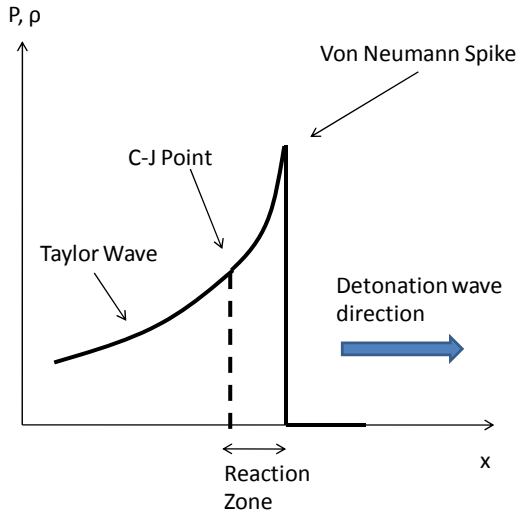

Figure 5. 1D detonation wave profile

To understand the relationship of the upstream and downstream gasdynamic properties, we apply the equation for the mass conservation, momentum, energy and equation as shown below. Figure 6 illustrates a 1D planar combustion wave in a long channel with a constant area, with the reference frame being the combustion wave itself. The combustion wave is assumed to have reached a steady state: - it is adiabatic and

remains in chemical and thermodynamic equilibrium [2]. The ideal gas law is an acceptable approximation for equation of state for gases during combustion.

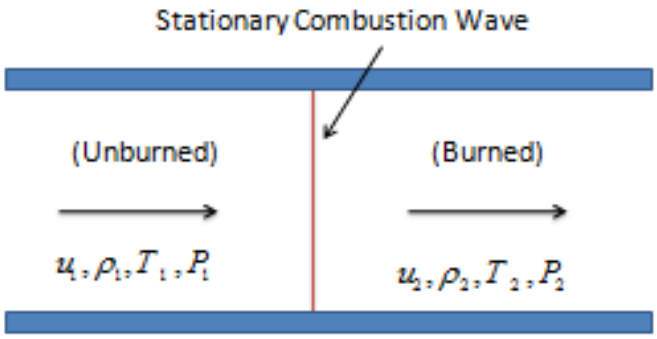

Figure 6. Schematic diagram of 1D combustion wave [From 2]

Conservation of Mass:

$$\rho_1 u_1 = \rho_2 u_2 \tag{1}$$

Conservation of Momentum:

$$P_1 + \rho_1 u_1^2 = P_2 + \rho_2 u_2^2 \tag{2}$$

Conservation of Energy:

$$C_p T_1 + \frac{u_1^2}{2} + q = C_p T_2 + \frac{u_2^2}{2} \tag{3}$$

Equation of State (Ideal Gas Law):

$$P = \rho R T \tag{4}$$

Specific Heat Relation:

$$C_p = \frac{\gamma}{\gamma - 1} R \tag{5}$$

where:

R = Specific Gas Constant = Universal Gas Constant / Molecular Weight

q = Specific heat energy added to the system via combustion process

C_p = Specific heat at constant pressure

γ = Ratio of specific heat

A relationship describing the solution for a steady state 1D combustion wave is derived by combining Equations (2) to (4). This relationship is known as Hugoniot relation as described by Equation (6).

Hugoniot relation

$$\frac{\gamma}{\gamma-1}\left(\frac{P_2}{\rho_2}-\frac{P_1}{\rho_1}\right)-\frac{1}{2}\left(P_2-P_1\right)\left(\frac{1}{\rho_1}+\frac{1}{\rho_2}\right)=q \qquad (6)$$

By plotting of pressure (P_2) versus specific volume ($\frac{1}{\rho_2}$), then we can obtain the Hugoniot curve. The Hugoniot curve represents the potential locus of end states behind the detonation wave. At each end state, the slope of the Hugoniot curve relates the velocity of the combustion wave.

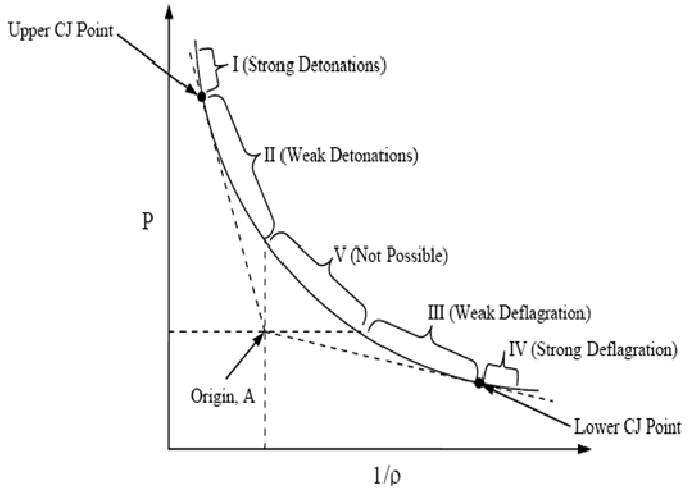

Figure 7. Hugoniot curve profile [From 2]

By combining Equations (1) and (2), the Rayleigh line relation shown in Equation (7) is formed. A Rayleigh line represents the path where the reactants at an initial state transiting into products in a final state and is represented by the dashed line from Origin A to the Upper CJ Point in Figure 7.

Rayleigh line Relation:

$$\rho_1^2 u_1^2 = \frac{P_2 - P_1}{\frac{1}{\rho_1} - \frac{1}{\rho_2}} \tag{7}$$

There are two possible final states that can occur using the Rayleigh line relation. Referring again to Figure 7, we see the product of initial pressure (P_1) and specific volume ($\frac{1}{\rho_1}$) represented by origin A. From the origin, two points the Rayleigh line is tangent to the Hugoniot curve at two points known as upper and lower CJ points. The upper CJ point represents the steady detonation velocity solution, while the lower CJ point represents a maximum deflagration point [3]. With this, the CJ points are obtained as follows:

By differentiating the Hugoniot relation, Equation (6), with respect to ($\frac{1}{\rho_2}$):

$$\frac{dP_2}{d\left(\frac{1}{\rho_2}\right)} = \frac{(P_2 - P_1) - \left(\frac{2\gamma}{\gamma - 1}\right) P_2}{\left(\frac{2\gamma}{\gamma - 1}\right)\frac{1}{\rho_2} - \left(\frac{1}{\rho_2} - \frac{1}{\rho_1}\right)} \tag{8}$$

Also, using the slope at the tangent of upper and lower CJ points:

$$\frac{dP_2}{d\left(\frac{1}{\rho_2}\right)} = \frac{(P_2 - P_1)}{\left(\frac{1}{\rho_2} - \frac{1}{\rho_1}\right)} \tag{9}$$

Using the speed of sound, c_2, for the products:

$$c_2 = \sqrt{\gamma RT} \tag{10}$$

Equating Equations (8) and (9) and substitute Equations (7) and (10):

$$u_2^2 = \frac{\gamma P_2}{\rho_2} = c_2^2 \tag{11}$$

$$\therefore \left| u_2 \right| = c_2 \tag{12}$$

From Equation (12), it can be concluded that the by-products leave the combustion wave is at sonic condition with respect to the combustion frame.

In addition, the solution on the Hugoniot curve can be divided into five regions. Region I is defined as the strong detonation region where strong overdriven detonations propagates above upper CJ point. The lead combustion wave front travels much faster than the products resulting in a larger induction zone. This induction zone increases till the reactants are unable to have any further effect on the wave front thus slowing it down. An overdriven detonation wave will always decay back to the CJ point.

Region II is defined as the weak detonation region where the velocity of the products travels faster than the lead combustion wave. This results in a reduction in the induction zone, where additional heat has to be supplied to increase the combustion wave speed back to the upper CJ point.

Region III is defined as the weak deflagration region. The combustion waves exist as expansion or rarefaction waves, which have lower product density than reactants. These waves are often observed experimentally in the deflagration to detonation phase.

Region IV is defined as the strong deflagration region. This is a physically impossible state as the combustion wave cannot accelerate from subsonic to supersonic speeds in a constant area duct.

Region V is mathematically impossible as the solution is imaginary number from the Rayleigh-line equation.

C. DETONATION WAVE STRUCTURE (ZND)

An extension of Chapman-Jouget's theory is a wave structure model known as ZND model developed by Zeldovich, von Neumann and Doring. As shown in Figure 8, the ZND model consists of gasdynamic properties across a detonation wave followed by a rarefaction region. In the shockwave, there is a sharp increase in pressure, temperature and density. The thickness of the shockwave region is very small, usually in the order of a few mean paths of gas molecules where reaction is limited. The rarefaction region consists of an induction zone and reaction zone. The properties in the induction zone remains constant except of the temperature profile which increases slowly. In the reaction zone, the high energy released from the reactions of the fuel-oxidizer mixtures causes the temperature profile to increase sharply whereas the pressure and density continues to decrease.

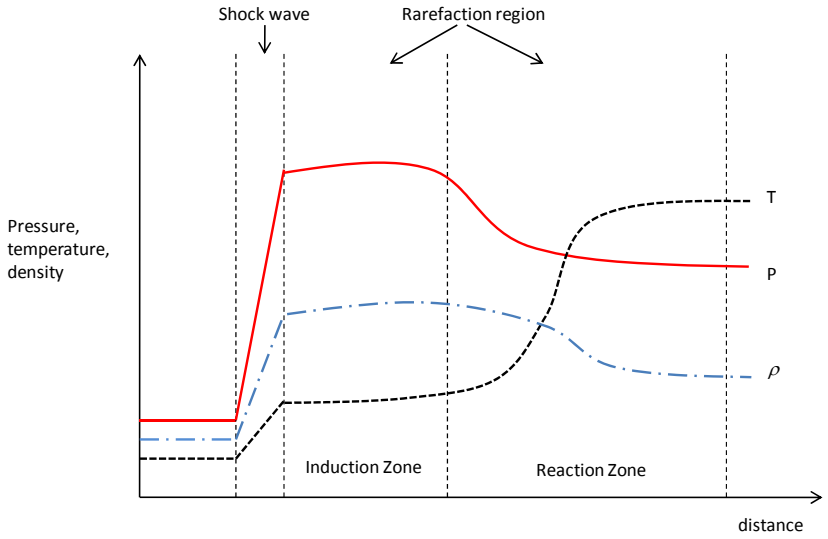

Figure 8. ZND model [From 2]

D. DETONATION INITIATION

There are two main processes to obtain a detonation wave, namely deflagration-to-detonation transition (DDT) and direct initiation. Under the appropriate boundary

conditions, a deflagration wave will accelerate to a high supersonic velocity and transit into a detonation wave. Figure 9 shows a fuel-oxidizer mixture filled tube undergoing the DDT process.

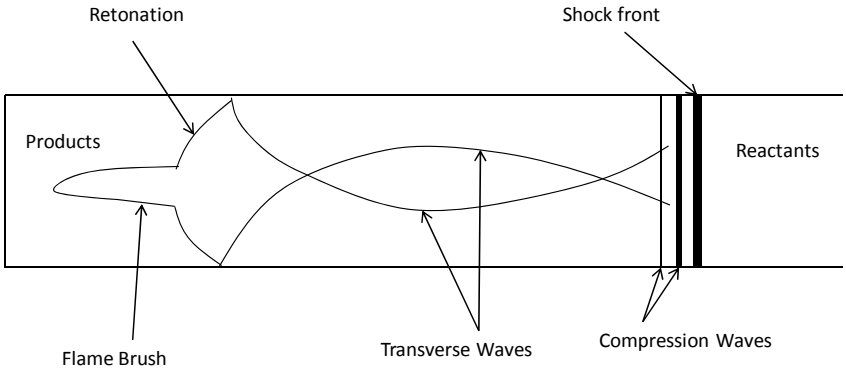

Figure 9. Schematic diagram of DDT process [From 2]

Upon ignition of the fuel-oxidizer mixture, a deflagration shock wave propagates into the reactants followed by a series of compression waves. These compression waves heat up the region behind the leading shock to create a localized high temperature region, which causes the velocity of the compression waves to increase further. The compression wave eventually catches up with the leading shock wave and coalesces into a sufficiently strong shock wave which can support a detonation wave [2]. The detonation wave in a confined tube causes the gas particles to move and create turbulence, which results in the onset of “an explosion in an explosion”. Two strong shock waves are created in the opposite direction: with the forward shock waves known as super detonation, and the shock waves that travel back towards the products known as retonation. When this process reaches a steady state, a self-propagating CJ detonation wave is formed.

It is also possible to initiate a detonation without going through the DDT process. Direct detonation refers to the spontaneous formation of a detonation wave without a predetonation deflagration regime. Here, the ignition source is responsible for the generation of the flow field and the formation of detonation wave [3]. There are several methods of direct detonation such as the use of powerful explosives; or photolysis and

turbulent mixing. In both processes, the important criterion towards achieving a self-sustaining detonation is the critical tube diameter (d_c) which is thirteen times the detonation cell width for a circular tube, and ten times the detonation cell width for a planar channel [2].

E. DETONATION CELL WIDTH

Detonation cells are formed through the interaction of the transverse and longitudinal compression waves. Detonation cell width is measured experimentally using a soot foil imprint technique where a detonation wave leaves a fish scale pattern on the soot coated aluminum sheeted lining the surface of a tube. Different concentration of fuel-oxidizer mixtures will have different cell sizes. Figure 10 shows the typical soot foil imprint from a Hydrogen-Oxygen mixture [4].

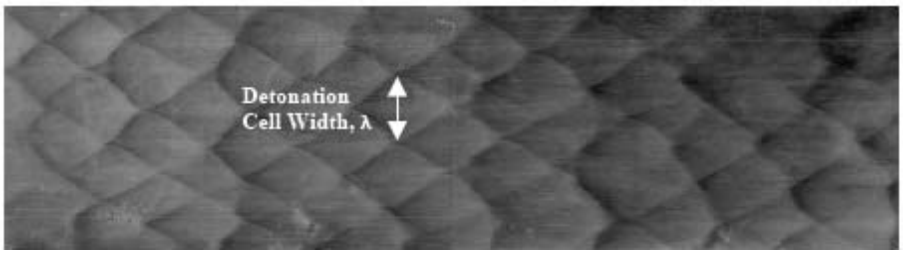

Figure 10. Soot foil imprint of Hydrogen-Oxygen mixture [From 4]

The detonation cell width is the transverse distance between each fish scale. Figure 11 shows the schematic of a detonation front cell structure. The non-planar shock front is induced by the energy release during the reactions within the fuel-oxidizer mixture. The Mach stem, incident shock, and reflected shock interact to produce a shear discontinuity known as the triple point.

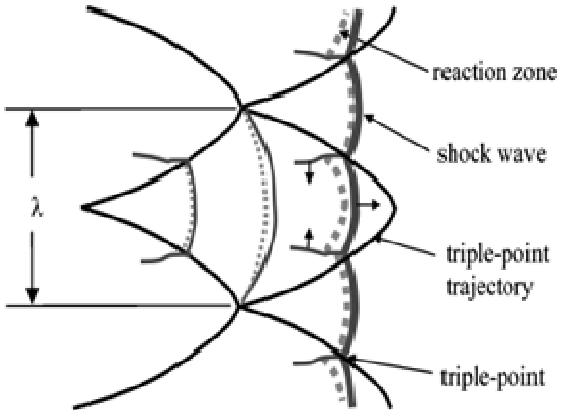

Figure 11. Schematic of detonation front structure [From 4]

The cell width is also an effective parameter used to characterize the detonability of fuel-oxidizer mixture. A more reactive fuel-oxidizer mixture such as Hydrogen-Oxygen will have smaller cell size than a typical hydrocarbon fuel such as Ethane (C_2H_6). Diluting the Hydrogen-Oxygen mixture with air however, reduces the reactivity hence increasing the cell size. To give us a sense of the scale, Kaneshige [5] reports that with an initial pressure of 101.5 atm and initial temperature of 293 K, a stoichiometric Hydrogen-Oxygen mixture diluted with N_2 has a cell size of 4.3 mm.

F. EQUIVALENCE RATIO OF FUEL-OXIDIZER MIXTURE

The equivalence ratio ϕ is defined as the actual fuel-oxidizer ratio to the stoichiometric fuel-oxidizer ratio. The stoichiometric reaction here means that the oxidizer has been completely used up when reacting with the fuel. It is a unique reaction for every different mixture. The equivalence ratio can be computed using either the mass fraction or mole fraction as shown in equation below.

$$\phi = \frac{m_{fuel} / m_{oxidizer}}{(m_{fuel} / m_{oxidizer})_{stoichiometric}} = \frac{n_{fuel} / n_{oxidizer}}{(n_{fuel} / n_{oxidizer})_{stoichiometric}} \tag{13}$$

where:

m = mass of molecules

n = number of moles

An equivalence ratio of more than one would imply that there is excess fuel, or that the mixture is fuel rich. Conversely, a ratio of less than one would imply excess oxidizer or a mixture that is fuel lean. The equivalence ratio will influence the thermodynamic property and composition of the fuel-oxidizer during detonation.

G. CHEMICAL KINETIC REACTION MODEL

During combustion or detonation, the chemical reactions take place at a finite rate. This rate is governed by chemical kinetics and depends on the concentration of the chemical compound, the prevailing temperature and pressure conditions; as well as the presence of a catalyst and radiative effects. The dependence of the reaction rate, *k*, is given by the Arrhenius Equation:

$$k = AT^{n} \exp\left(-\frac{E_a}{RT}\right) \tag{14}$$

where:

A= collision frequency for the species

n= represents the temperature dependency of the reaction.

E_a = amount of activation energy required for the reaction to occur

R = universal gas constant

A detail chemical reaction model of a fuel-oxidizer mixture will have hundreds of reaction and species under all operating conditions. Therefore, it is computationally demanding especially for complex detonation like RDE. Hence, it is important to use a reduced chemical model, which allows us to capture the detonation process and provide the accurate gasdynamic properties at the same time.

H. INVISCID NAVIER-STOKES OR THE EULER EQUATION

For the purpose of this thesis, the fuel-oxidizer mixture used is Hydrogen-Air mixture, and is assumed to be ideal gas and inviscid. During detonation, the interaction between the shock and combustion wave dominates over the effects of transport properties such as viscosity, thermal conduction and mass diffusion. Therefore, the governing equation used for this study is the 2D inviscid Navier-Stokes, which simply reduces to the well known Euler equations below.

$$\frac{\partial \vec{Q}}{\partial t} + \frac{\partial (\vec{F}_1)}{\partial x} + \frac{\partial (\vec{F}_2)}{\partial y} = \vec{S} \tag{15}$$

$$\vec{Q} = \begin{pmatrix} e \\ \rho \\ \rho u \\ \rho v \\ \rho \sigma_k \end{pmatrix}, \vec{F}_1 = \begin{pmatrix} (e+p)u \\ \rho u \\ \rho u^2 + p \\ \rho v u \\ \rho v \sigma_k \end{pmatrix}, \vec{F}_2 = \begin{pmatrix} (e+p)v \\ \rho v \\ \rho u v \\ \rho v^2 + p \\ \rho v \sigma_k \end{pmatrix}, \vec{S} = \begin{pmatrix} 0 \\ 0 \\ 0 \\ 0 \\ \dot{\omega}_k \end{pmatrix} \tag{16}$$

where:

Q = the dependent variable vector

$\vec{F}_i$ = the inviscid flux vectors

$\vec{S}$ = the source term vector

e = total energy

ρ = density

p = pressure

σ_k = the species mass fraction from species 1 to k

$\dot{\omega}_k$ = the rate of mass production for each species

I. COMPUTATIONAL NUMERICAL SCHEMES

There are two main categories of time integration scheme in computational numerical schemes, namely the implicit and explicit schemes. It is important to understand the differences between the two schemes to properly set up the simulation. Equation (17) shows a simple scalar equation which has to be discretized using the data from some time level, where the terms on the right hand side of the equation are the source term solutions required at each time step. An explicit integration will use the known data U^n and results in Equation (18). For an implicit integration, the right hand side term is discretized using time advanced term U^{n+1} shown in Equation (19).

$$\frac{\partial U}{\partial t} = RHS^n \tag{17}$$

$$\frac{U^{n+1} - U^n}{\Delta t} = RHS^n \tag{18}$$

$$\frac{U^{n+1} - U^n}{\Delta t} = RHS^{n+1} \tag{19}$$

To solve for Equation (19), there will be a linear system of equations relating the current time level to the time advanced level.

$$\frac{U^{n+1} - U^n}{\Delta t} = RHS^n + \left(\frac{\partial RHS}{\partial U}\right)^n (U^{n+1} - U^n) \tag{20}$$

The implicit scheme is generally known to be more stable as the forward solution is coupled together with the previous solution as shown by Equation (20), and will not generate an overly large value. There is also no restriction on the time step size but will require additional computation on the linear systems of equations.

The explicit scheme generally requires small time steps for stability and accuracy. This can impose restrictions on chemistry terms. The time step is being prescribed by the Courant-Friedrichs-Lewy (CFL) number, which relates the time domain to the spatial domain and is shown in Equation (21). CFL can be defined using the computational mesh

size or a fixed time step, and small CFL number implies a finer resolution in the computation and will generally require more computational resources. It is therefore important to optimize the simulation by selecting the suitable CFL number. Ho et al. [4] investigated the cell size suitable for hydrogen-air mixtures for computation simulation and found that a cell size of 0.0625 mm is sufficient.

$$CFL = a\frac{\partial t}{\partial x} \tag{21}$$

where:

a = maximum signal speed.

Beside the main integration schemes, there are two methods that are generally employed to improve the convergence and accuracy of the solution by making the system less stiff and allow dissipation. The first method is to use a spatially varying local CFL numbers, which varies the CFL number at each cell or time step. The second method is dual time stepping which appends a pseudo time derivative term by having a pseudo time step as shown in Equation (22).

$$\frac{U^{n+1}-U^{n}}{\Delta\tau}+\frac{U^{n+1}-U^{n}}{\Delta t}=RHS^{n}+\left(\frac{\partial RHS}{\partial U}\right)^{n}(U^{n+1}-U^{n}) \tag{22}$$

Dual time stepping allows inner iterations to use the pseudo time step $\Delta\tau$ and at convergence, disappears with the solution advancing by an actual physical time step of Δt.

Currently, there is no standard scheme to adopt for RDE simulation. A simpler method will be to use implicit scheme since it is more efficient. However, this is not always the case for reactive flow simulation involving a large number of species conservation Equations [6]. One example is using 4th-order Runge-Kutta explicit method, which requires less time than an implicit method since matrix inversion for the linear system of equations is not necessary.

THIS PAGE INTENTIONALLY LEFT BLANK

III. LITERATURE REVIEW

A. NUMERICAL SIMULATION

In 1959, Voitsekhovskii [7] was the first researcher to pioneer the use of one or more detonation waves spinning in an annular tube which was constantly filled by a combustible mixture from one end. As RDE began to receive more attention as an alternative propulsion concept, more numerical simulations were conducted. Zhdan et al. [8] used a 2D unsteady mathematical model with a Hydrogen-Oxygen mixture and found that a rotating detonation wave formed when the combustor length was 1.5 times or more than the rotating detonation wave.

Davidenko et al. [9] used a 6 species, 7 reactions chemical kinetic model for stoichiometric Hydrogen-Oxygen mixture to investigate the effects of the injector relative area and injection pressure. The numerical simulation used an Euler code based on a shock capturing, weighted essentially non-oscillatory (WENO) scheme with semi-implicit additive Runge-Kutta scheme. The CFL number used was 0.5 to 0.7, with the conclusion that the injection pressure acted as a scaling factor for the injection mass flux and wall pressure. The propagation velocity of the detonation wave matched the ideal CJ velocity and was found to be insensitive to the changes in the chamber height. The frequency between the detonation wave and fuel-air mixture height were inversely proportional to the azimuthal distance.

Yi et al. [10] conducted both 2D and 3D simulations using adaptive mesh refinement to achieve numerical efficiency and accuracy. The simulations employed second-order, three-step Runge-Kutta method for the temporal terms. A one-step chemical reaction model for Hydrogen-Air mixture was adopted. The numerical model of the annular chamber with length 0.177 m, outer diameter of 0.15 m and inner diameter 0.13 m was used for the simulation. For both cases, the denotation wave velocity propagated close to the CJ velocity. Yi et al. [11] further investigated the effects of nozzle shapes on the performance of RDE using 3D simulation. It was concluded that

since the flow at the chamber exit had already reached supersonic speeds, there was no further requirement to attach a convergent-divergent nozzle.

Hishida et al. [12] recommended using a fourth ordered Runge-Kutta time integration to resolve unsteady RDE problems and presented the fundamental flow field of rotating detonation. Yamada et al. [13] investigated the effects of doubling the computation area and increase in ignition energy on two different reservoir pressures at 2.7 MPa and 7.0 MPa. It was found that the upper detonation limit does not have any size effects unlike the lower limit. Sun et al. [14] used a simplified implicit method to deal with the stiffness generated by the chemical reacting source term in the species equation. A 9 species 19 reactions chemical mechanism was used, and a rotating detonation wave was achieved successfully. Schwer et al. [15] further developed a numerical procedure for investigating the flow field using algorithms used for PDEs. This pressure study was conducted by varying the inlet stagnation pressure and back pressure, and it was found that the height of the detonation wave generally decreases with decreasing pressure ratio, whereas mass flow depends mostly on the inlet stagnation properties.

B. RDE DEMONSTRATORS

In order to better design a computational setup for RDE, numerous practical experiments and RDE demonstrators were being reviewed. Nicholls et al. [16] performed experiments to determine the feasibility of RDE. Zhdan et al. [17] performed experiments on a simple annular chamber and they recorded transverse detonation waves. The parameters used are detonation velocities of 1,100 to 1,430 m/s with an equivalence ratio of 0.8 to 1.94. Bykovskii et al. [18] investigated the rotating detonation in various combustion chambers with hydrogen-air mixtures, and measured wave speeds of 1880m/s and observed 1 to 2 oblique shockwaves between the incident and reflected waves.

In recent years, France, Russia and Japan had successfully built RDE demonstrators to verify the propulsion performance, mechanical vibrations and thermal aspects of the ignition system and fuel injection system. Laboratory of Combustion and

Detonation in Poitiers, France [19] used an annular chamber of 100 mm diameter, 2.5 mm height and 40 mm length with no nozzle connected as their demonstrator as shown in Figure 12 to 13.

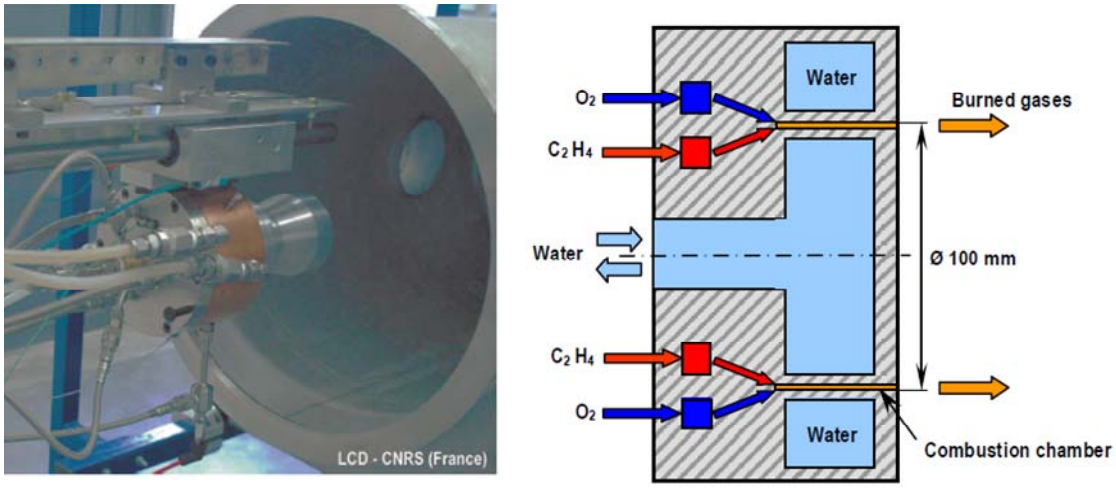

Figure 12. RDE demonstrator [From 19]

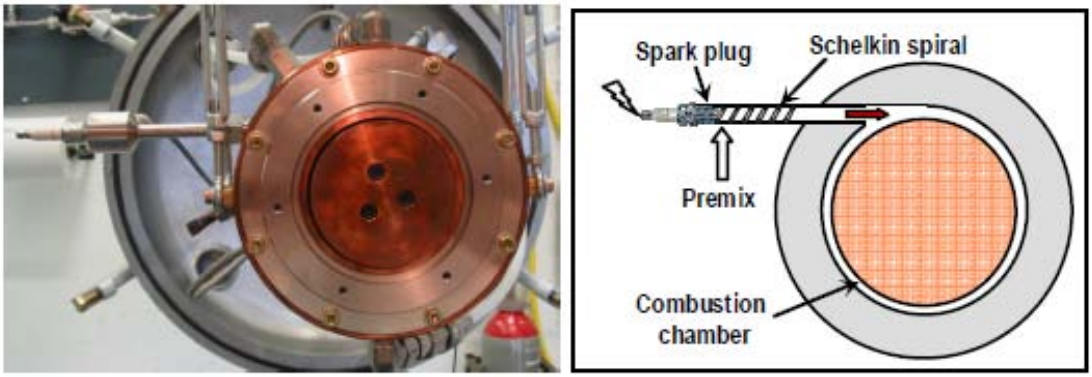

Figure 13. Ignition System [From 19]

Hayashi et al. [20] had also developed a RDE system to compare experimental and numerical solutions. The RDE system is shown in Figure 14.

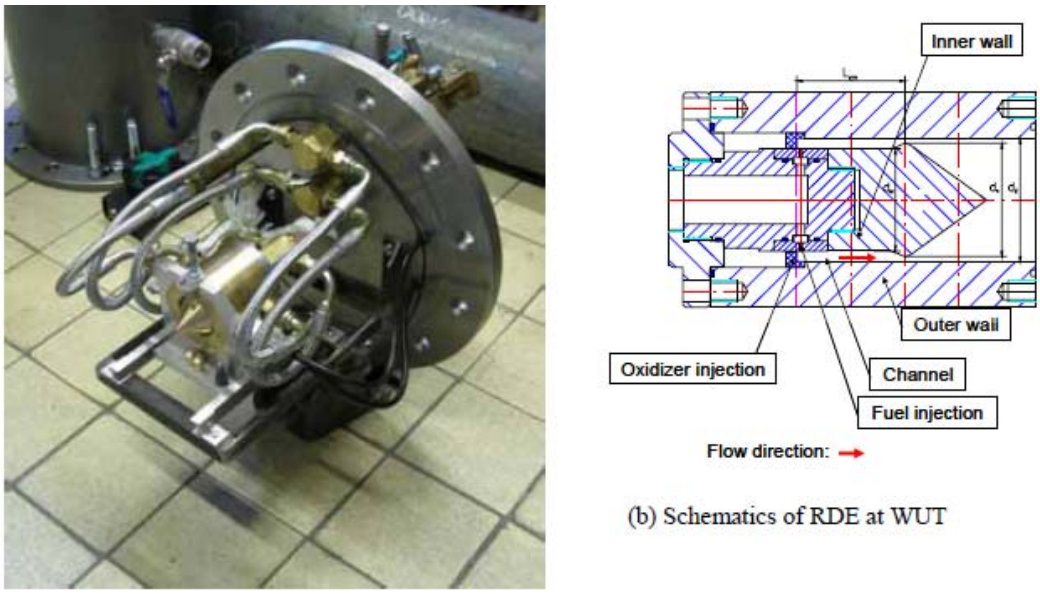

(a) RDE system of Warsaw University of Technology

(b) Schematics of RDE at WUT

Figure 14. RDE System [From 20]

In 2009, Lavrentyev Institute of Hydrodynamics and MBDA-France [21] had designed a full scale demonstration engine of 350 mm external diameter and 280 mm internal diameter as shown in Figure 16.

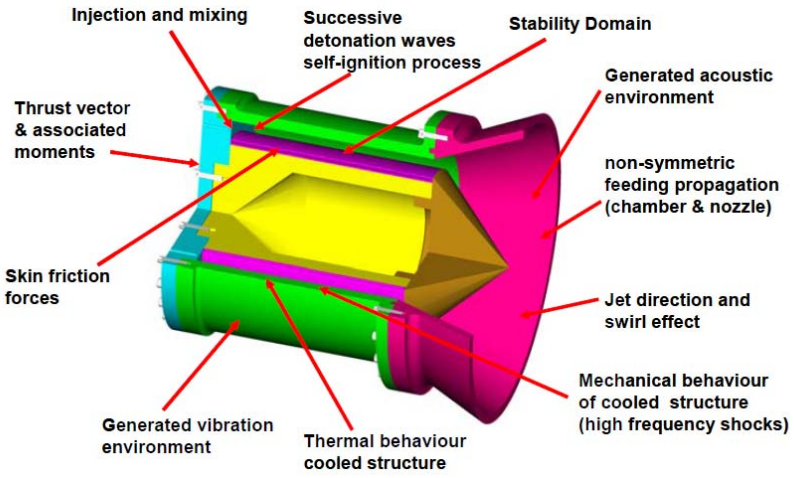

Figure 15. RDE Demonstrator Engine [From 21]

The review of various RDE demonstrators provided a better understanding on the practicality of RDE thus allowing a more robust computational domain to be formulated.

THIS PAGE INTENTIONALLY LEFT BLANK

IV. COMPUTATIONAL SETUP

A. 2D COMPUTATIONAL DOMAIN

A complete 3D numerical simulation of an RDE as a first approach was deemed to be too computationally intensive and expensive. Therefore, the 3D RDE was simplified into a 2D domain as shown in Figure 16. The 3D annular combustion chamber had been projected as a 2D rectangular chamber. The height of the annular chamber in the radial direction was assumed to be relatively small compared to the arc length in the azimuthal direction. Therefore, the effect of the height was neglected and the domain could be represented by a 2D planar chamber.

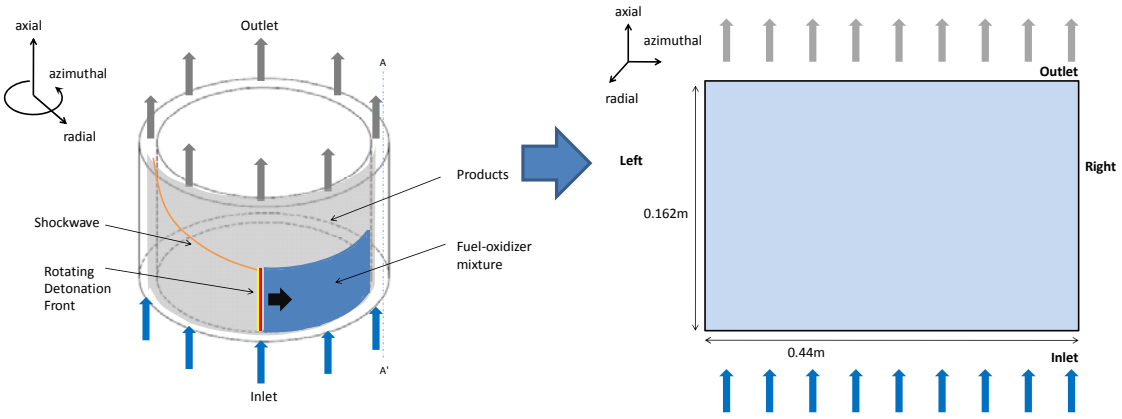

Figure 16. Schematic of the 2D computational domain

An incremental approach was taken for the simulation of RDE. The first step was to use a smaller domain to create a shock wave. Once a shockwave was achieved, the next step was to reliably reproduce the CJ conditions. Chemical reactions were first added to produce a detonation wave. Various simulation parameters were explored such as time integration scheme, CFL number, mesh cell size, unstructured and structured mesh topology. Once the CJ conditions were reproduced, different fuel-oxidizer ratios

were then compared to the CJ conditions to select the final simulation parameters. The suitable boundary conditions for the RDE simulation were finally selected by looking at the overall flow field of the detonation wave. A full RDE simulation was thus carried out to characterize the inlet. Finally, a novel simulation set-up was conducted to better depict the actual RDE operation.

B. BASIC SHOCKTUBE SIMULATION

It was first necessary to understand the basics of shock physics and the methods to setup a CFD simulation. A shocktube of length 0.1 m and height 0.02 m was used to represent a subset of the 2D computational domain as shown in Figure 17. The initial and boundary conditions were shown in Table 1. The 2D computational domain was created using Solidworks CAD software. The domain was exported to Multipurpose Intelligent Meshing Environment (MIME) software to create triangular unstructured meshes. A coarse mesh size of 0.1 mm was used for this simulation as shown in Figure 18. The commercial computational software, CFD++, was used to simulate the gasdynamics and flow field of a RDE.

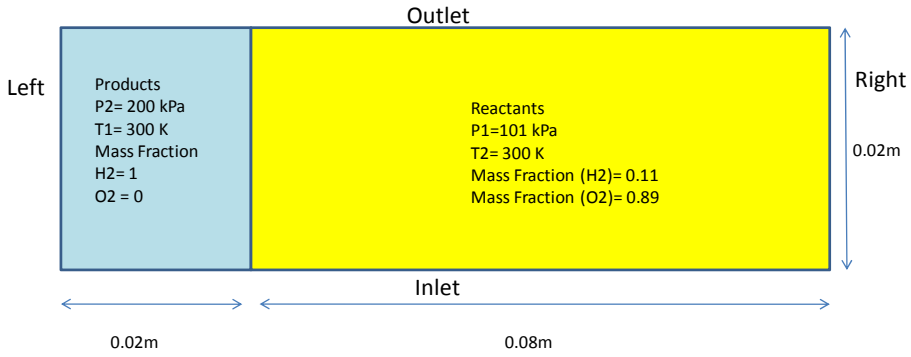

Figure 17. Schematic of basic shocktube simulation

Table 1. Simulation parameters for basic shocktube simulation

Basic Shocktube Simulation	
Parameters	**Settings**
Dimensions	0.1 x 0.02 m
Initial Conditions	Products: 200 kPa, 300 K Reactant: 101 kPa, 300 K
Boundary Conditions	Inlet: Multi-species inviscid surface tangency (Wall) Outlet: Multi-species inviscid surface tangency (Wall) Left: Multi-species inviscid surface tangency (Wall) Right: Multi-species inviscid surface tangency (Wall)
Equation Set	Compressible Euler Equation Equation of State: Ideal Gas
Spatial Discretization	2^{nd} order accuracy in space 2D Total Variation Diminishing (TVD): Continuous
Riemann Solver	Minimum Dissipation: LHS & RHS Activate pressure switch: Supersonic Activate pressure gradient switch: Normal
Time Integration	Point implicit Dual time stepping Global CFL: 1e15 Local CFL: 0.95
Mesh Size	0.1mm 532766 triangles Topology: Unstructured
Reaction	None

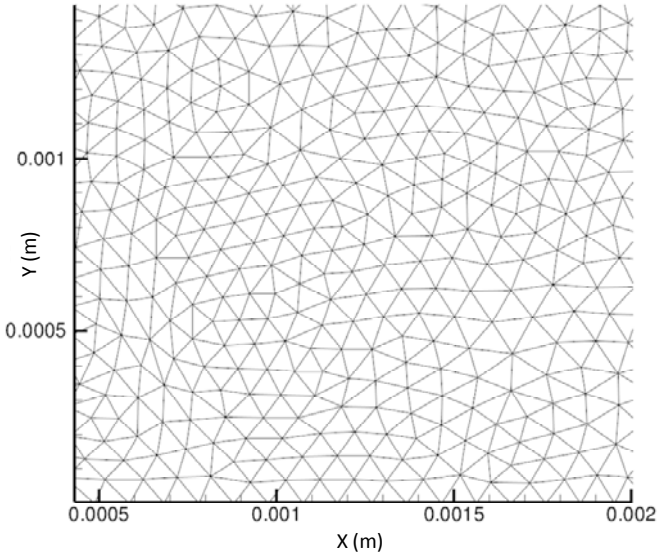

Figure 18. Unstructured mesh topology

C. RELIABLE REPRODUCTION OF CJ CONDITIONS

It was important to make reliable reproductions of detonation waves with CJ conditions since this research uses a commercial CFD code. The next step was to include chemical reactions in the shocktube to produce a detonation wave. Here, a one step reaction as shown by Equation (23) for a stoichiometric H_2-Air mixture was used conjunction with a Hydrogen-Air mixture ($\phi = 1.0$).

$$H_2 + 0.5(O_2 + 3.76N_2) \rightarrow H_2O + 0.5(3.76)N_2 \tag{23}$$

where the respective mass fractions X_i for reactants and Y_i for products were:

$$X_{H_2} = \frac{H_2}{H_2 + 0.5(O_2 + 3.76N_2)} = \frac{2}{2 + 0.5(32 + 3.76 * 28)} = 0.02831$$

$$X_{O_2} = \frac{0.5O_2}{H_2 + 0.5(O_2 + 3.76N_2)} = \frac{0.5 * 32}{2 + 0.5(32 + 3.76 * 28)} = 0.22650$$

$$X_{N_2} = \frac{0.5(3.76)N_2}{H_2 + 0.5(O_2 + 3.76N_2)} = \frac{0.5 * 3.76 * 28}{2 + 0.5(32 + 3.76 * 28)} = 0.74519$$

$$Y_{H_2O} = \frac{H_2O}{H_2O + 0.5(3.76N_2)} = \frac{18}{18 + 0.5*3.76(28)} = 0.25481$$

$$Y_{N_2} = \frac{0.5(3.76N_2)}{H_2O + 0.5(3.76N_2)} = \frac{0.5*3.76(28)}{18 + 0.5*3.76(28)} = 0.74519$$

Subsequently, a 2 step chemical reaction [22] was used. The reactions were as follows:

$$H_2 + O_2 \leftrightarrow 2OH \quad (24)$$

$$2OH + H_2 \leftrightarrow 2H_2O \quad (25)$$

Finally, a reduced chemical mechanism of 18 reactions and 9 species [23] was used to achieve high fidelity in the solution shown in Table 2. Both implicit and explicit time integration with various CFL numbers were investigated to determine the detonation flow field. In addition, the mesh size had been reduced to 0.05 mm and there were a total 2,113,220 triangles as shown in Figure 19. A summary of various setting of the computational set-up was shown in **Appendix A**.

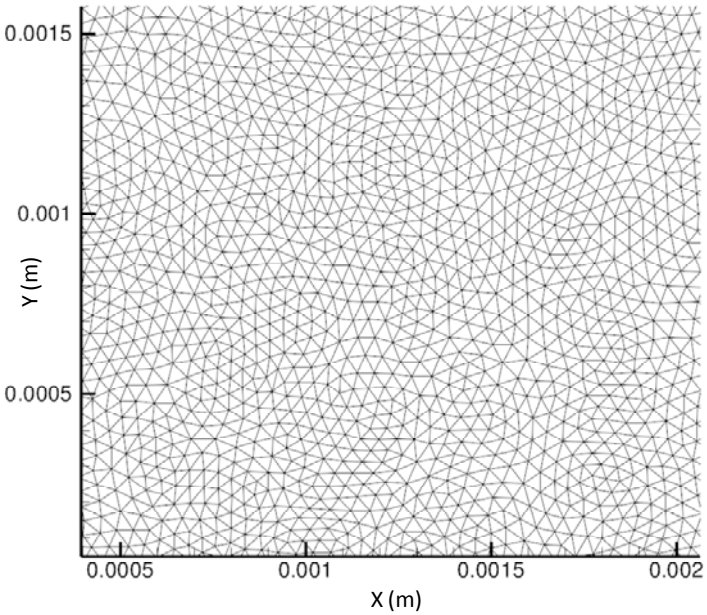

Figure 19. Reduced mesh size topology

Table 2. Reduced chemical mechanism for Hydrogen-Air mixture

#	Reaction	Frequency factor (Nm/kilomole)	Temperature exponent	Activation energy ($s^{-1}[m^3/kilomole]^{N-1}$)
1	$H_2 + O_2 <-> 2OH$	0.17e11	0	0.20159e9
2	$O_2 + H <-> OH + O$	0.142e+12	0	0.6866e+08
3	$H_2 + OH <-> H_2O + H$	0.316e+05	1.8	0.12686e+08
4	$H_2 + O <-> OH + H$	0.207e+12	0	0.57568e+08
5	$2OH <-> H_2O + O$	0.55e+11	0	0.29307e+08
6	$OH + H + M <-> H_2O + M$	0.2211e+17	-2.0	0
7	$H + H + M <-> H_2$	0.653e+12	-1.0	0
8	$O_2 + H + M <-> HO_2 + M$	0.32e+13	-1.0	0
9	$OH + HO_2 <-> O_2 + H_2O$	0.5e+11	0	0.4186e+07
10	$H + HO_2 <-> H_2 + O_2$	0.253e+11	0	0.29307e+07
11	$H + HO_2 <-> 2OH$	0.199e+12	0	0.7536e+07
12	$O + HO_2 <-> O_2 + OH$	0.50e+11	0	0.4186e+07
13	$2HO_2 <-> O_2 + H_2O_2$	0.199e+10	0	0
14	$H_2 + HO_2 <-> H + H_2O_2$	0.301e+09	0	0.7829e+08
15	$OH + H_2O_2 <-> H_2O + HO_2$	0.102e+11	0	0.7954e+07
16	$H + H_2O_2 <-> H_2O + OH$	0.5e+12	0	0.4186e+08
17	$O + H_2O_2 <-> OH + HO_2$	0.199e+11	0	0.247e+08
18	$H_2O_2 + M <-> 2OH + M$	0.121e+15	0	0.19049e+09

Once the detonation wave was established, the mesh topology was changed to structured meshes to allow for more efficiency computation. Using the commercial meshing software, Pointwise, structured rectangular meshes were generated for the computational domain. The mesh size was 0.05 mm and the total number of meshes increased to 409,200 rectangles, with the structure mesh topology is shown in Figure 20.

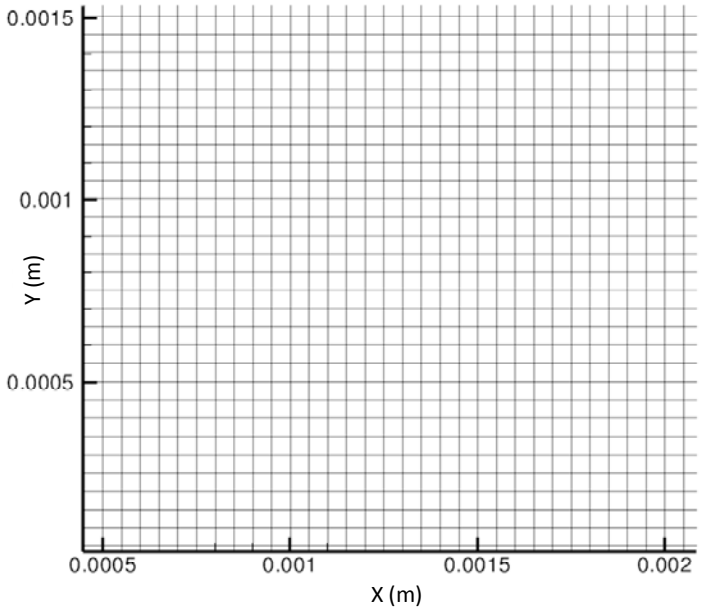

Figure 20. Structured mesh topology

D. CJ CONDITIONS WITH DIFFERENT FUEL-AIR RATIOS

The next step was to determine the CJ conditions such as temperature and velocity for fuel lean, stoichiometric and fuel rich conditions. The ratios selected were 0.7 and 2.2. The mass fractions of each species were calculated as follows:

For a Fuel Lean mixture ($\phi = 0.7$),

$$0.7H_2 + 0.5(O_2 + 3.76N_2) \rightarrow 0.7H_2O + 0.15O_2 + 0.5(3.76)N_2 \qquad (23)$$

where the respective mass fractions X_i for reactants and Y_i for products were:

$$X_{H_2} = \frac{0.7H_2}{0.7H_2 + 0.5(O_2 + 3.76N_2)} = \frac{0.7*2}{0.7*2 + 0.5(32 + 3.76*28)} = 0.01999$$

$$X_{O_2} = \frac{0.5O_2}{0.7H_2 + 0.5(O_2 + 3.76N_2)} = \frac{0.5*32}{0.7*2 + 0.5(32 + 3.76*28)} = 0.22844$$

$$X_{N_2} = \frac{0.5(3.76)N_2}{0.7H_2 + 0.5(O_2 + 3.76N_2)} = \frac{0.5*3.76*28}{0.7*2 + 0.5(32 + 3.76*28)} = 0.75157$$

$$Y_{H_2O} = \frac{0.7H_2O}{0.7H_2O + 1.5(O_2) + 0.5(3.76N_2)} = \frac{0.7(18)}{0.7(18) + 1.5(32) + 0.5*3.76(28)} = 0.17990$$

$$Y_{O_2} = \frac{1.5(O_2)}{0.7H_2O + 1.5(O_2) + 0.5(3.76N_2)} = \frac{1.5(32)}{0.7(18) + 1.5(32) + 0.5*3.76(28)} = 0.68532$$

$$Y_{N_2} = \frac{0.5(3.76N_2)}{0.7H_2O + 1.5(O_2) + 0.5(3.76N_2)} = \frac{0.5*3.76(28)}{0.7(18) + 1.5(32) + 0.5*3.76(28)} = 0.75157$$

For a Fuel Rich mixture ($\phi = 0.7$),

$$2.2H_2 + 0.5(O_2 + 3.76N_2) \rightarrow H_2O + 1.2H_2 + 0.5(3.76)N_2 \qquad (25)$$

where the respective mass fractions X_i for reactants and Y_i for products were:

$$X_{H_2} = \frac{2.2H_2}{2.2H_2 + 0.5(O_2 + 3.76N_2)} = \frac{2.2*2}{2.2*2 + 0.5(32 + 3.76*28)} = 0.06024$$

$$X_{O_2} = \frac{0.5O_2}{2.2H_2 + 0.5(O_2 + 3.76N_2)} = \frac{0.5*32}{2.2*2 + 0.5(32 + 3.76*28)} = 0.21905$$

$$X_{N_2} = \frac{0.5(3.76)N_2}{2.2H_2 + 0.5(O_2 + 3.76N_2)} = \frac{0.5*3.76*28}{2.2*2 + 0.5(32 + 3.76*28)} = 0.72070$$

$$Y_{H_2O} = \frac{H_2O}{H_2O + 1.2(H_2) + 0.5(3.76N_2)} = \frac{18}{18 + 1.2(2) + 0.5*3.76(28)} = 0.24644$$

$$Y_{H_2} = \frac{1.2(H_2)}{H_2O + 1.2(H_2) + 0.5(3.76N_2)} = \frac{1.2(2)}{18 + 1.2(2) + 0.5*3.76(28)} = 0.03286$$

$$Y_{N_2} = \frac{0.5(3.76N_2)}{H_2O + 1.2(H_2) + 0.5(3.76N_2)} = \frac{0.5*3.76(28)}{18 + 1.2(2) + 0.5*3.76(28)} = 0.72070$$

Both the implicit and explicit time integration schemes were used to determine the CJ conditions.

E. CONFIRMATION OF PERIODIC BOUNDARY CONDITION

For this study, it was important to create periodic boundary conditions to allow the left and right boundary to be connected during the simulation (Figure 21). Hence, several iterations were done to ensure that the detonation wave was able to flow through the connecting boundary. The high-pressure region was being offset from the centre of the shocktube so that the detonation waves could be differentiate when it propagate through the boundaries. The simulation set up was shown in Table 3.

Table 3. Simulation parameters for periodic boundary simulation

Periodic simulation	
Dimensions	0.1 x 0.02 m
Initial Conditions	Products: 200 kPa, 3,000 K Reactant: 101 kPa, 300 K
Boundary Conditions	Inlet: Multi-species inviscid surface tangency (Wall) Outlet: Multi-species inviscid surface tangency (Wall) Left: Periodic Zonal Right: Periodic Zonal
Equation Set	Compressible Euler Equation Equation of State: Ideal Gas
Spatial Discretization	2^{nd} order accuracy in space 2D Total Variation Diminishing (TVD) limiter: Minmod
Riemann Solver	Minimum Dissipation: LHS only
Time Integration	4^{th} order explicit Runge-kutta CFL: 1
Mesh Size	0.05 mm 797,601quadilateral Topology: Structured
Reaction	9 species 18 reactions

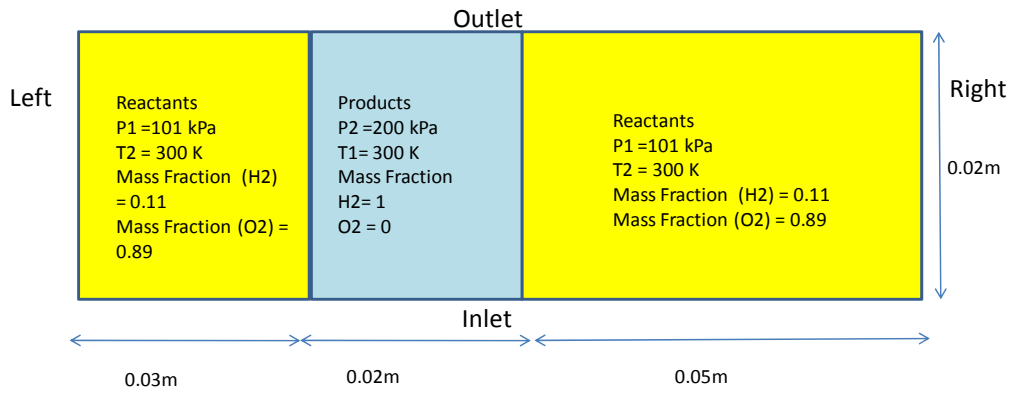

Figure 21. Schematic of periodic boundary simulation

F. FULL RDE SIMULATIONS

Using a RDE with diameter of 0.14 m and length of 0.162 m, the computational domain dimensions were of the width 0.44 m and length 0.162 m (Figure 22). This dimension was chosen so that the computational domain was comparable to the physical RDE demonstrators.

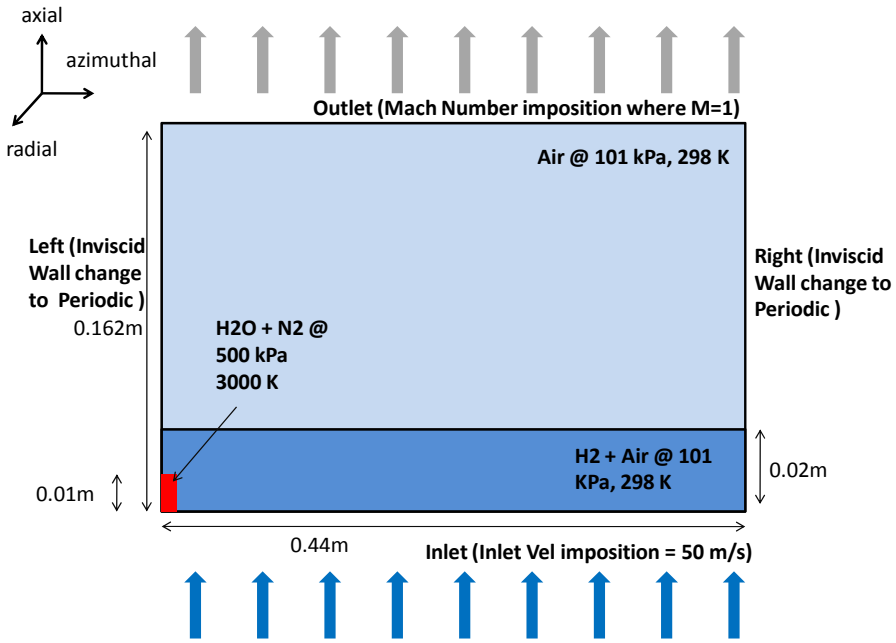

Figure 22. Schematic of full RDE simulation

The main challenge for this research was to select the appropriate boundary conditions to represent the RDE. For the RDE combustor inlet, pre-mixed fuels were injected into the combustion chamber via micro nozzles. By assuming that the distance between each nozzle was very small, the inlet could be simplified to be a continuous boundary that allows flow into the chamber.

Next, there were various approaches to specify the inflow of the Hydrogen-Air mixture. Usually, the inlet could be treated as valves, which would open and close depending on the reservoir stagnation pressures or the static pressure at the chamber inlet. Since the detonation wave would be at a higher pressure than the static or stagnation pressure, the inlet would need to be choked for those conditions. The mass flow rates could also be specified for the pre-mixed fuel. However, it would be more insightful to allow the interaction to determine the mass flow rate of the inlet. To better characterize the gasdynamic at the inlet, the inlet should be constraint to as small an extent as possible. For this study, only the injection velocities and temperatures were specified. Other important gasdynamics parameters such as pressure, mass flow rate and density would be determined by the interaction of the detonation wave and inflow. The inlet velocity was determined from the height of the premixed fuel required to be filled to continuously support the detonation wave.

$$V_{In} = \frac{H_f}{t_d} = \frac{H_f}{W_{rde} / V_{CJ}} \tag{23}$$

where:

V_{in} = injection or inlet velocity (m/s)

H_f = Height of premixed fuel required (m)

t_d = time for detonation wave to travel a complete cycle (s)

W_{rde} = width chamber (m)

V_{CJ} =Detonation wave speed at CJ condition (m/s)

$$V_{In} = \frac{H_f}{t_d} = \frac{H_f}{W_{rde}/V_{CJ}} = \frac{0.01}{0.44/1971} = 44.79m/s \approx 45m/s$$

As shown above, the injection velocity was calculated to be approximately 45 m/s. To account for a certain degree of variability, an injection velocity of 50 m/s was used as the baseline simulation.

When the computational domain was simplified into a 2D planar chamber, there would be a need to connect the left and right boundary to allow the detonation wave front to propagate continuously around the domain. The type of boundary condition employed was known as periodic boundaries. A negative offset in distance equivalent to the width of the chamber was applied to the right boundary and a positive offset was applied to the right boundary so that the two boundaries were connected numerically. To ensure that the detonation wave propagates in a specific direction, the boundary conditions were set as a wall initially. The high-pressure segment located on the left bottom of the domain would initialize the detonation and send the detonation wave propagating to the right. Before the detonation wave impacts the right wall, we changed the boundary conditions to periodic without affecting the detonation front, since the detonation wave travelled at a supersonic speed.

For this study, the outflow boundary represented the outlet of the combustion chamber. There would be no nozzle attached to the outlet as it was not the focus of this research. The design of nozzle could be subsequently introduced after the inlet had been characterized. Several possible boundary conditions could be assumed for the outlet: - either supersonic outflow, sonic outflow or pressure dependent outflow. The boundary condition selected as a baseline set-up is a sonic outflow condition of Mach 1. Table 4 summarized the simulation parameter used for the full RDE simulation.

Table 4. Simulation parameters for full RDE simulation

Full RDE Simulation	
Parameters	**Settings**
Dimensions	0.44 x 0.162 m
Initial Conditions	Products: 500 kPa, 3,000 K Reactant: 101 kPa, 300 K
Boundary Conditions	Inlet: Pressure Temperature using normal velocity Outlet: Multi-species inviscid surface tangency (Wall) & periodic zonal Left: Multi-species inviscid surface tangency (Wall) & periodic zonal Right: Direct Mach Number Imposition
Equation Set	Compressible Euler Equation Equation of State: Ideal Gas
Spatial Discretization	2^{nd} order accuracy in space 2D Total Variation Diminishing (TVD) limiter: Mimod
Riemann Solver	Minimum Dissipation: LHS only
Time Integration	4^{th} Order Runge-kutta explicit CFL: 1
Mesh Size	0.05 mm to 0.1 mm 5261802 Quadrilaterals Topology: Structured
Reaction	9 Species 18 reactions

G. NOVEL RDE SIMULATIONS

Instead of starting the simulation with wall boundary conditions for the left and right boundaries, the high-pressure ignition source could be shifted to the centre of the domain. Half the domain was filled with pre-mixed fuel as illustrated in Figure 23. Once the simulation commenced, shockwaves would be sent in the all directions. The shockwave travelling in the pre-mixed fuel region would transit into a detonation wave while the other shockwaves should turn into an expansion wave after some time. Thus, the need to pause the simulation to change the periodic boundary conditions was eliminated. In addition, this simulation depicted an actual RDE that had an omni-directional igniter and would send shockwaves in all directions from the ignition point.

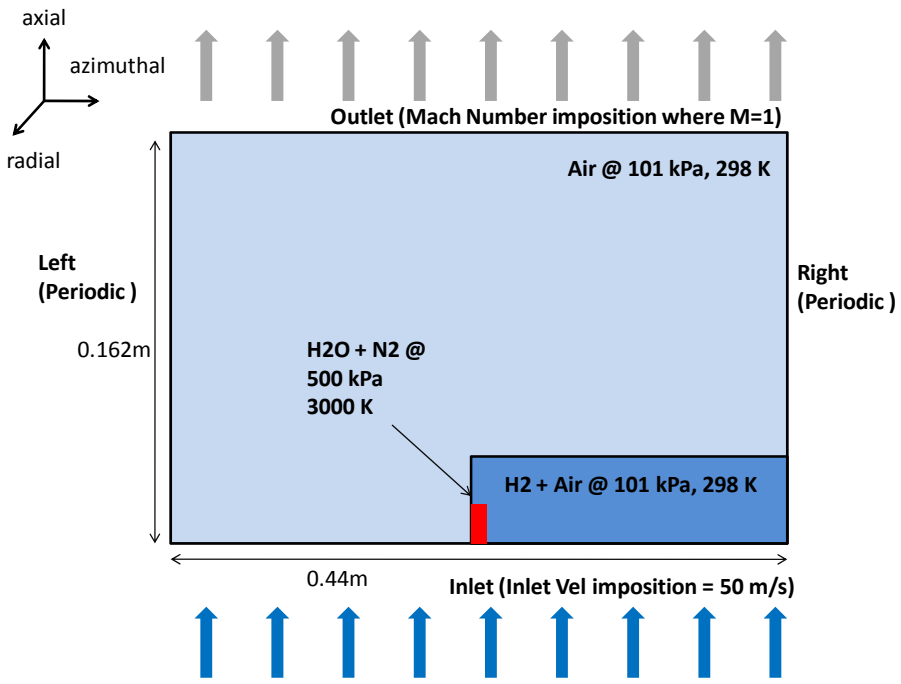

Figure 23. Schematic of novel RDE simulation

V. DISCUSSION OF RESULTS AND ANALYSIS

From the literature review, there were many different conflicting approaches to properly simulate detonation wave. Hence, the first step was to determine the best numerical scheme to adopt. A shocktube simulation was used to investigate various schemes such as implicit, explicit, low, high order Runge-kutta with different number of chemical reactions. The effects of mesh resolution and mesh topology such as unstructured and structured were also investigated. Once the numerical scheme was identified with the right mesh resolution and topology, a full RDE simulation was carried out to characteristic the inlet. Finally, with the insights gain from the full RDE simulation, a novel simulation set-up was formulated to eliminate the need to pause the simulation to change the periodic boundary conditions.

A. BASIC SHOCKTUBE SIMULATION

Figure 24 showed the initial condition of the shocktube. The high-pressure region was in red and the low pressure region was in blue. From Figures 25, a shock front could be observed at the 100^{th} time step ($t = 1\ \mu s$). Using Equation 24 to compute the average shock velocity and measuring pressure and temperature at Mach 1 (Figure 26), the following conditions were observed:

- Pressure – 2 MPa.
- Temperature at the shock front – 692 K.
- Average shock velocity – 1 km/s.

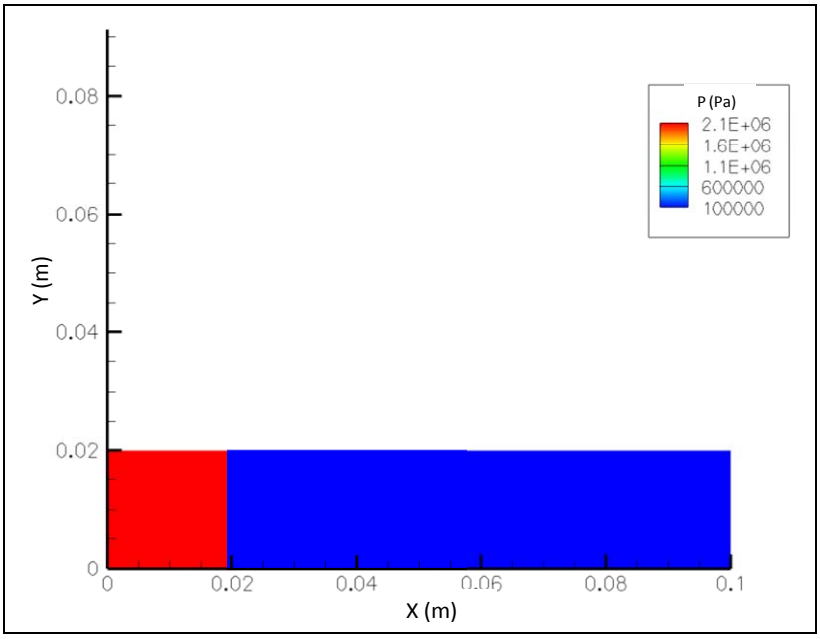

Figure 24. Pressure contour for basic shocktube simulation at 0 μs

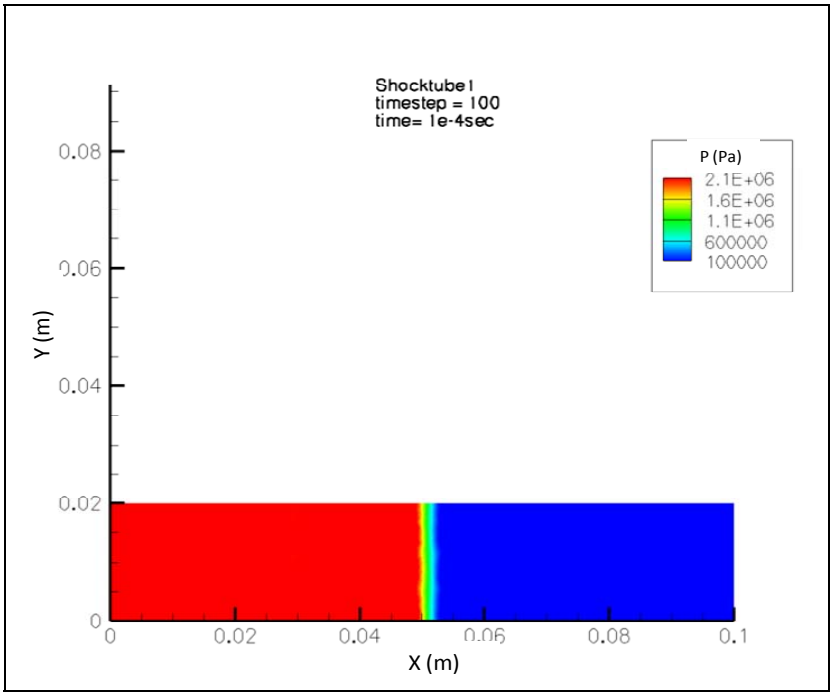

Figure 25. Pressure contour for basic shocktube simulation at 1 μs

The pressure, temperature and Mach number profile was extracted from a horizontal line (Y= 0.01 m). The temperature drop observed at around 0.03 m due to the absences of reactants in that region. The resolution of the shock wave was poor since a large mesh size of 0.1 mm was used. Since a shock was achieved, the next step was to include chemical reactions to obtain a detonation wave.

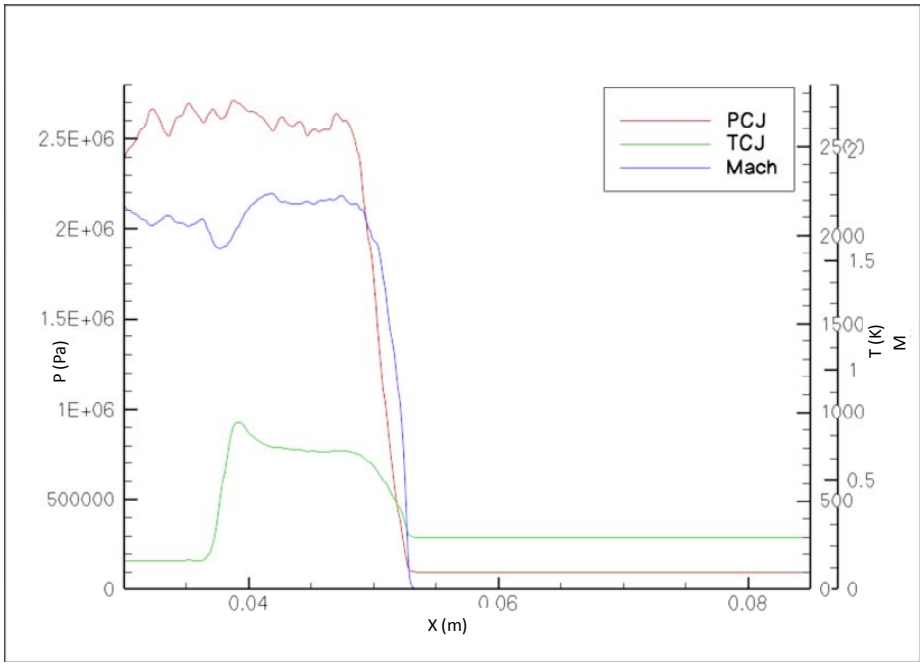

Figure 26. Pressure, temperature and Mach number profile for basic shocktube simulation at 1 μs

$$V_{Ave} = \frac{1}{n}\sum_{i=1}^{n}\frac{\Delta x_n}{\Delta t_n} = \frac{1}{n}\left(\frac{\Delta x_1}{\Delta t_1} + \frac{\Delta x_2}{\Delta t_2} + \frac{\Delta x_3}{\Delta t_3} + \ldots + \frac{\Delta x_n}{\Delta t_n}\right) \tag{24}$$

where

Δx = distance travelling from time from one time step to the next.

Δt = time step

B. RELIABLE REPRODUCTION OF CJ CONDITIONS

As mentioned previously, it was important to make reliable reproductions of CJ conditions. It was not trivial to find the suitable simulation parameters to achieve a detonation wave that meets CJ conditions. The main iterations conducted to reproduce the CJ conditions were highlighted in this section.

The CJ conditions for stoichiometric Hydrogen-Air mixture were outlined in as follows:

- Pressure: 1.58 MPa
- Temperature: 2,942 K
- Average Shock Velocity: 1.965 km/s

Initially, a one step chemical reaction was used, where several iterations had to be carried out to find the suitable simulation parameters to achieve detonation. The first series of iterations included varying the global CFL number with a fixed local CFL number of 1. The explicit multi-stage Runge-kutta time integration scheme was used. Figure 27 and 29 showed the pressure contours using the various global CFL numbers and a fixed local CFL = 1.0

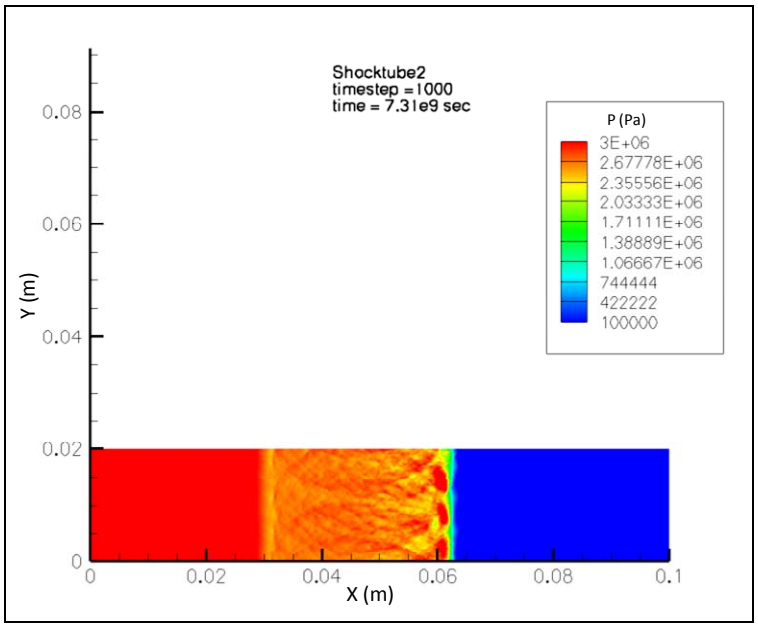

Figure 27. Pressure contour for global CFL of 1e15 at 7.31e9 sec

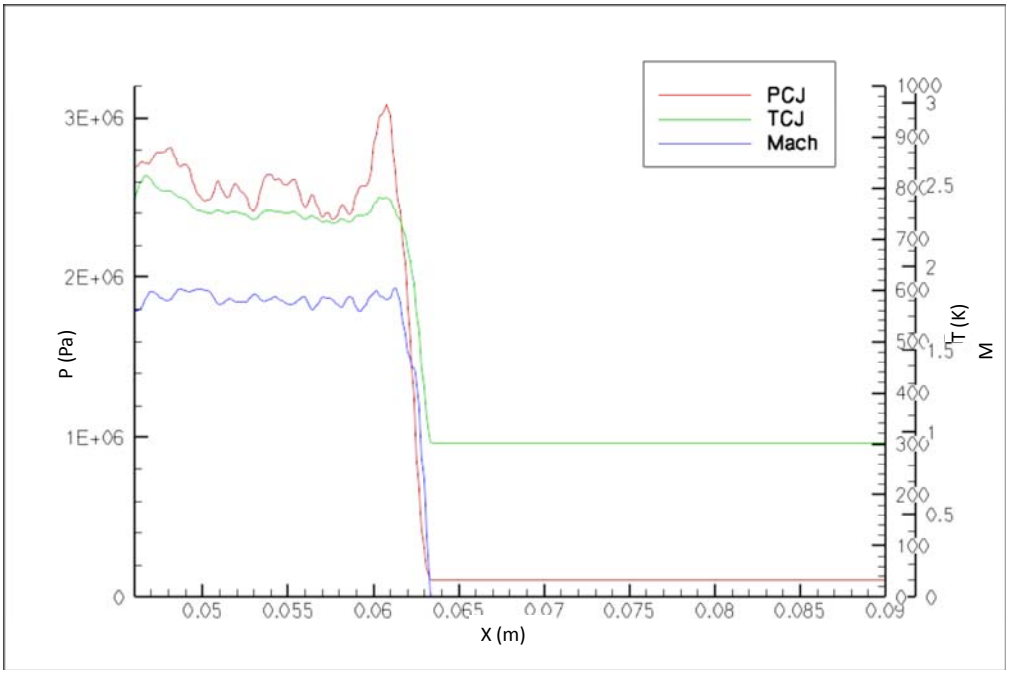

Figure 28. Pressure, temperature and Mach number profile for global CF of 1e15 at 7.31e9 sec

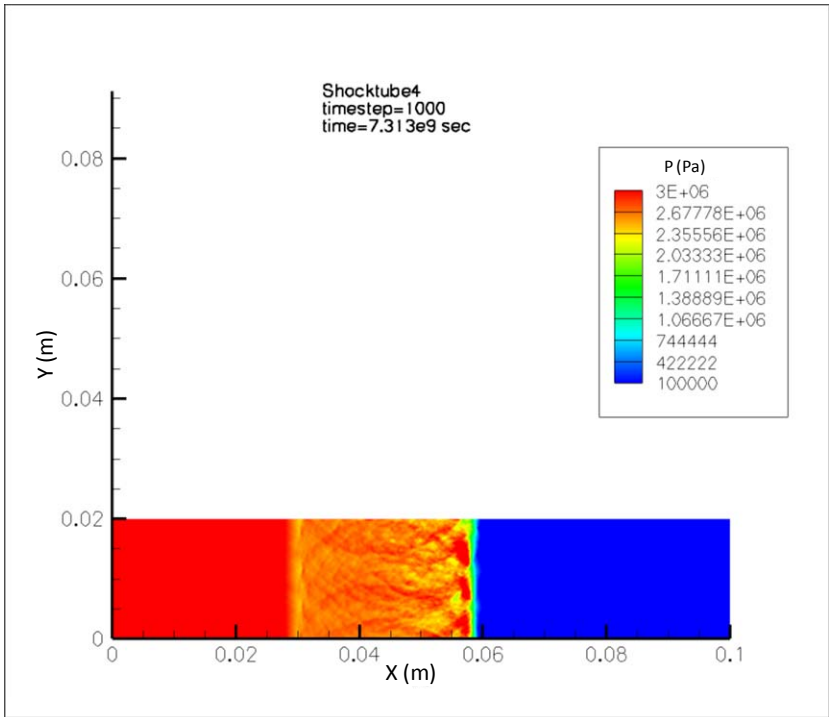

Figure 29. Pressure contour for global CFL of 1e16 at 7.31e9 sec

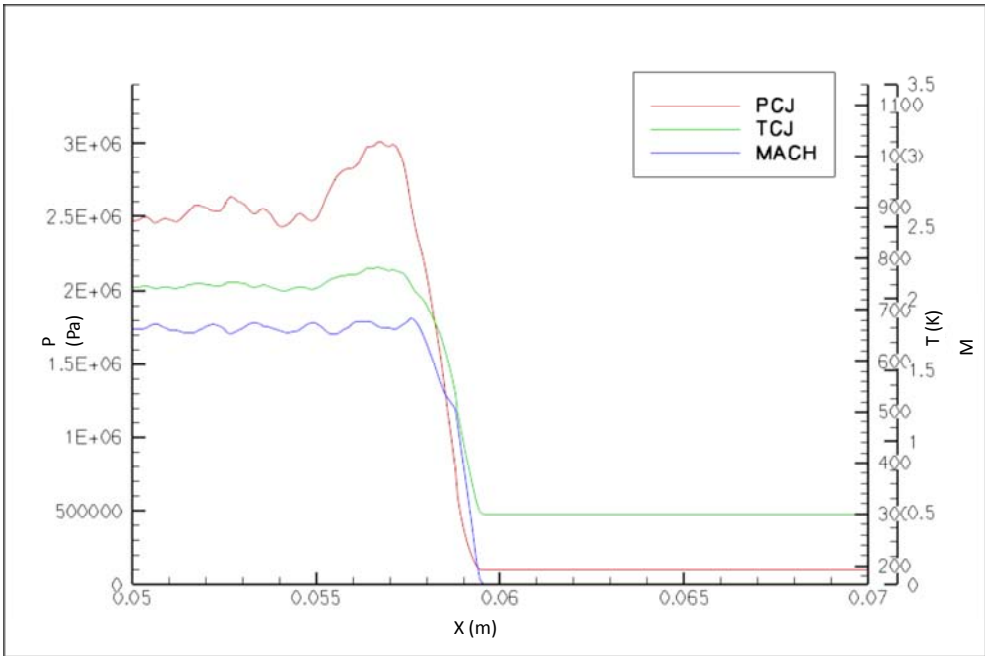

Figure 30. Pressure, temperature and Mach number profile for global CF of 1e16 at 7.31e9 sec

It was observed that the local number CFL number of 1 was able to reliably reproduce detonation waves. Setting a high global CFL number did not affect the computation. However, the CJ conditions were not reproduced.

For global CFL of 1e15 (Figure 28), the measurements achieved were:

- Pressure: 3 MPa
- Temperature: 800 K
- Average shock velocity: 6.38e-12 m/s

Whereas for a global CFL of 1e16 (Figure 29), the measurements achieved were:

- Pressure: 3.1 MPa
- Temperature: 790 K
- Average shock velocity: 5.73e-12 m/s

It might be due to the one step chemical reactions which might have been over-simplified to reach the CJ conditions, since the difference in the number of integration steps did not have any effects on the one-step chemical reaction.

The subsequent iterations were employed to investigate a 2 step chemical reaction with a CFL number of 1. The time integration schemes adopted were an explicit 2nd order Runge-kutta scheme and point implicit scheme. The dissipation function had been switched to aggressive mode. From Figure 31 and 33, there was no detonation wave structure observed in the flow field. The measurements for the explicit scheme (Figure 32) were:

- Pressure: 2.2 MPa
- Temperature: 250 K
- Average shock velocity: 6 km/s

Whereas the measurements for the implicit scheme (Figure 34) were:

- Pressure: 1.8 MPa
- Temperature: 1,100 K
- Average shock velocity: 6.515 km/s

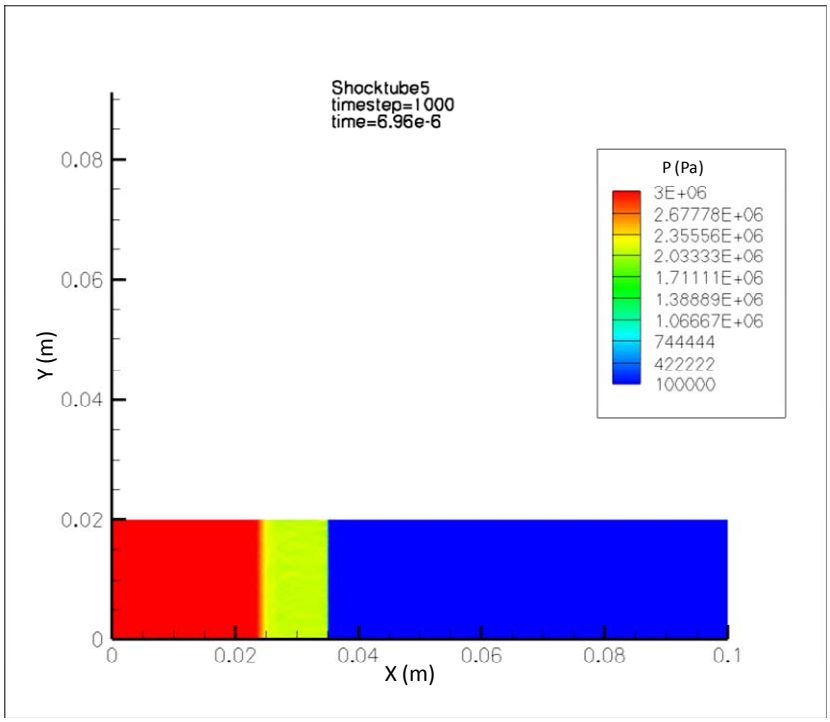

Figure 31. Pressure contour for explicit 2nd order Runge-kutta scheme at 6.96 μs

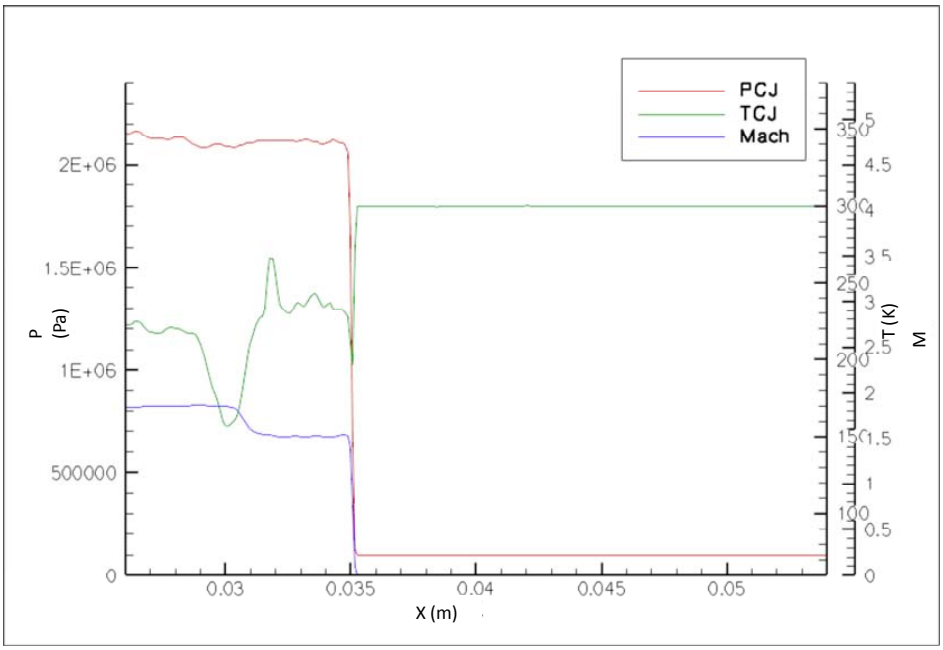

Figure 32. Pressure, temperature and Mach number profile for explicit 2nd order Runge-kutta scheme at 6.96 μs

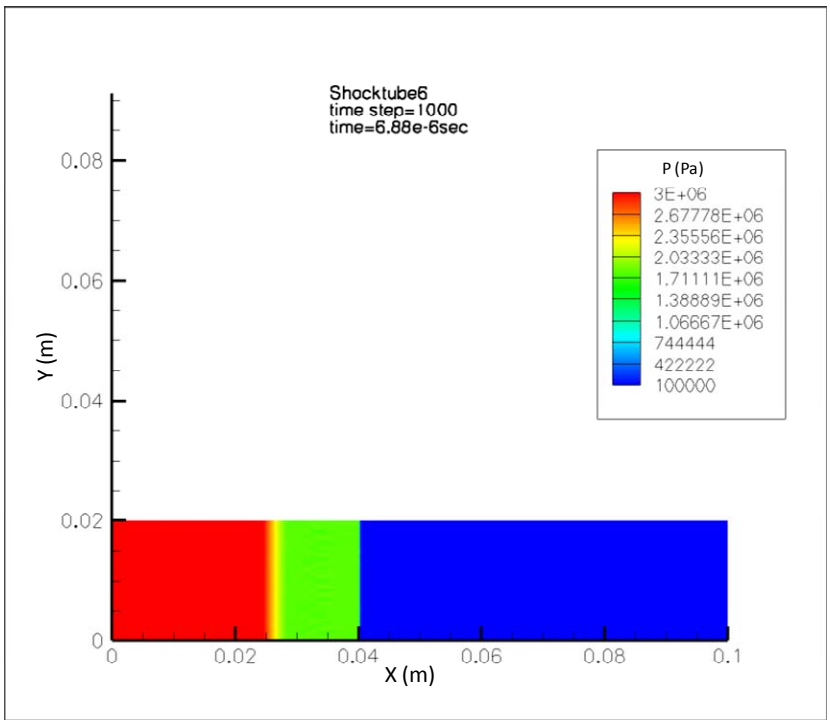

Figure 33. Pressure contour for point implicit scheme at 6.88 μs

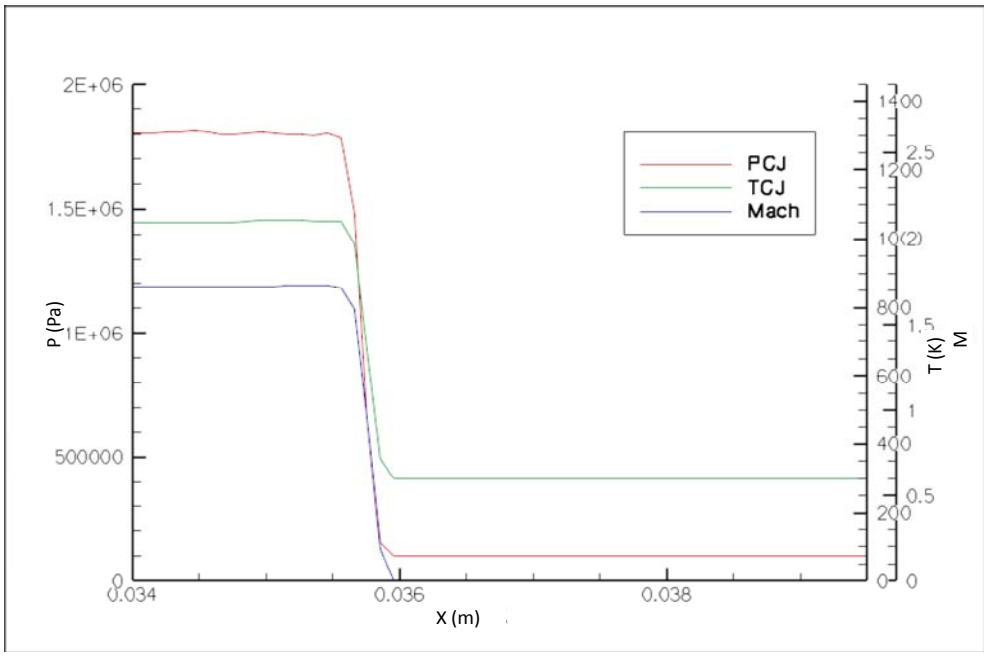

Figure 34. Pressure, temperature and Mach number profile for point implicit scheme at 6.88 μs

There were two possible reasons why there was no detonation: (1) the choice of the two step reactions was not suitable for detonation and (2) the mesh cell size might be too coarse. Hence, the cell size was reduced to 0.05mm. From Figure 35, we observed that the next simulation also did not achieve detonation. The measurements for the implicit scheme (Figure 36) were:

- Pressure: 3.1 MPa
- Temperature: 3,800 K
- Average shock velocity: 2.255 km/s

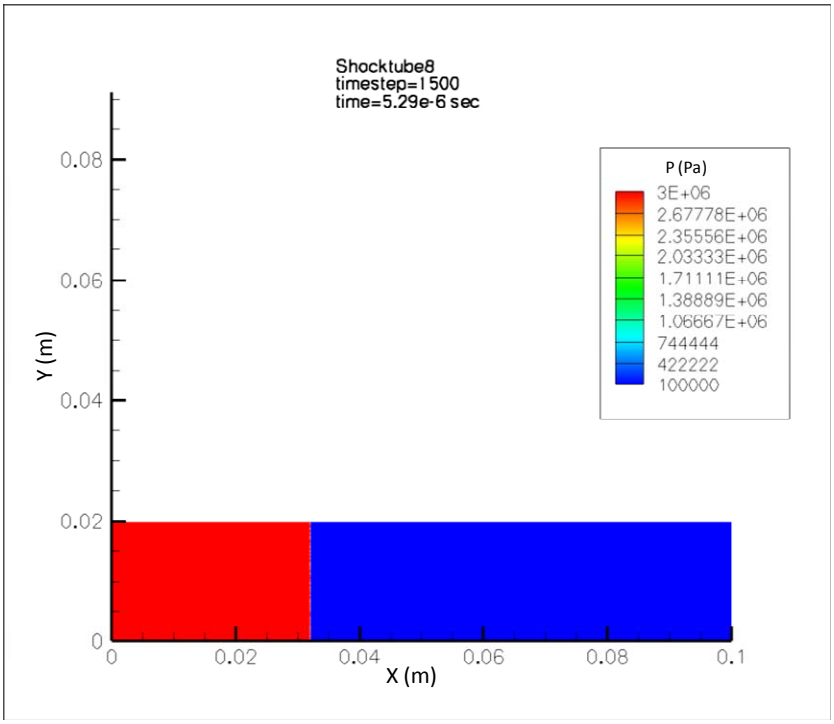

Figure 35. Pressure contour for point implicit scheme with reduced mesh size of 0.05 mm at 5.29 μs

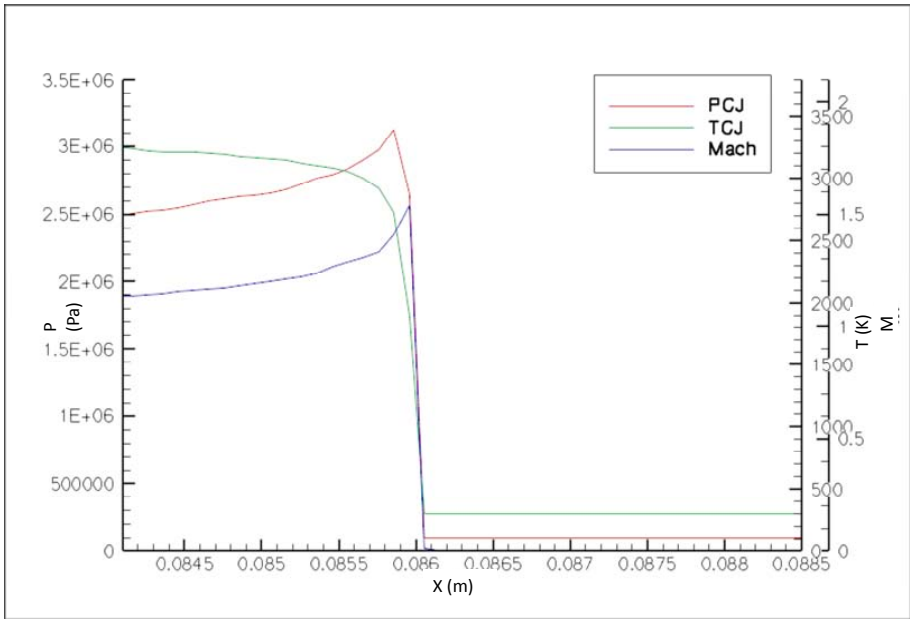

Figure 36. Pressure, temperature and Mach number profile for point implicit scheme with reduced mesh size of 0.05 mm at 5.29 μs

Since detonation was still not achieved using the 2 step chemical reaction, 9 species 18 step chemical reactions would be able to provide sufficient fidelity. The next simulations used a reduced unstructured mesh size of 0.05 mm. For Figure 37, a detonation wave was observed. However, the gasdynamic parameters were not at CJ conditions. The measurements for were:

- Pressure: 3.1 MPa
- Temperature: 2,600 K
- Average shock velocity: 2.234 km/s

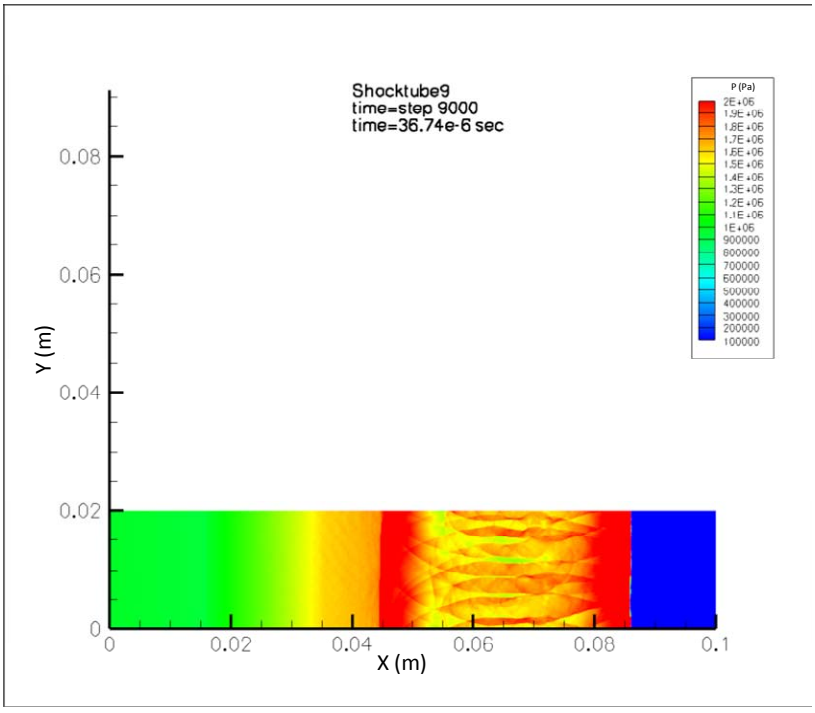

Figure 37. Pressure contour for point implicit scheme with 9 species 18 step chemical reaction at 36.74 μs

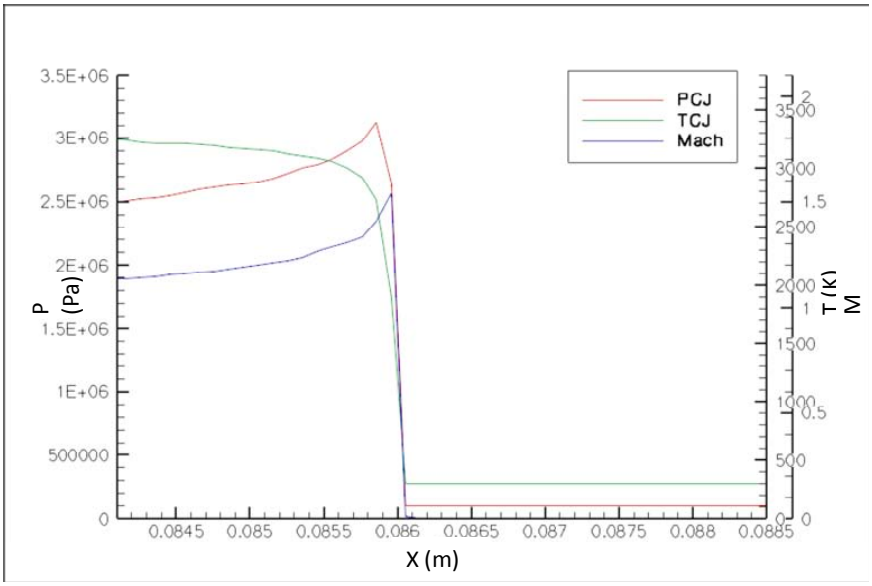

Figure 38. Pressure, temperature and Mach number profile for point implicit scheme with 9 species 18 step chemical reaction at 36.74 μs

To further refine the simulation, structured mesh topology was explored. Both explicit 4th order Runge-kutta scheme and point implicit scheme were investigated. It could be observed that the explicit 4th order Runge-kutta scheme produced the CJ conditions for the detonation wave. The measurements were as follows:

From Figure 40, the point implicit scheme produced:

- Pressure: 2 MPa
- Temperature: 2,722 K
- Average shock velocity: 2.077 km/s

From Figure 42, the explicit scheme produced:

- Pressure: 1.8 MPa
- Temperature: 2,868 K
- Average shock velocity: 1.971 km/s

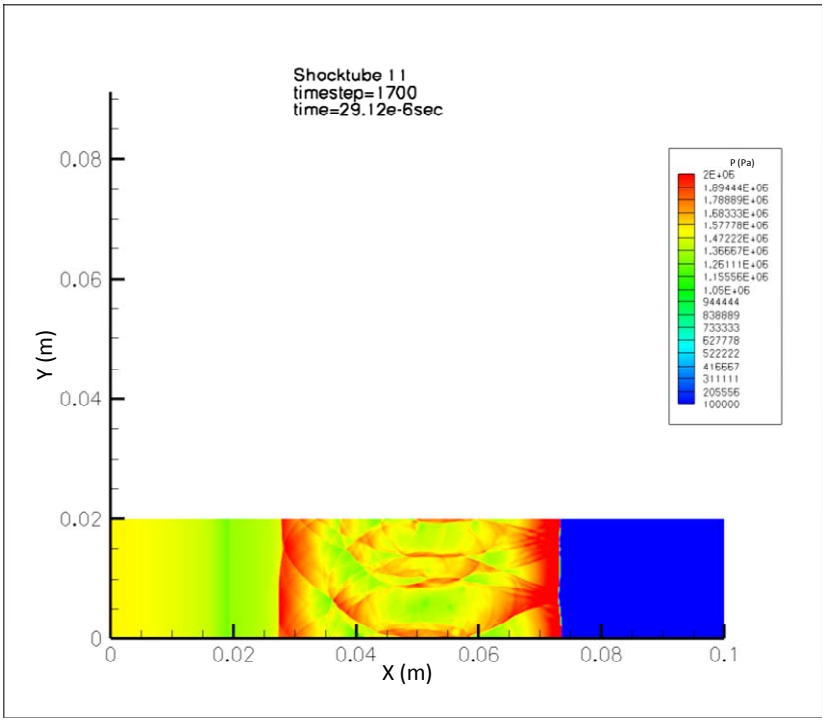

Figure 39. Pressure contour for point implicit scheme with 9 species 18 step chemical reaction (structured mesh topology) at 29.12 μs

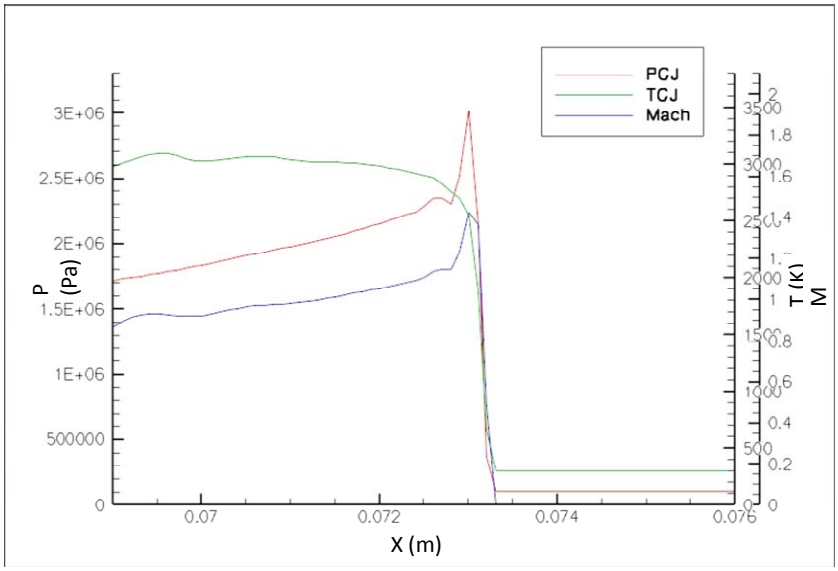

Figure 40. Pressure, temperature and Mach number profile for point implicit scheme with 9 species 18 step chemical reaction (structured mesh topology) at 29.12 μs

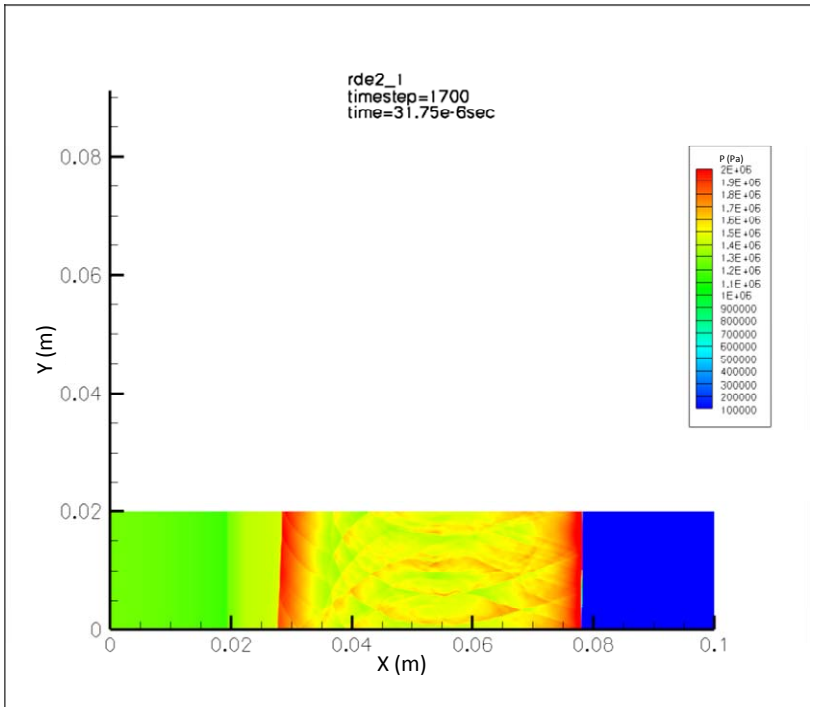

Figure 41. Pressure contour for explicit 4th order Runge-kutta scheme with 9 species 18 step chemical reaction (structured mesh topology) at 31.75 μs

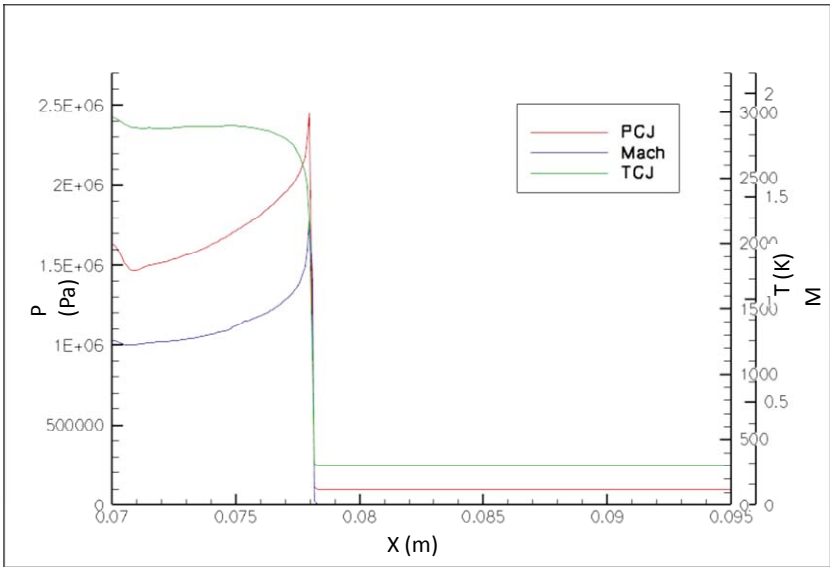

Figure 42. Pressure, temperature and Mach number profile for explicit 4th order Runge-kutta scheme with 9 species 18 step chemical reaction (structured mesh topology) at 31.75 μs

The CJ conditions have been reliability reproduced using the explicit 4th order Runge-kutta scheme with 9 species 18 step reactions (structured mesh topology). Table 5 summarized the results obtain from the various iterations.

Table 5. Summary of results to produce CJ conditions

Simulation	V_{CJ} (m/s)	T_{CJ} (K)	P_{CJ} (MPa)
CJ Conditions	1,964.8	2,942	1.58
Figure 27-shocktube2	6.38e-12	800	3.0
Figure 29-shocktube4	5.73e12	790	3.1
Figure 31-shocktube6	6,000	250	2.2
Figure 33-shocktube7	6,515	1,100	1.8
Figure 35-shocktube8	2,255	3,800	3.1
Figure 37-shocktube9	2,234	2,600	3.1
Figure 39-shocktube11	2,077	2,722	2.0
Figure 41-rde2_1	1,971	2,868	1.8

C. CJ CONDITIONS FOR DIFFERENT FUEL-AIR RATIOS

To further confirm the accuracy of the implicit and explicit integration scheme, simulations using different fuel-air ratios were conducted. The results were summarized in Table 6. It could be observed that explicit 4th order Runge-kutta scheme was more accurate. The various pressure profiles at the same time step were shown in Figure 36 to 39.

Table 6. Comparison with CJ conditions

ϕ	Scheme	V_{CJ} (m/s)	T_{CJ} (K)	P_{CJ} (MPa)
1	Theory	1,964.8	2,942	1.58
1	Implicit	2,077	2,722	2.0
1	Explicit	1,971	2,868	1.8
0.7	Theory	1,788	2,598	13.9
0.7	Implicit	2,065	3,003	3.6
0.7	Explicit	1,817	2,557	1.8
2.2	Theory	2,165	2,655	14.2
2.2	Implicit	2,609	3,086	1.8
2.2	Explicit	2,206	2,674	2.2

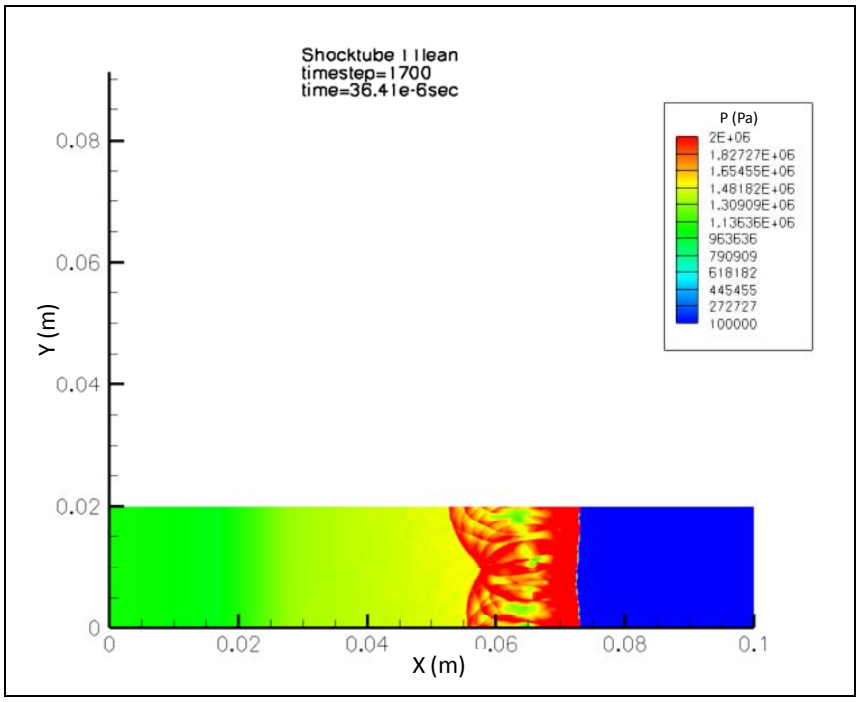

Figure 43. Pressure contour for fuel lean point implicit scheme at 36.41 μs

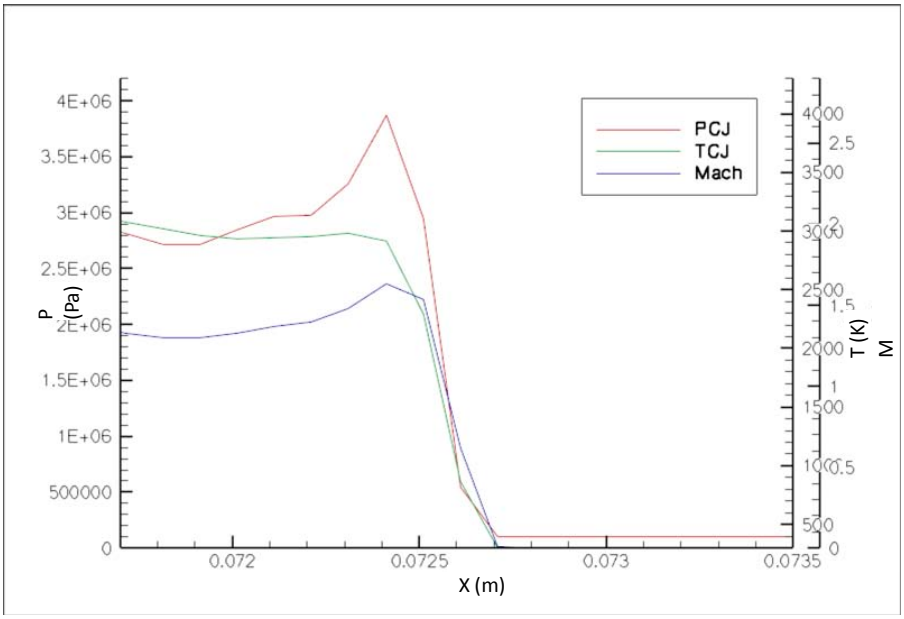

Figure 44. Pressure, temperature and Mach number profile for fuel lean point implicit scheme at 36.41 μs

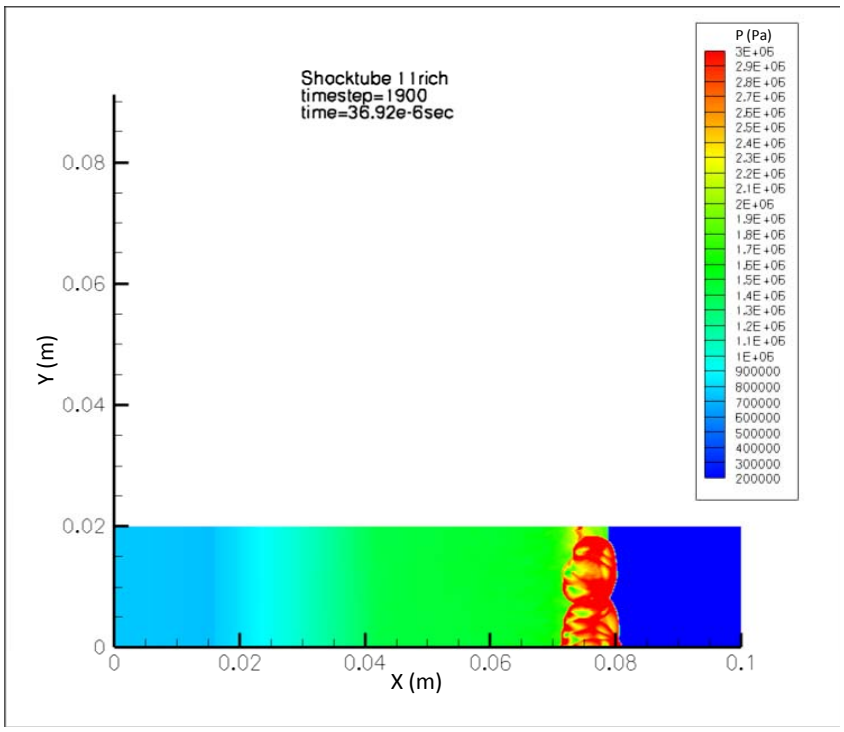

Figure 45. Pressure contour for fuel rich point implicit scheme at 36.92 μs

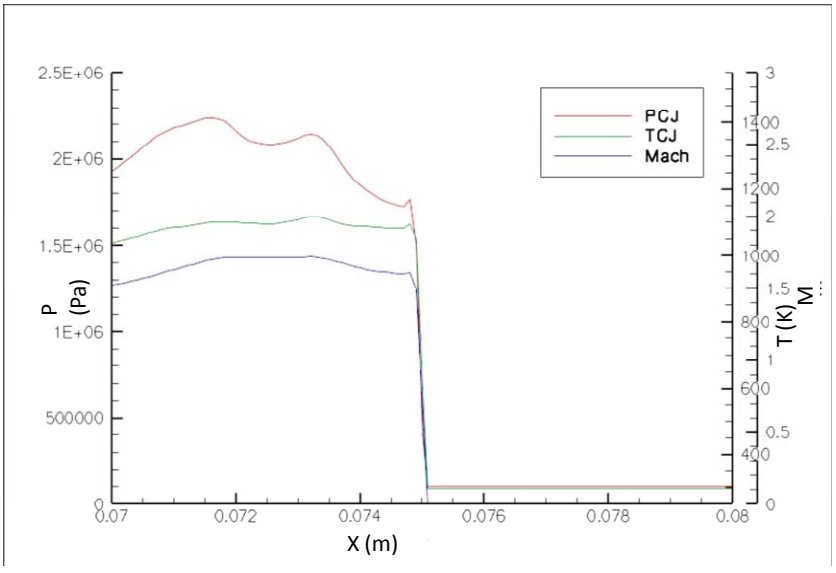

Figure 46. Pressure, temperature and Mach number profile for fuel rich point implicit scheme at 36.92 μs

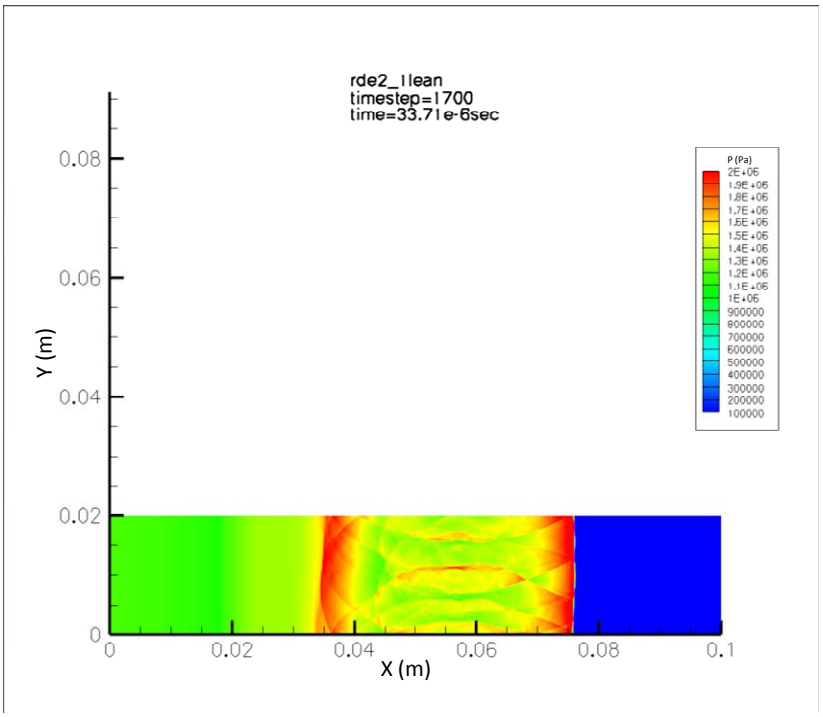

Figure 47. Pressure contour for fuel lean explicit scheme at 31.75 μs

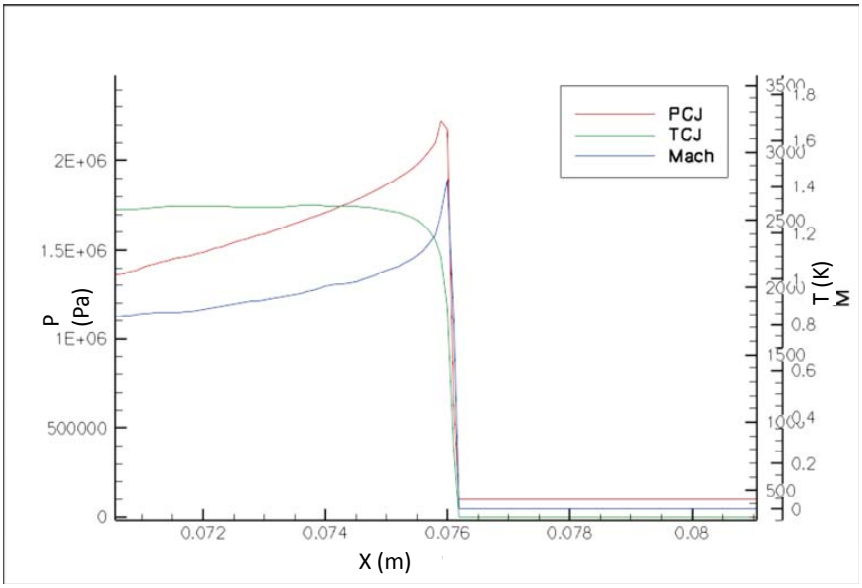

Figure 48. Pressure, temperature and Mach number profile for fuel lean explicit scheme at 31.75 μs

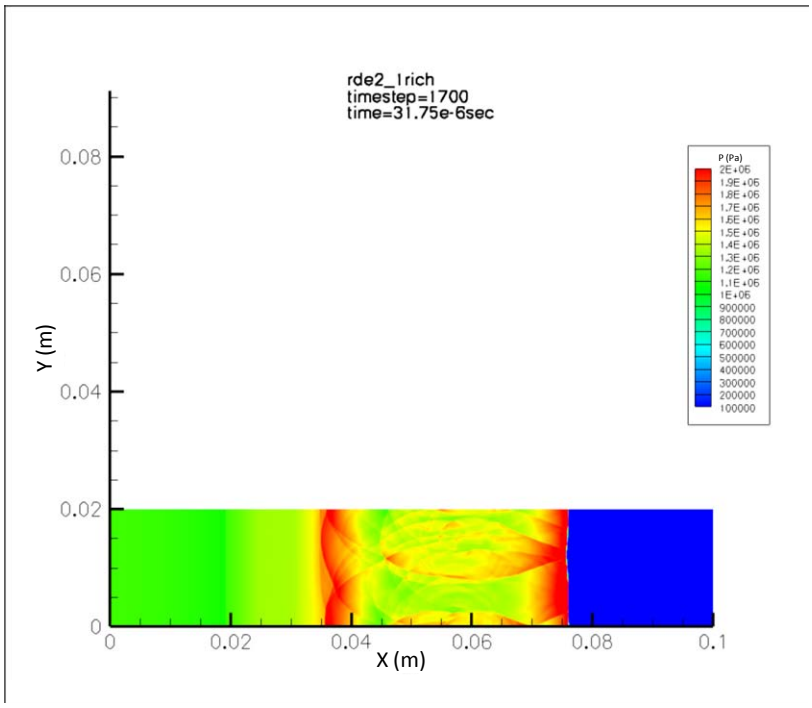

Figure 49. Pressure contour for fuel rich explicit scheme at 31.75 μs

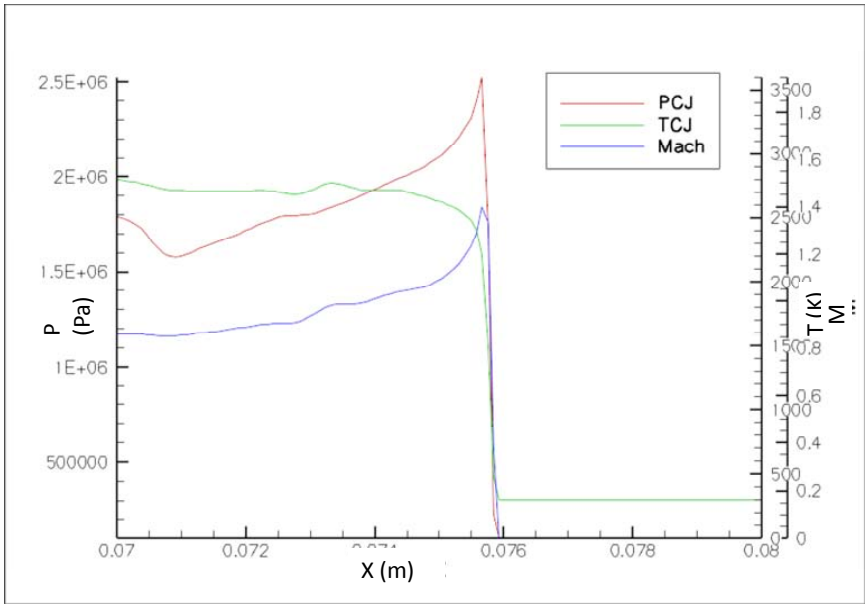

Figure 50. Pressure, temperature and Mach number profile for fuel rich explicit scheme at 31.75 μs

D. PERIODIC BOUNDARY SIMULATIONS

For the periodic boundary, there was a need to apply an offset of 0.44 m for each of the boundary in order for the detonation wave to flow through continuously. Again, several iterations were conducted before able to simulate the 2D cyclic domain. Figures 51 to 53 showed the shock wave successfully flowed through the boundary.

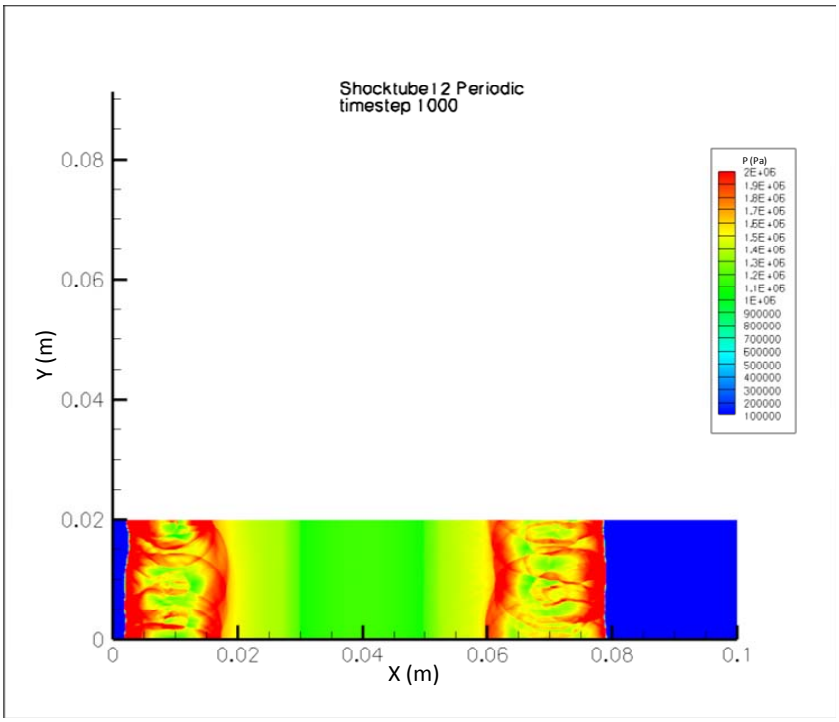

Figure 51. Pressure contour for periodic boundary simulation at timestep 1,000

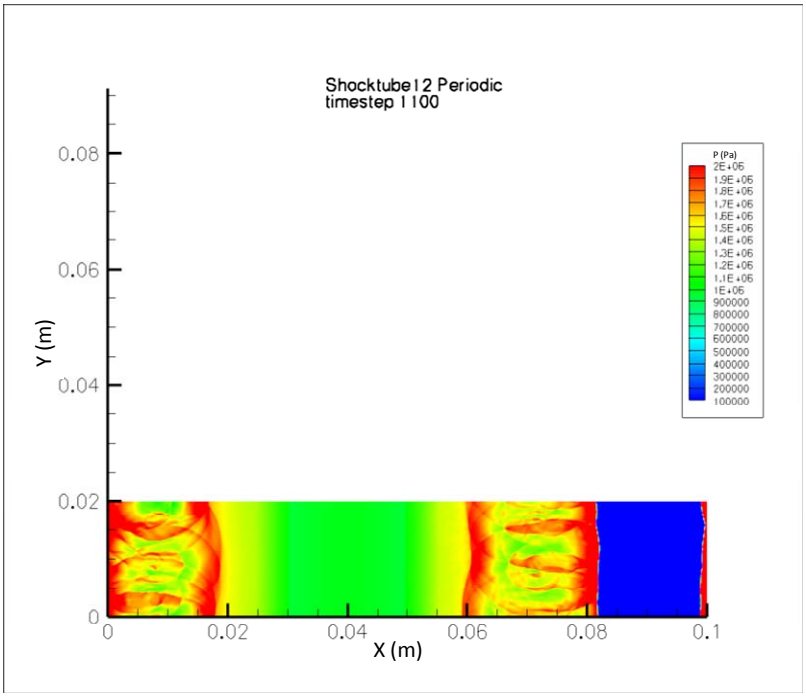

Figure 52. Pressure contour for periodic boundary simulation at timestep 1,100

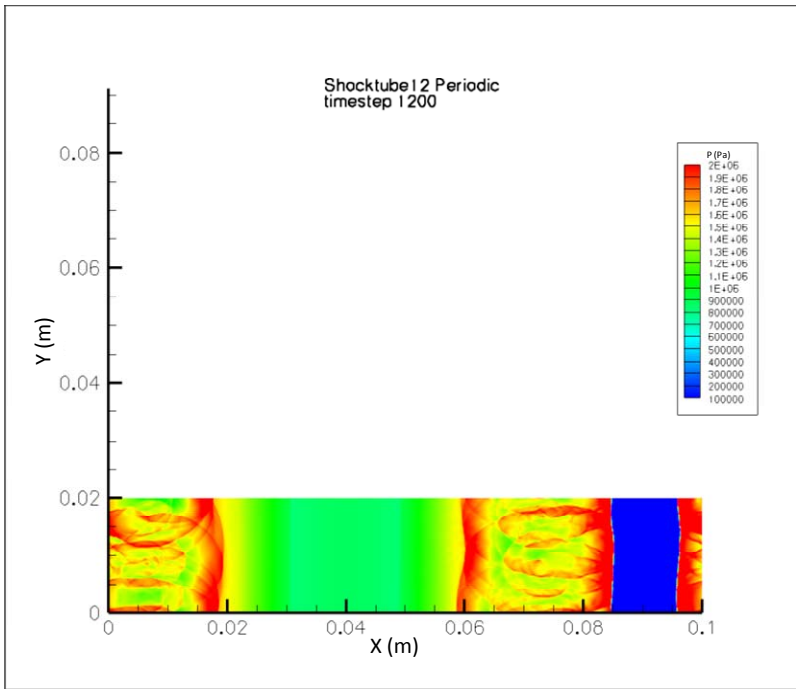

Figure 53. Pressure contour for periodic boundary simulation at timestep 1,200

E. FULL RDE SIMULATIONS ANALYSIS

The analysis of the inlet gasdynamic consists of four main phases of the simulation, namely the ignition, flow through periodic boundary, the second RDE cycle and third RDE cycle. For each of the phases, the flow field, gasdynamic parameters such as pressure, temperature, Mach number, velocity, density and mass flow rate were analysed. The data were extracted from a horizontal line along the inlet axis (x-axis).

1. Ignition Phase

A 1 mm x 10 mm high-pressure region which represents the igniter was inserted at the bottom left corner of the domain as shown in Figure 55. Once the simulation commenced, a detonation wave was generated and propagate towards the right at an average velocity of 1.8 km/s. The flow field for temperature and pressure was shown in Figure 54.

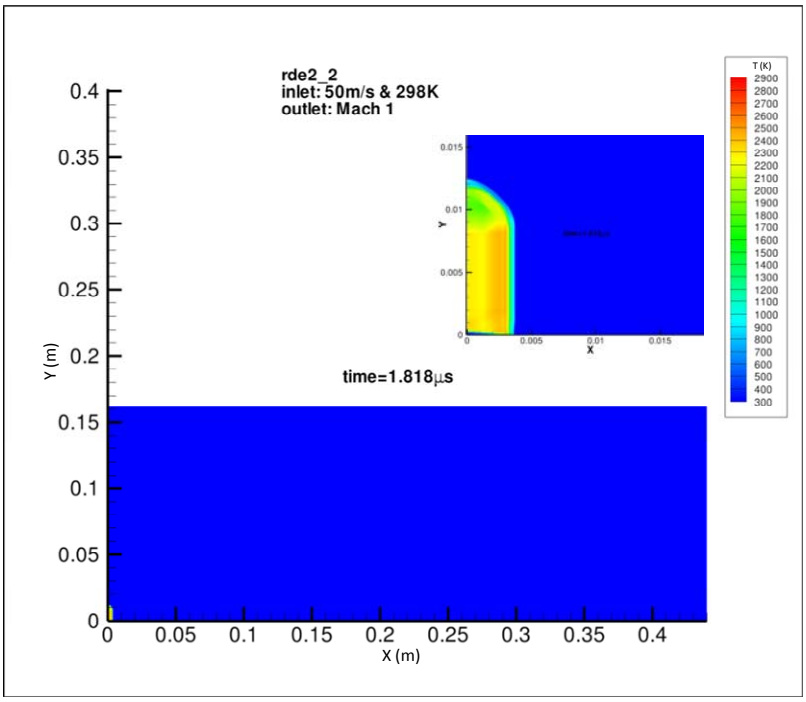

Figure 54. Temperature contour for ignition phase at 1.818 μs

Once the high-pressure region began to expand, a shock wave propagated into the pre-injected Hydrogen-Air mixture and detonation occurred. Since there was no Hydrogen-Air mixture above the igniter, a shock wave was generated and propagated towards the outlet. The shockwave propagated in an oblique direction due to the forward movement of the detonation wave. Figure 55 showed the initial development of the flow field from 1.818 μs to 10.757 μs .

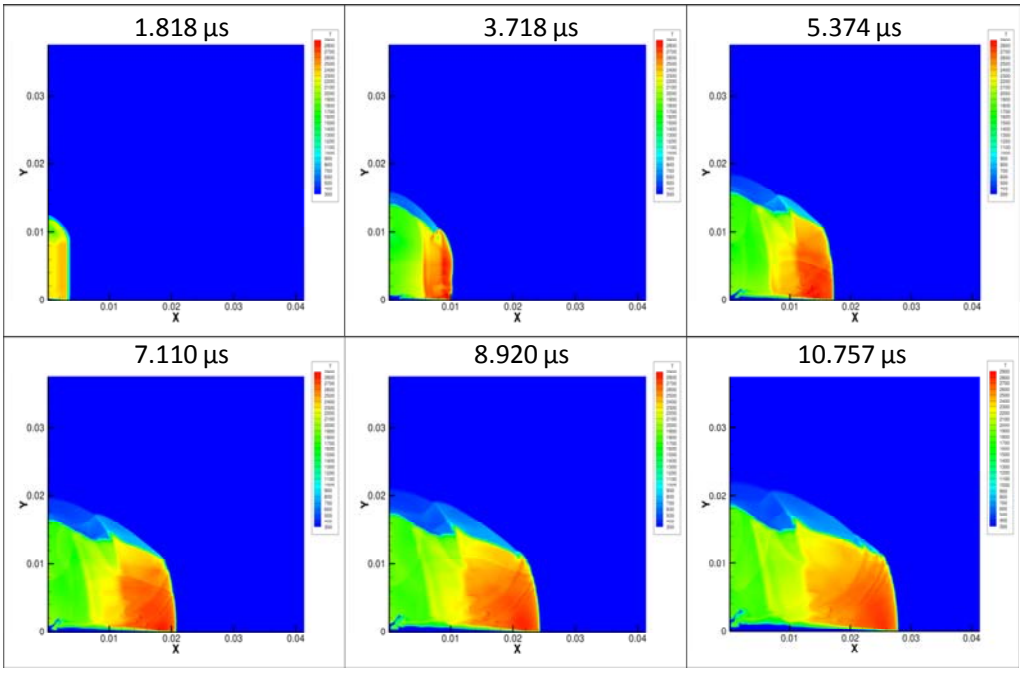

Figure 55. Flow field structure of ignition phase from 1.818 μs

As the transverse wave interacted with the denotation shock front, the “fish scale” structure was formed around 54.447 μs as shown in Figures 56 and 57. The cell dimension measured was 3 mm. From Figure 58, it could be observed that the pressure, temperature and Mach number increased after the detonation front as expected. The rotating detonation wave produced the following:

- Pressure: 1.93 MPa
- Temperature: 2,338.52 K
- Average shock velocity: 1.829 km/s

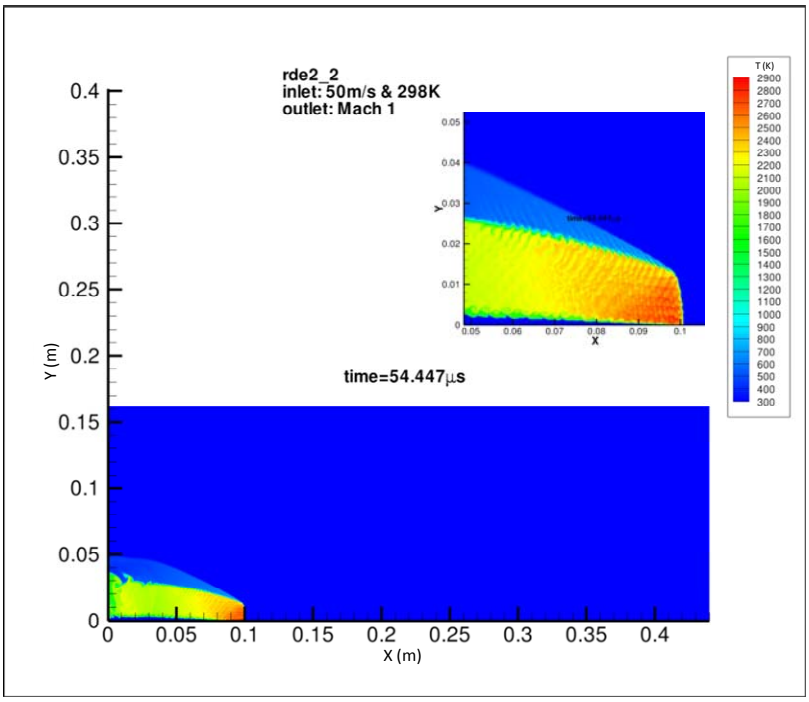

Figure 56. Temperature contour for ignition phase at 54.447 μs

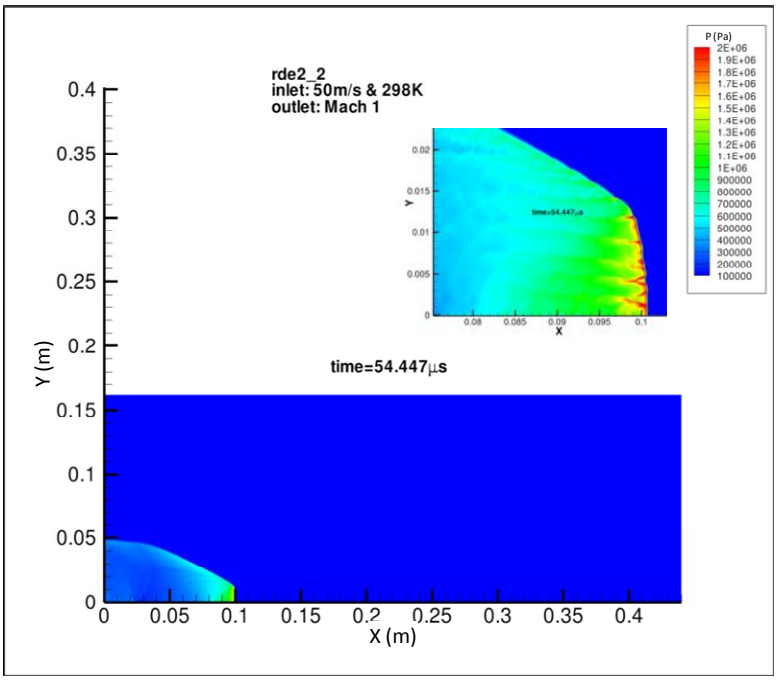

Figure 57. Pressure contour for ignition phase at 54.447 μs

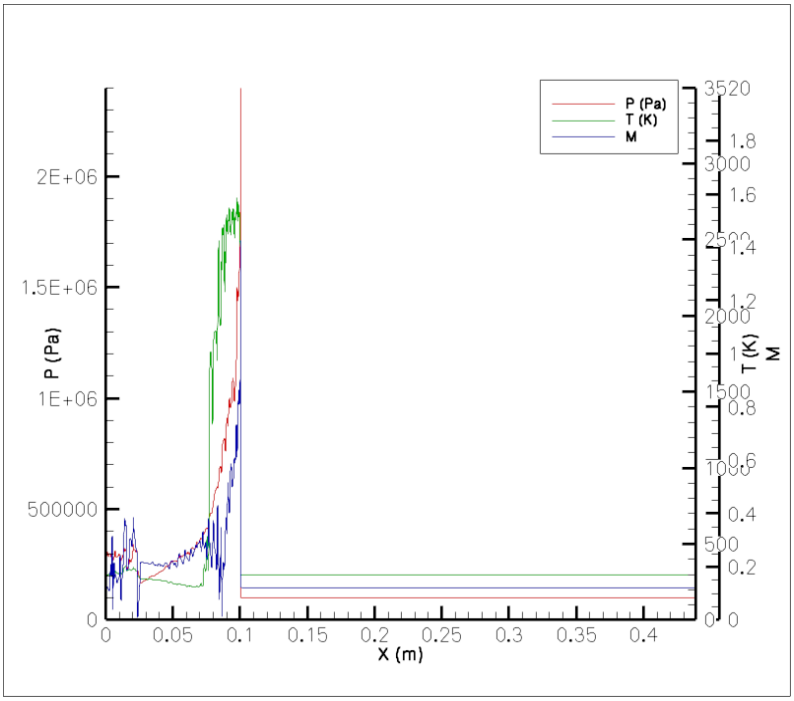

Figure 58. Pressure, temperature and Mach number profile for ignition phase at 54.77 μs

From Figure 59, the injection velocity had large fluctuation between -104.54 m/s and 313.48 m/s just behind the detonation front. For the inlet density, it was relatively low at 0.75 kg/m^3 at the detonation front and increased immediately after the detonation front to 4.27 kg/m^3. In addition, the mass flow rate at the combustor inlet large fluctuated between -234.99 kg/s and 934.46 kg/s. After the detonation shock front, the mass flow rate fluctuated around 100 kg/s.

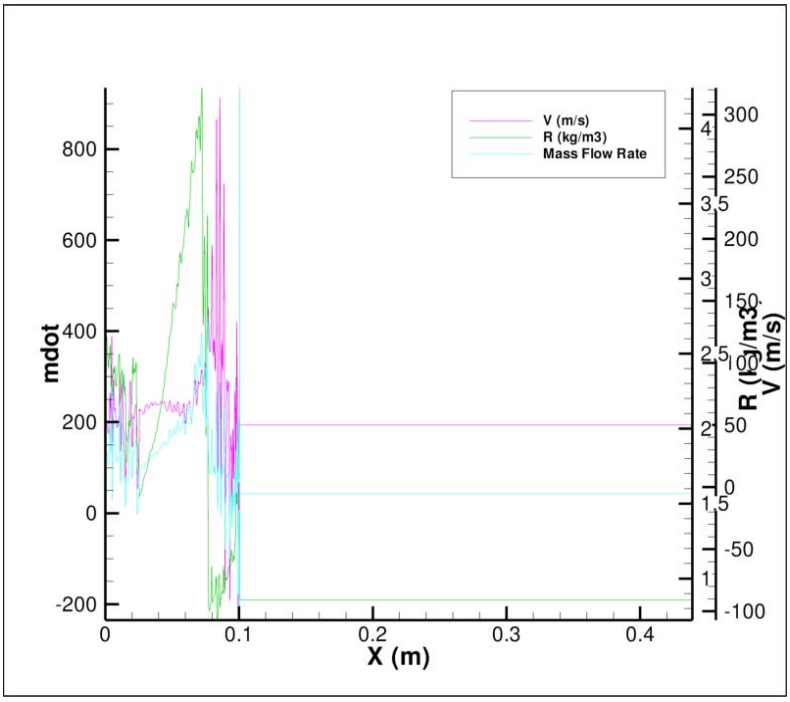

Figure 59. Inlet velocity and density profile for ignition phase at 54.77 μs

2. Flow Through Periodic Boundary

At 213.31 μs, the simulation was paused and both the left and right boundaries were changed to periodic boundaries. Figure 60 and 61 showed the temperature and pressure profile of the denotation wave just before it reached the periodic boundary. From Figure 63, the rotating detonation wave produced the following:

- Pressure: 1.725 MPa
- Temperature: 2,598 K
- Average shock velocity: 1.88 km/s

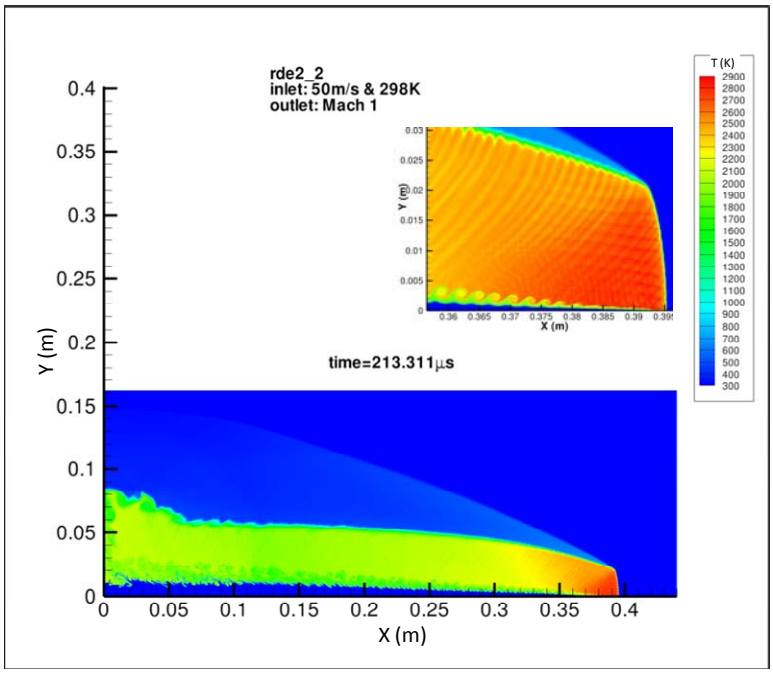

Figure 60. Temperature contour for flow through periodic boundary at 213.31 μs

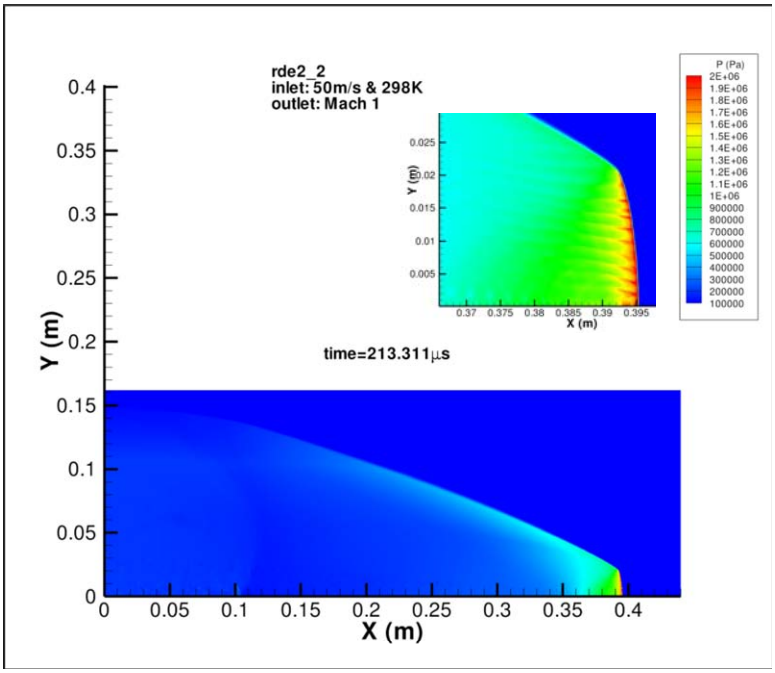

Figure 61. Pressure contour for flow through periodic boundary at 213.31 μs

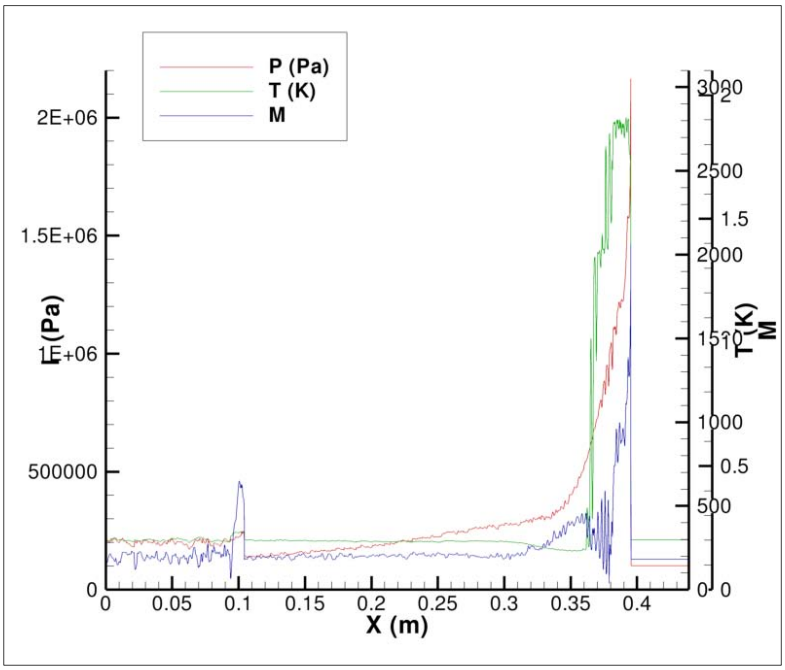

Figure 62. Pressure, temperature and Mach number profile for flow through periodic boundary at 213.31 μs

From Figure 63, the injection velocity and mass flow rate continued to have large huge fluctuations. The injection velocity varied between -46.45 m/s and 309.62 m/s whereas the mass flow rate varied between -51.68 kg/s and 376.94 kg/s. For the inlet density, it maintained the profile where it was relatively low at 0.38 kg/m^3 at the detonation front and increased immediately after the detonation front to 5.78 kg/m^3. One interesting observation was that pressure, density, injection velocity and mass flow had a sharp increase in magnitude at 0.10 m, which was downstream of the detonation wave. A closer examination of the flow field using Figure 64 showed that the expansion waves from the detonation front hit the freshly injected Hydrogen-Air mixture and was reflected into a shockwave since the Hydrogen-Air mixture had high impedance.

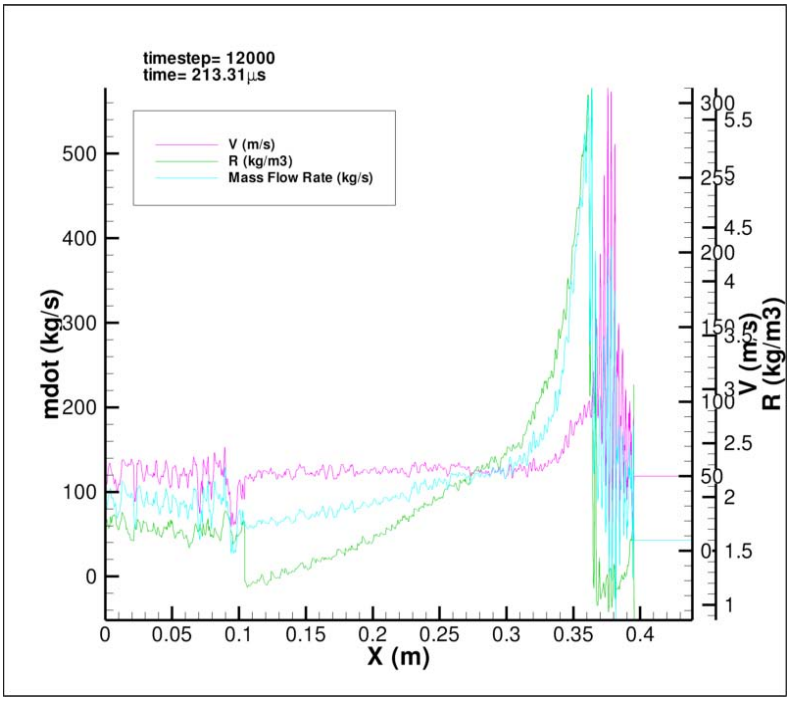

Figure 63. Inlet velocity and density profile for flow through periodic boundary at 213.31 μs

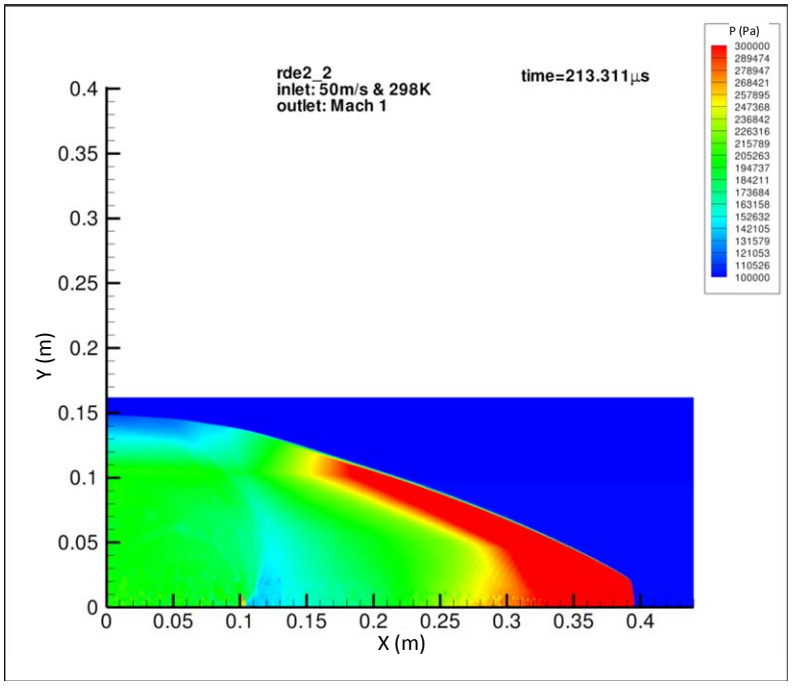

Figure 64. Pressure contour for flow through periodic boundary with lower maximum pressure range at 213.31 μs

Once the simulation restarted, the products from the left boundary flow into the domain via the right boundary as shown in Figures 66 and 67. The height of the detonation wave front was 0.026 m. In addition, the height of the freshly injected Hydrogen-air mixture was measured and plotted in Figure 67. It could be observed that the height increased linearly from the detonation until 0.25 m away from the detonation front.

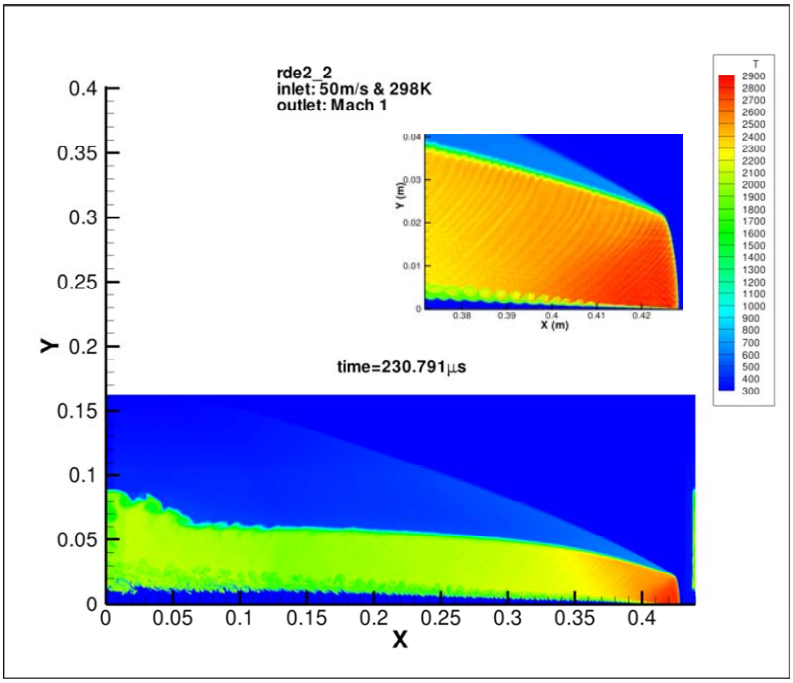

Figure 65. Temperature contour for flow through periodic boundary at 230.79 μs

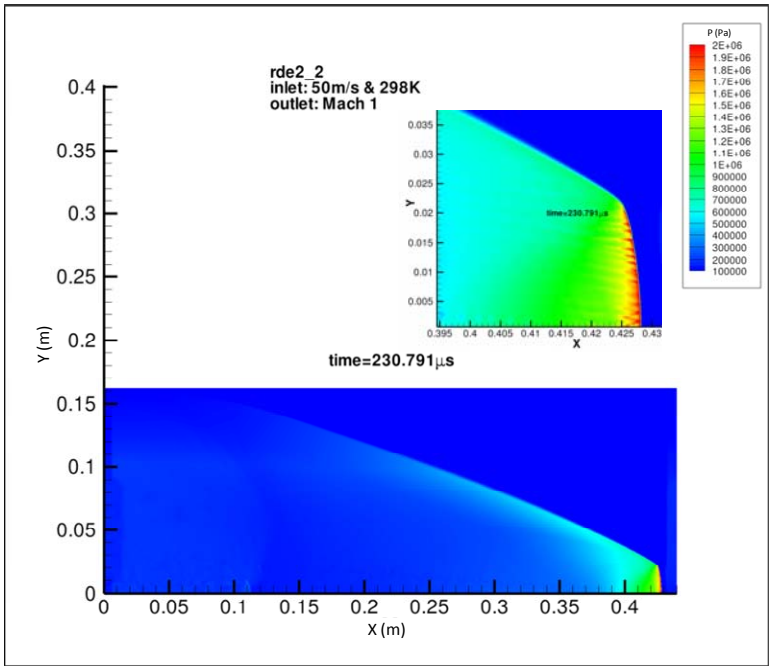

Figure 66. Pressure contour for flow through periodic boundary at 230.79 μs

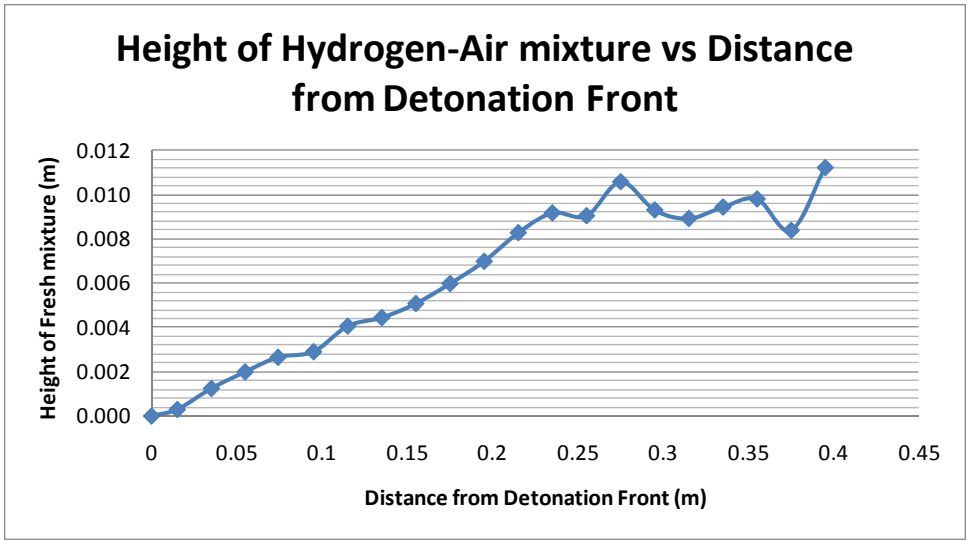

Figure 67. Height variation of Hydrogen-Air mixture from detonation front at 230.79 μs

Due to the discontinuities in density, the denotation wave that re-entered the domain mixed the freshly injected Hydrogen-Air mixture and the burn products. This resulted in a second denotation. Figure 68 showed the flow field of mixing detonation wave.

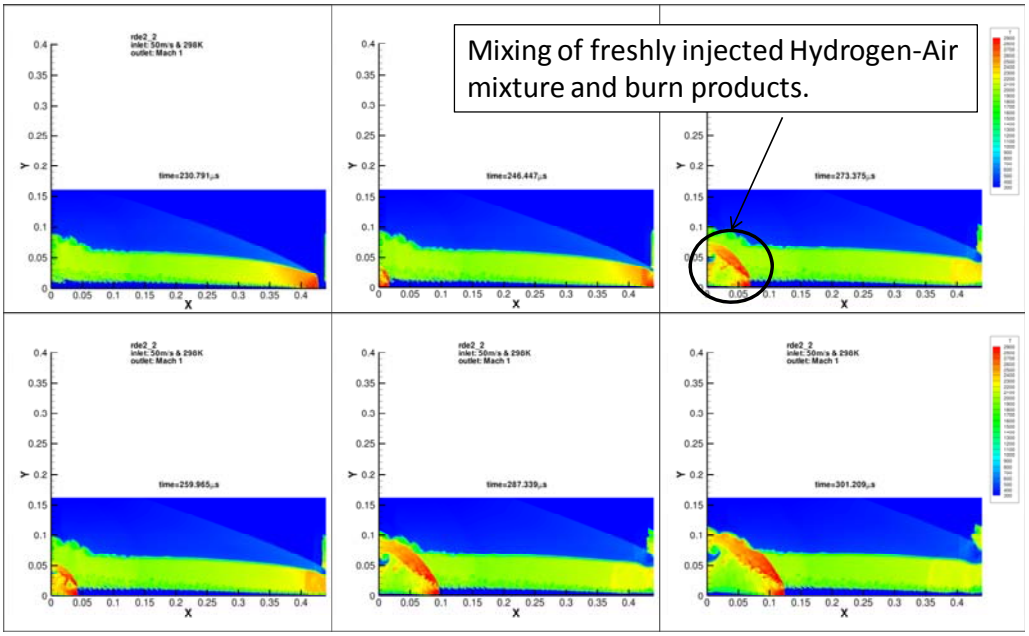

Figure 68. Flow through periodic boundary from 230.79 μs to 301.21 μs

The detonation wave profiles were shown in Figures 69 and 70. The measurements were as follows:

- Pressure: 3.54 MPa
- Temperature: 2,829.9 K
- Average shock velocity: 1.98 km/s

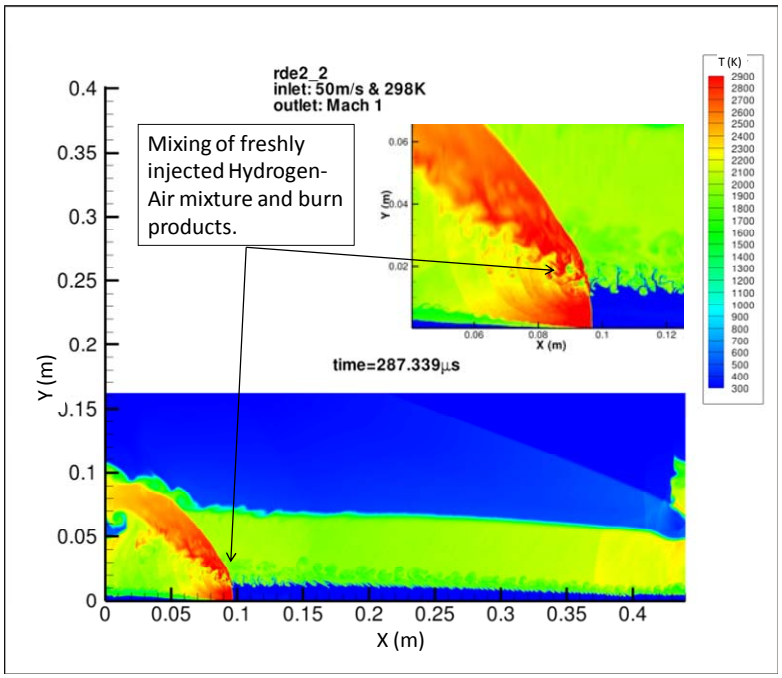

Figure 69. Temperature contour for flow through periodic boundary at 287.34 μs

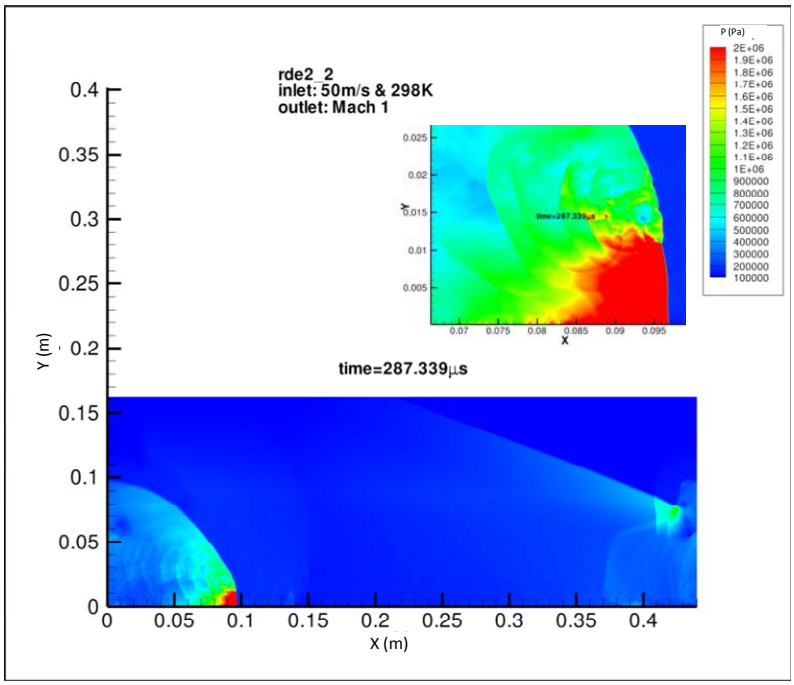

Figure 70. Pressure contour for flow through periodic boundary at 287.34 μs

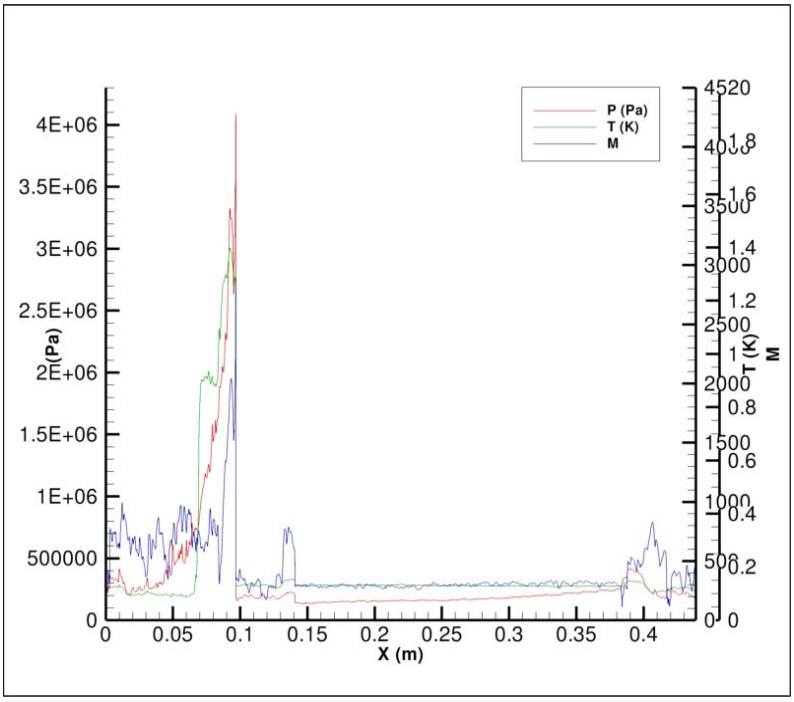

Figure 71. Pressure, temperature and Mach number profile for flow through periodic boundary at 287.34 μs

There was no back flow of the combustor inlet as injection velocity varied between 20.67 m/s and 262.65 m/s and the mass flow rate varies between 33.93 kg/s and 1000.84 kg/s. For the inlet, density varies between 1.35 kg/m^3 and 8.66 kg/m^3. These observations are illustrated in Figure 73. The expansion wave profile observed in Figure 65 is also observed in Figure 74.

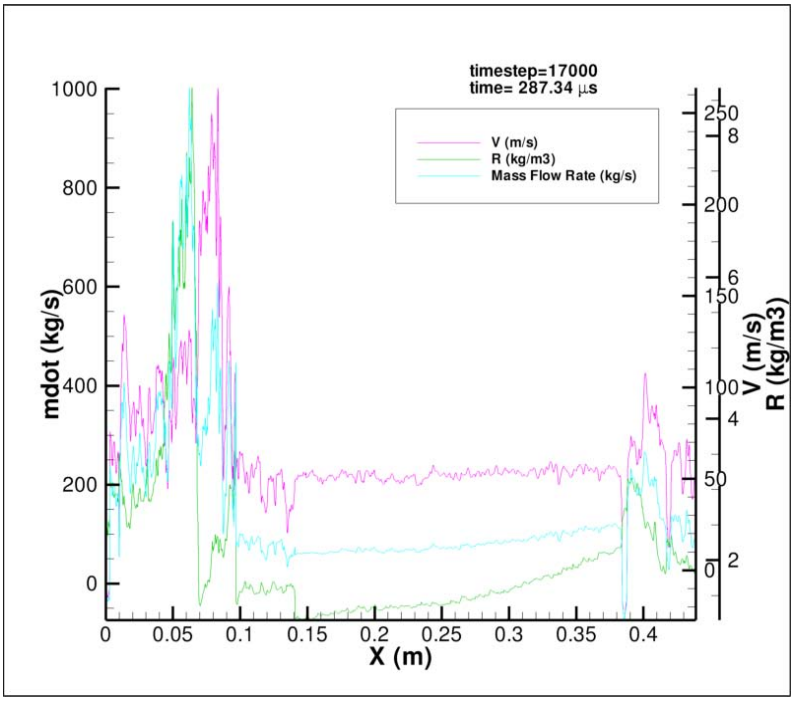

Figure 72. Inlet velocity and density profile for flow through periodic boundary at 287.34 μs

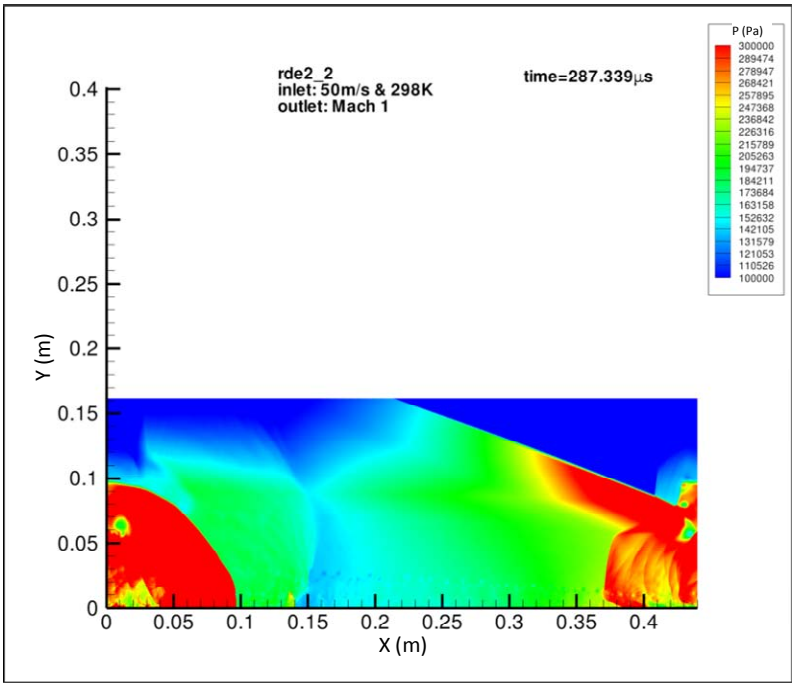

Figure 73. Pressure contour for flow through periodic boundary using lower pressure range at 287.34 μs

3. Second RDE Cycle

As the detonation continued to propagate, the combustion chamber was completely filled with products and reached a quasi-steady state. The detonation wave profiles were shown in Figures 74 and 75. The measurements were as follows:

- Pressure: 3.54 MPa
- Temperature: 2,829.9 K
- Average shock velocity: 1.98 km/s

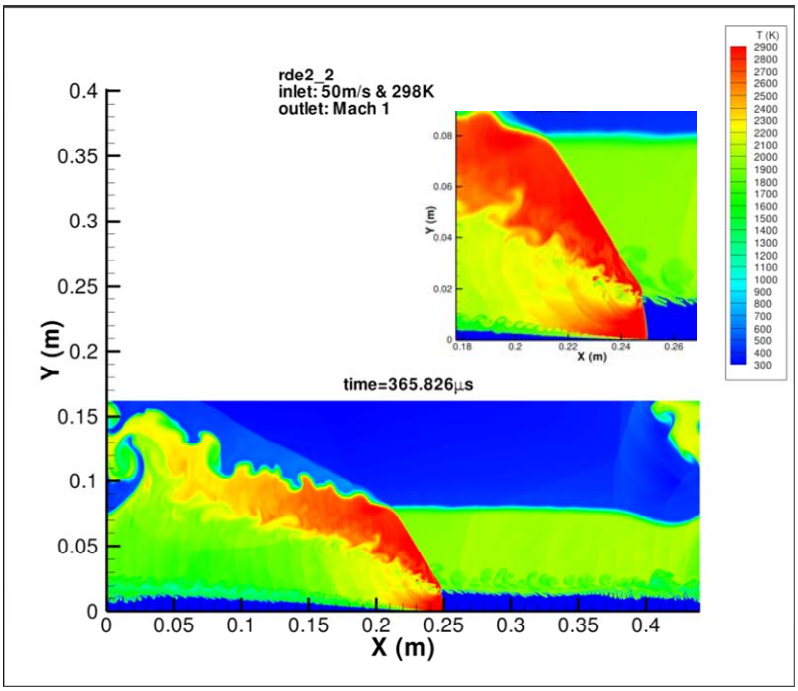

Figure 74. Temperature contour for 2nd RDE cycle simulation at 365.8 μs

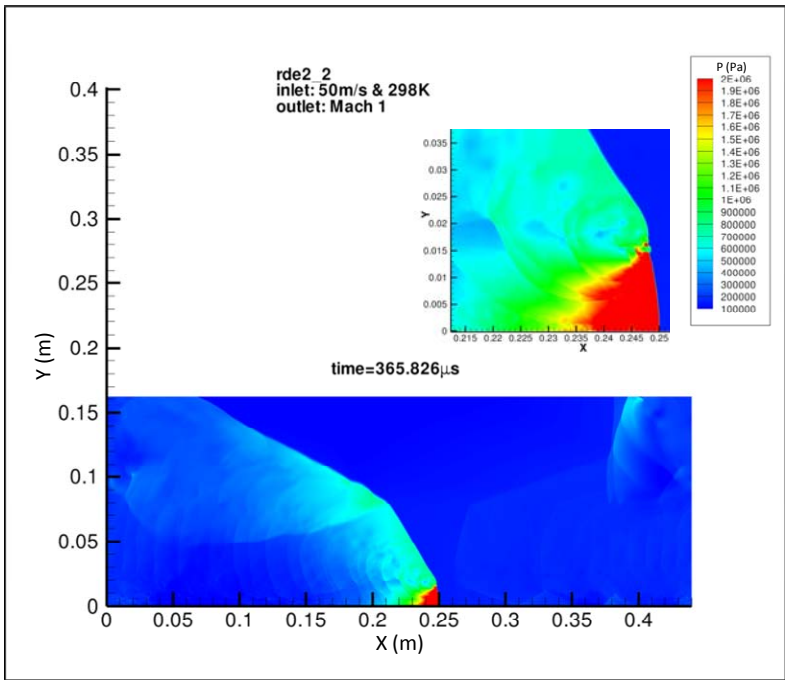

Figure 75. Pressure contour for 2nd RDE cycle simulation at 365.8 μs

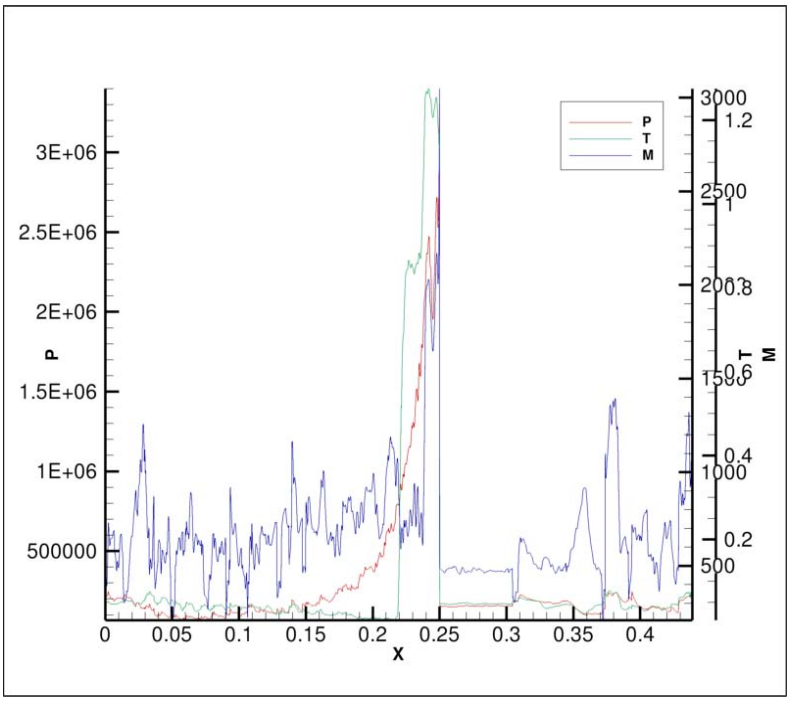

Figure 76. Pressure, temperature and Mach number profile for 2nd RDE cycle simulation at 365.8 μs

The fluctuation of the injection velocity and mass flow rate varies between -23.30 m/s and 241.91 m/s with the mass flow rate varies between -50.51 kg/s and 1117.88 kg/s. For the density varies between 1.46 kg/m^3 and 8.80 kg/m^3. These observations were illustrated in Figure 77. We could also observed that the flow field was complex with expansion waves interacting with the detonation wave as well as small pockets of high-pressure region in the combustor as shown in Figure 79.

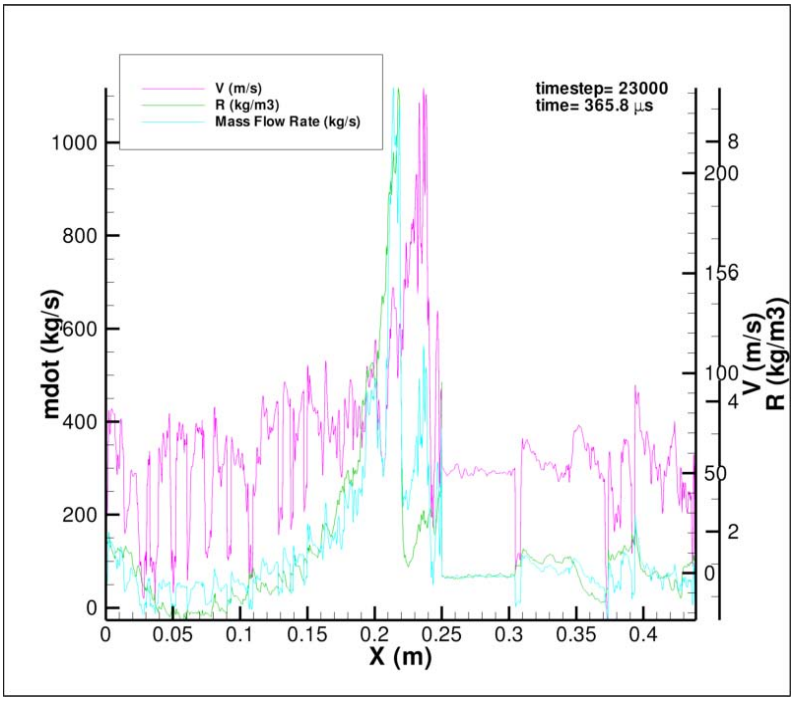

Figure 77. Inlet velocity and density profile for 2nd RDE cycle simulation at 365.8 μs

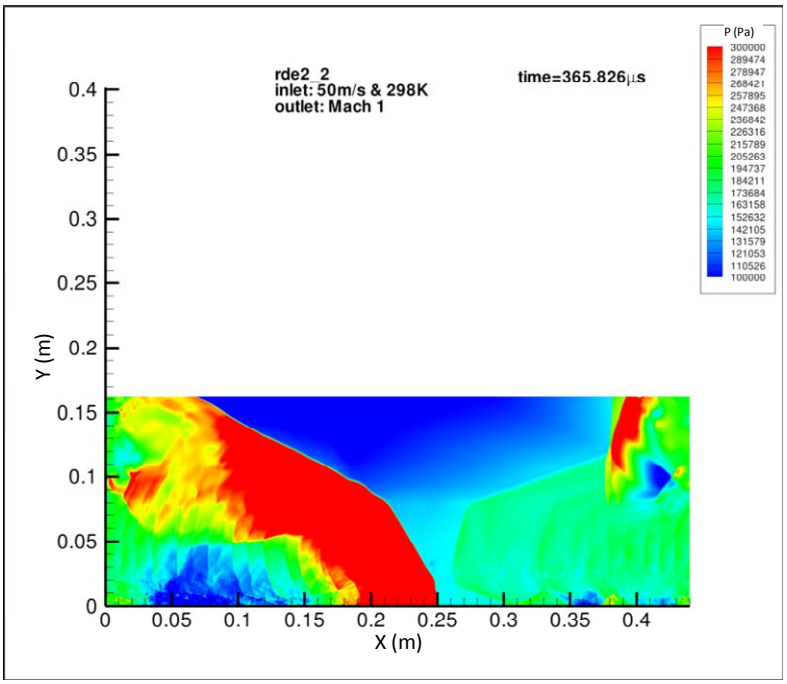

Figure 78. Pressure contour for 2nd RDE cycle simulation using lower pressure range at 365.8 μs

Although the focus of this thesis was to characterize the inlet, the gasdynamic parameters at the combustor outlet were also measured for the steady state. Figure 80 and 81 showed the various gasdynamic profiles. The measurements were as follows:

- Maximum pressure: 502 kPa
- Maximum temperature: 2,172.12 K
- Outlet axial velocity: 406.71 m/s
- Maximum mass flow rate: 261.792 m/s

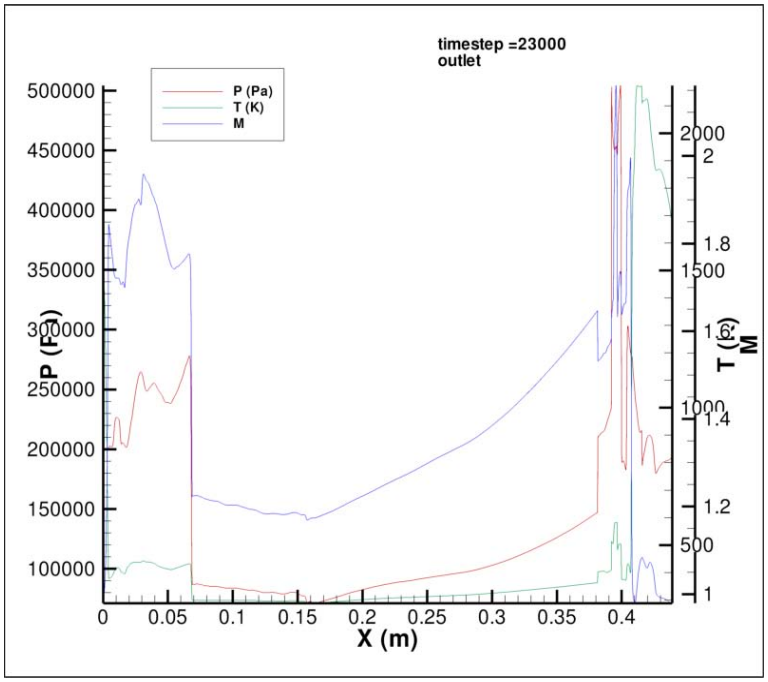

Figure 79. Pressure, temperature and Mach number profile for 2nd RDE cycle simulation (outlet) at 365.8 μs

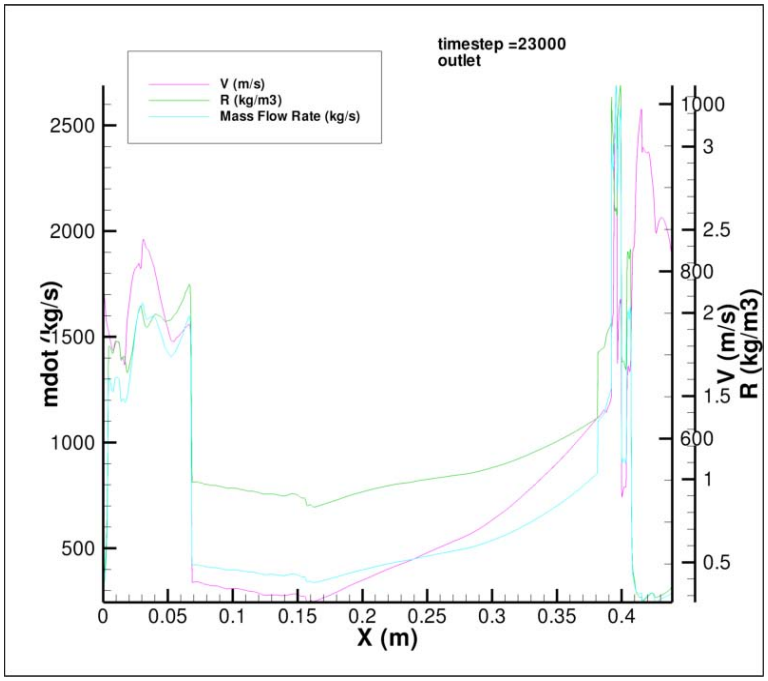

Figure 80. Velocity and density profile for 2nd RDE cycle simulation (outlet) at 365.8 μs

4. Third RDE Cycle

Figures 81 to 86 showed the flow field of the detonation wave rotating in the 3rd cycle. As the detonation continued to propagate, the combustion chamber was completely filled with product. The measurements were as follows:

- Pressure: 3.25 MPa
- Temperature: 2,790.8 K
- Average shock velocity: 1.91 km/s

The fluctuation of the injection velocity varies between -102.15 m/s and 331.08 m/s with the mass flow rate varied between -95.70 kg/s and 1083.93 kg/s. For the density varied between 0.71 kg/m3 and 8.46 kg/m3. These observations were illustrated in Figure 84. We could observed that the flow field was similar to the 2nd cycle which had complex interaction between the expansion waves interacting with the detonation wave as well as small pockets of high-pressure region in the combustor.

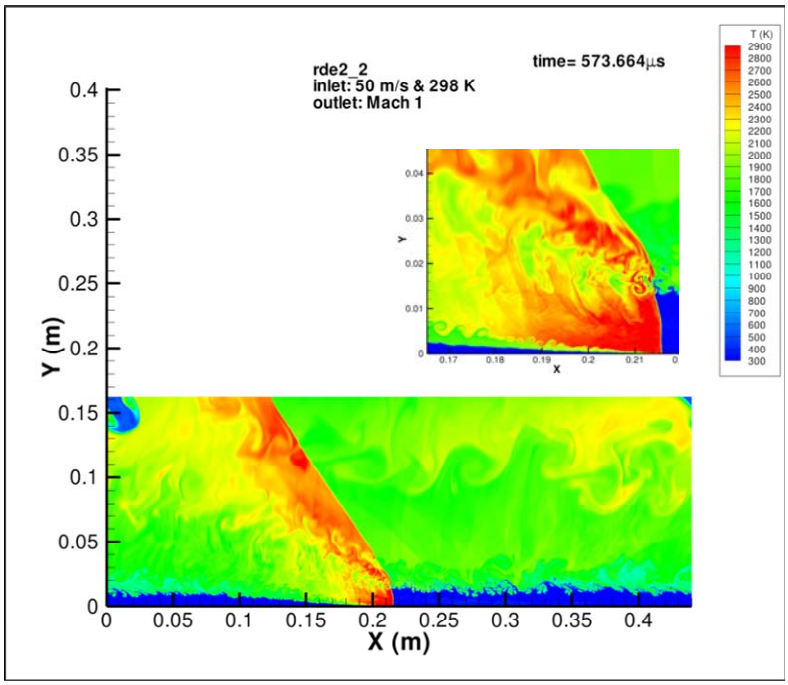

Figure 81. Temperature contour for 3rd RDE cycle simulation at 573.66 μs

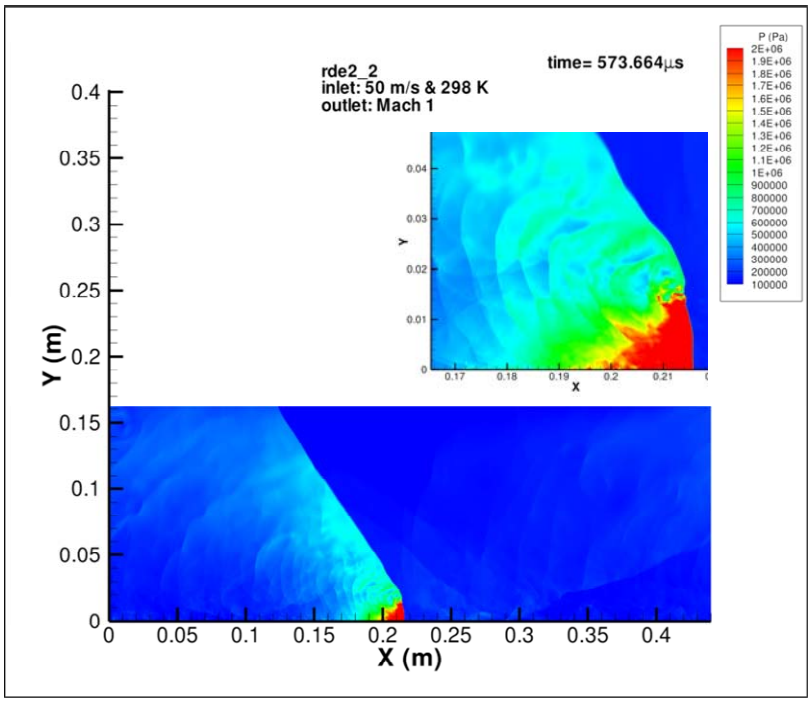

Figure 82. Pressure contour for 3rd RDE cycle simulation at 573.66 μs

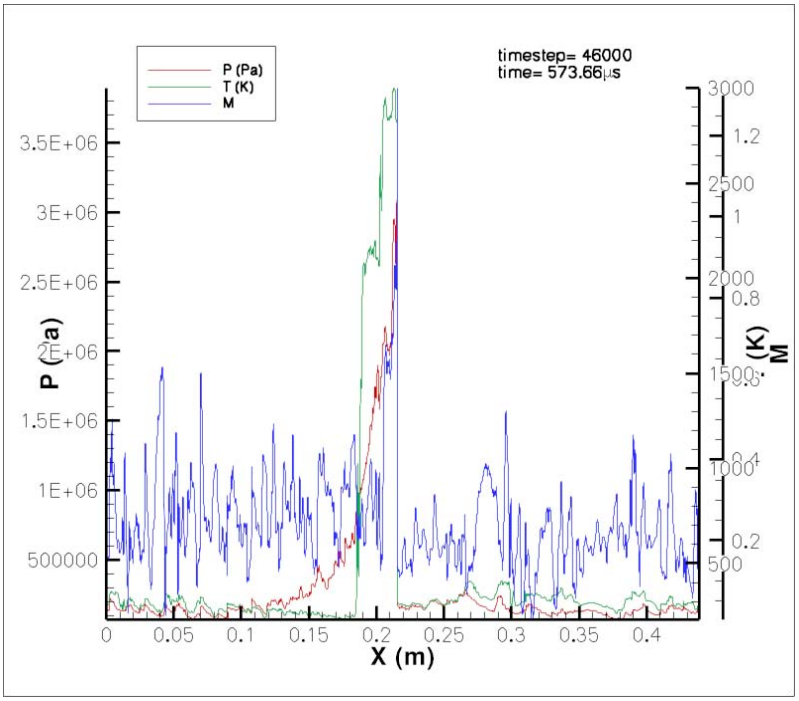

Figure 83. Inlet pressure, temperature and Mach number profile for 3rd RDE cycle simulation at 573.66 μs

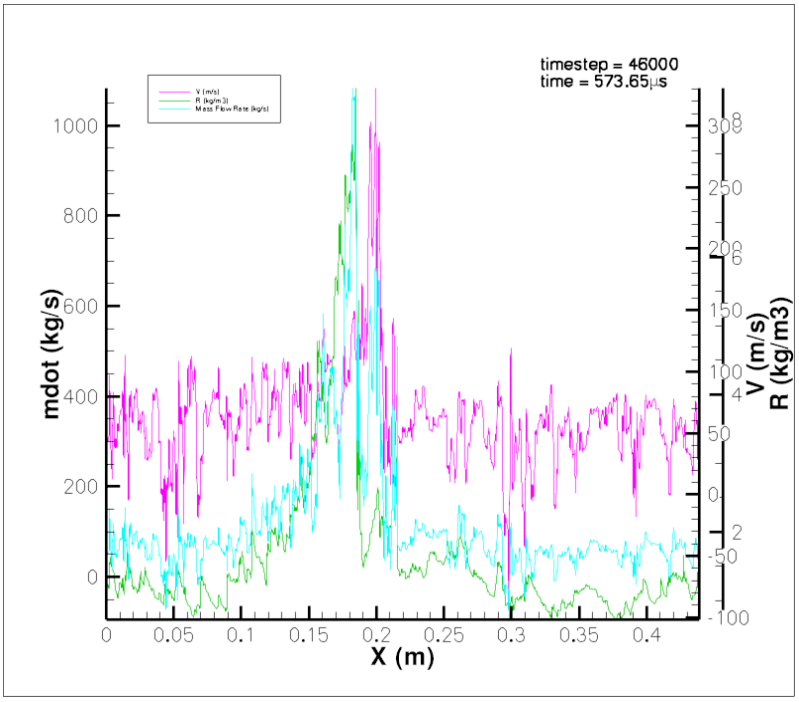

Figure 84. Inlet velocity and density plot for 3rd RDE cycle simulation at 573.66 μs

The combustor outlet was also measured for the 3rd cycle steady state conditions. Figure 85 and 86 showed the various gasdynamic profiles. The measurements were as follows:

- Maximum pressure: 269 kPa
- Maximum temperature: 2,578.1 K
- Outlet axial velocity: 1,377.81 m/s
- Maximum mass flow rate: 856.9 kg/s

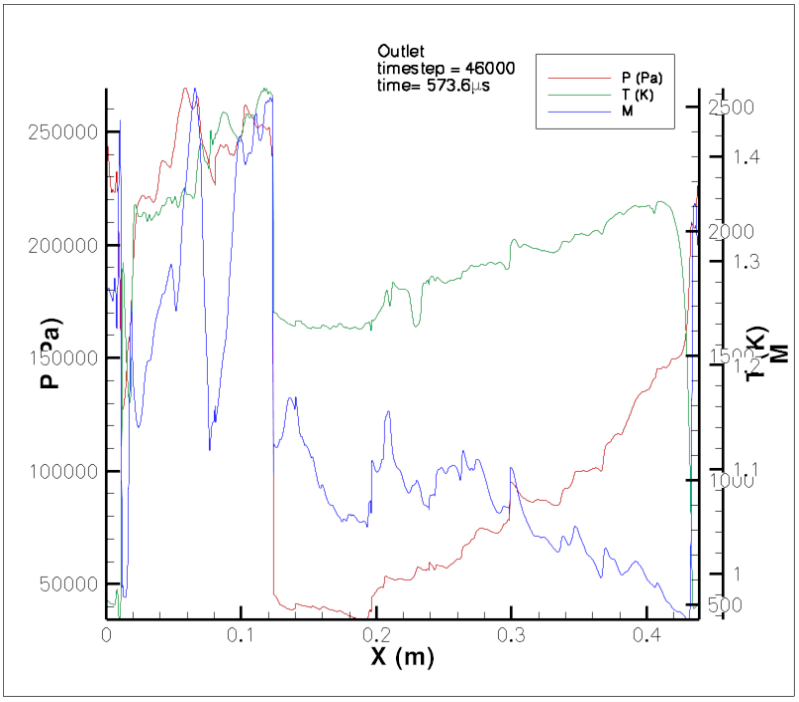

Figure 85. Outlet pressure, temperature and Mach number profile for 3rd RDE cycle simulation at 573.66 μs

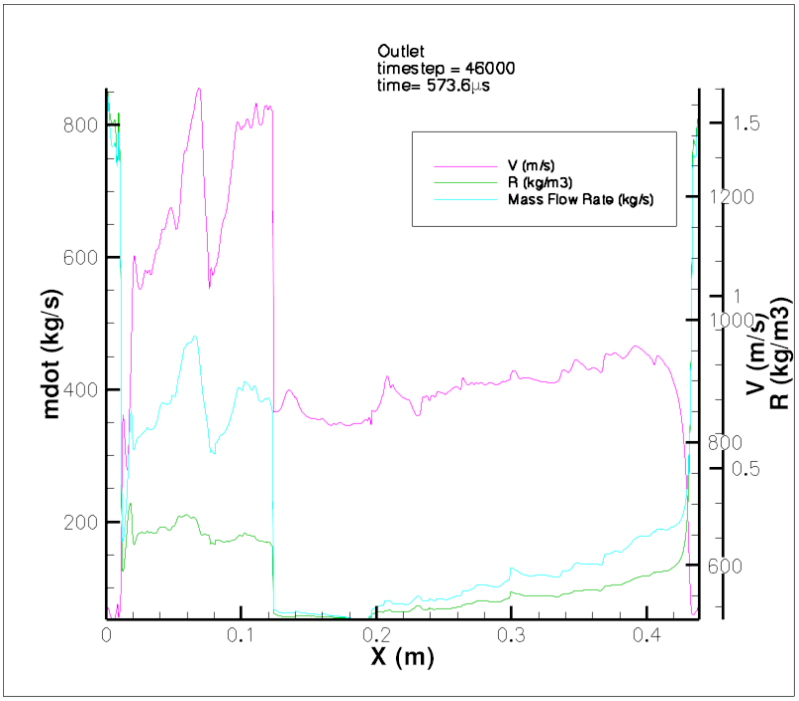

Figure 86. Outlet velocity and density profile for 3rd RDE cycle simulation at 573.66 μs

F. NOVEL RDE SIMULATIONS

A novel simulation set-up was implemented to eliminate the need to pause the simulation to change to periodic boundaries. Figure 87 showed the high-pressure ignition being ignited at the start of the simulation.

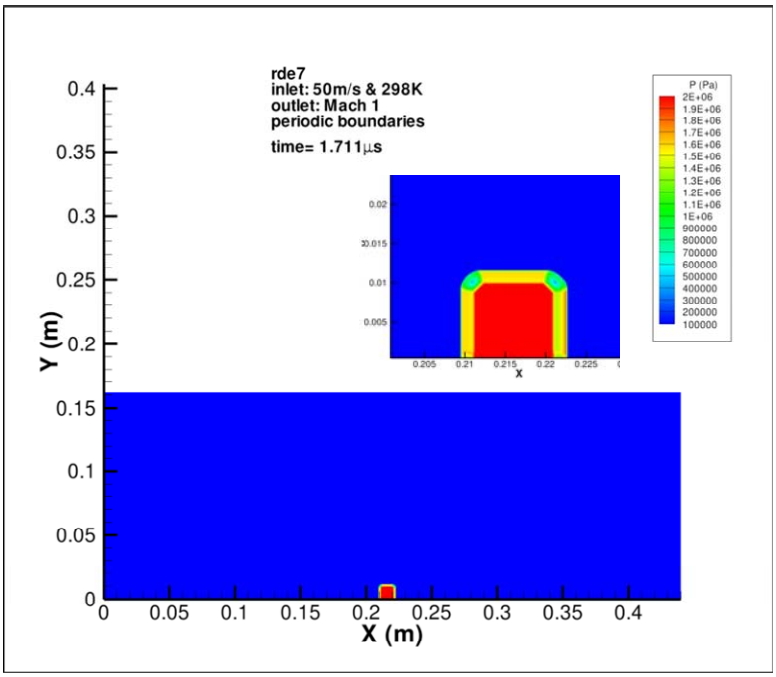

Figure 87. Pressure contour for novel RDE simulation at 1.711 μs

As the simulation progressed, a shockwave propagated radically from the ignition source. Figures 88 to 90 showed the shockwave moving towards the right transiting into a detonation wave when the shockwave interacted with the Hydrogen-Air mixture. For the rest of the shockwave, it continued to propagate away from the source.

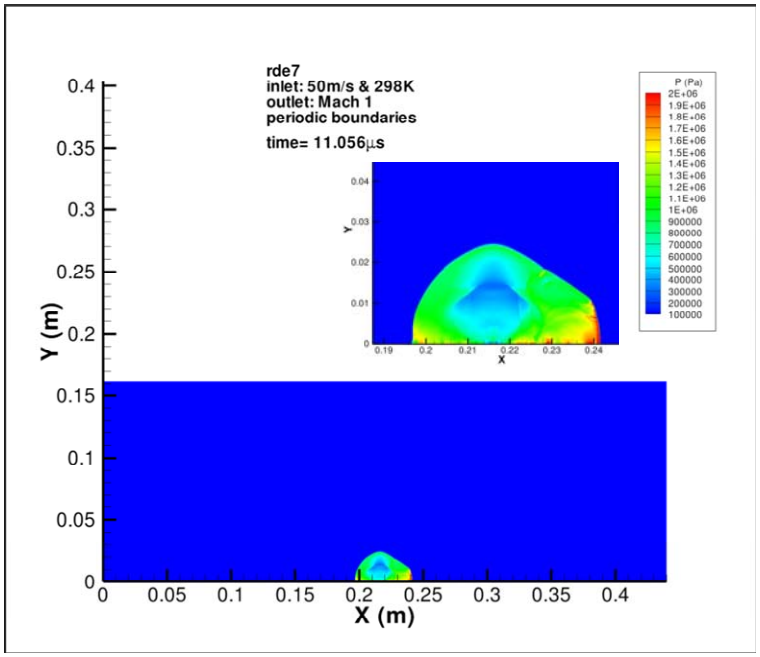

Figure 88. Pressure contour for novel RDE simulation at 11.056 μs

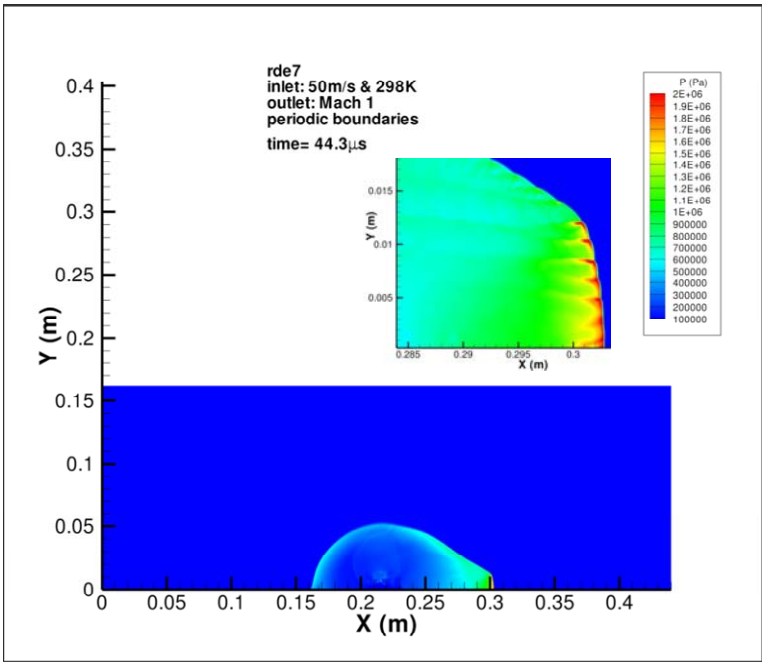

Figure 89. Pressure contour for novel RDE simulation at 44.3 μs

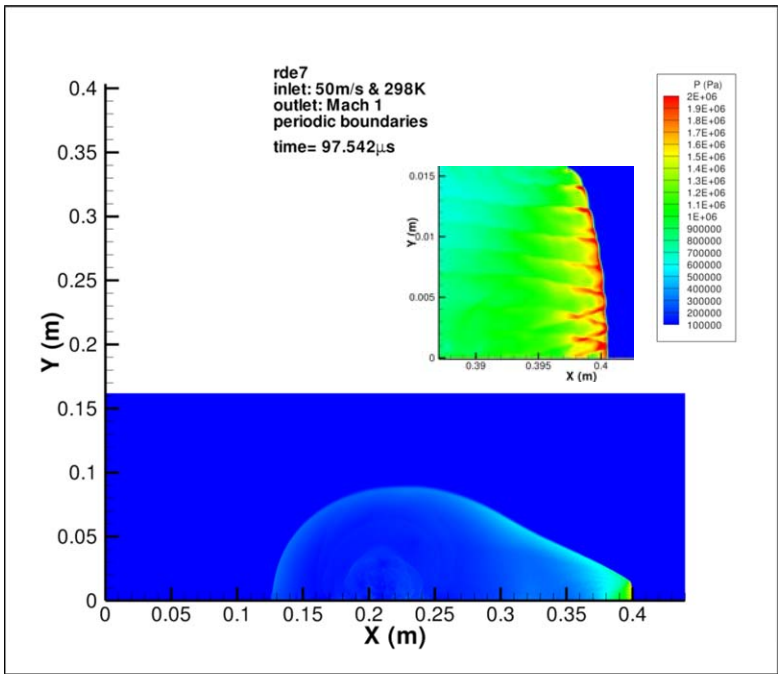

Figure 90. Pressure contour for novel RDE simulation at 97.542 μs

The left propagating shockwave prevented freshly injected Hydrogen-Air mixture from being injected from the inlet. As it propagated, the region behind the shockwave was not filled with Hydrogen-air mixture. Hence, when the right propagating detonation wave front encountered the region behind the shockwave, it ran out of fuel and failed. The gases started to expand with the pressure, temperature and density decreasing in time. This was shown using the pressure contour in Figures 91 and 92. The plots had been adjusted to show a lower pressure range. This simulation gave us valuable insights that the ignition source must directional in order to achieve a rotating detonation wave. Furthermore, it showed that the injection of the Hydrogen-Air mixture must be continuous to maintain the detonation wave.

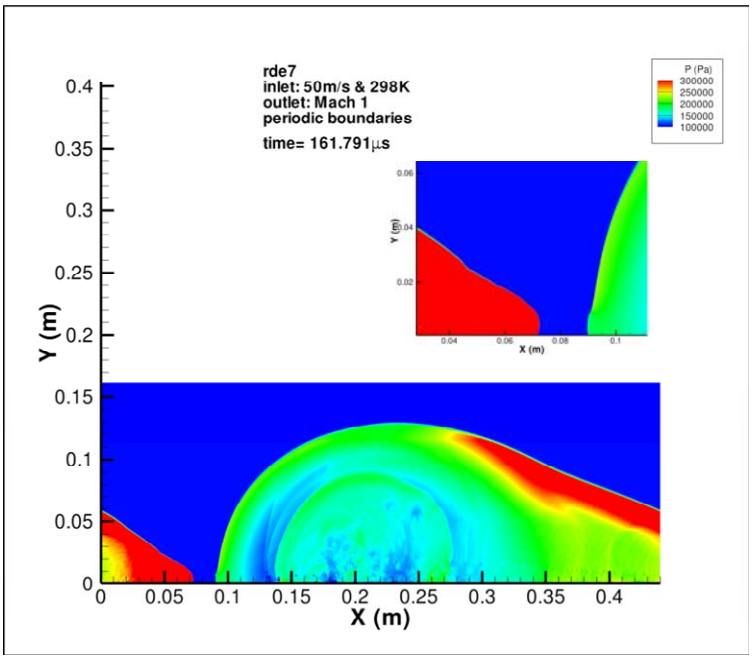

Figure 91. Pressure contour for novel RDE simulation with lower pressure range at 161.791 μs

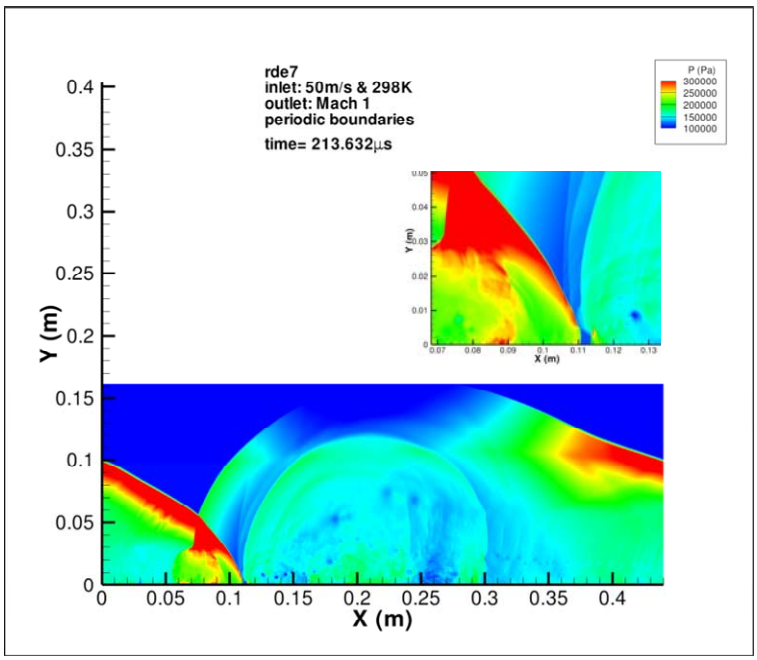

Figure 92. Pressure contour for novel RDE simulation with lower pressure range at 213.632 μs

VI. CONCLUSION

This study had provided valuable insights of the gasdynamic conditions that existed at the combustor inlet. These insights would help engine designer to properly design the inlet of the RDE by taking advantage of the existing gasdynamic data to help isolate the rotating detonation in the combustor chamber.

In this study, various numerical schemes, number of chemical reactions, mesh topology and mesh refinement were investigated to reliable reproduce the Chapman-Jouguet conditions. A set of simulations using a shocktube were carried out and it was found that explicit 4^{th} Order Runge-kutta scheme using structured mesh topology, 18 species and 9 reactions with a maximum mesh cell size of 0.05 mm was required to reproduce the Chapman-Jouguet conditions.

By simplifying the RDE into a 2D domain, simulations were carried out to characterize the gasdynamics at the combustor inlet. It was found that the detonation wave travels at CJ conditions and affects the inflow of the fresh reactants (fuel-oxidizer mixture).

A novel method of simulation was also investigated where there is no need to pause the simulation to change into periodic boundary conditions. It was found that the shockwave from the ignition source affected the propagation of the denotation wave and prevented the newly injected Hydrogen-Air mixture to be fed to the detonation wave. This resulted in detonation failure. Hence, the direction of the ignition source would need to be considered for the engine design.

THIS PAGE INTENTIONALLY LEFT BLANK

VII. FUTURE WORK AND RECOMMENDATIONS

Since the flow field of a RDE has been successfully achieved, the next step is to better model the inlet of the RDE. Instead of using a continuous inflow boundary condition, the computational domain can be modeled with micro nozzles as shown in Figure 94. The set-up allows the flow field in the nozzles to be studied. The micro nozzles need to be smaller than the detonation cell size of the fuel-air mixture so that the detonation wave will not propagate upstream of the nozzle and disturb or even unstart the supersonic inlet. Different design of the micro nozzles can be studied to gain further inside to better design the inlet. A parametric study can also be conducted on the dimensions such as length and diameter of the nozzles.

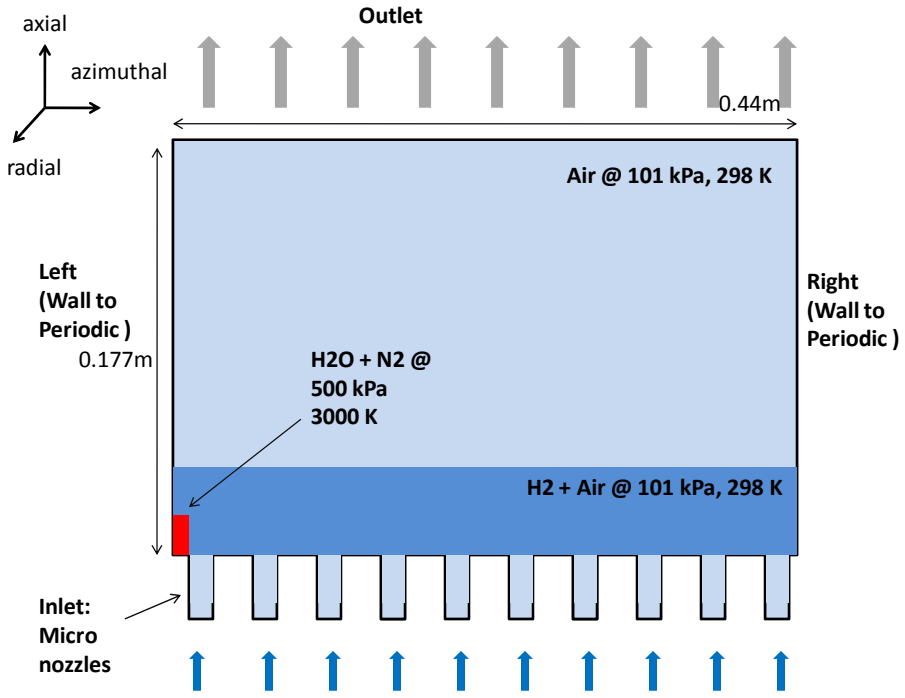

Figure 93. Schematic of full RDE domain with micro nozzles

Once the optimal configuration has been established, other fuel-oxidizer mixture such as JP10-air and ethylene-air can be investigated. JP10 is a military qualified jet aviation fuel with high energy density and is suitable choice for RDE application.

Next, adaptive mesh refinement can be introduced to reduce the number of cells required for the domain. The adaptive mesh refinement will be able to provide higher resolution with smaller cells at the shock fronts and bigger cells in the products region where much smaller gradients are present. This will lower the overall computational requirement hence reducing computational time.

APPENDIX A: SUMMARY OF SIMULATION SET-UP PARAMETERS

CJ simulation	
Parameters	**Settings**
Figure 27 - 28 (Shocktube2)	
Dimensions	0.1 x 0.02 m
Initial Conditions	Products: 200 kPa, 300 K Reactant: 101 kPa, 300 K
Boundary Conditions	Inlet: Multi-species inviscid surface tangency (Wall) Outlet: Multi-species inviscid surface tangency (Wall) Left: Multi-species inviscid surface tangency (Wall) Right: Multi-species inviscid surface tangency (Wall)
Equation Set	Compressible Euler Equation Equation of State: Ideal Gas
Spatial Discretization	2^{nd} order accuracy in space 2D Total Variation Diminishing (TVD) limiter: Continuous
Riemann Solver	Minimum Dissipation: LHS & RHS Activate pressure switch: Supersonic Activate pressure gradient switch: Normal
Time Integration	Multi-stage explicit Runge-kutta Dual time stepping Global CFL: 1e15 Local CFL: 0.95
Mesh Size	0.1 mm 532,766 triangles Topology: Unstructured
Reaction	1 step
Figure 29 - 30 (Shocktube4)	
Dimensions	0.1 x 0.02 m
Initial Conditions	Products: 200 kPa, 300 K Reactant: 101 kPa, 300 K
Boundary Conditions	Inlet: Multi-species inviscid surface tangency (Wall) Outlet: Multi-species inviscid surface tangency (Wall) Left: Multi-species inviscid surface tangency (Wall) Right: Multi-species inviscid surface tangency (Wall)
Equation Set	Compressible Euler Equation Equation of State: Ideal Gas
Spatial Discretization	2^{nd} order accuracy in space 2D Total Variation Diminishing (TVD) limiter: Continuous

Riemann Solver	Minimum Dissipation: LHS & RHS Activate pressure switch: Supersonic Activate pressure gradient switch: Normal
Time Integration	Multi-stage explicit Runge-kutta Dual time stepping Global CFL: 1e16 Local CFL: 0.95
Mesh Size	0.1 mm 532,766 triangles Topology: Unstructured
Reaction	1 step
Figure 31 - 32 (Shocktube5)	
Dimensions	0.1 x 0.02 m
Initial Conditions	Products: 200 kPa, 300 K Reactant: 101 kPa, 300 K
Boundary Conditions	Inlet: Multi-species inviscid surface tangency (Wall) Outlet: Multi-species inviscid surface tangency (Wall) Left: Multi-species inviscid surface tangency (Wall) Right: Multi-species inviscid surface tangency (Wall)
Equation Set	Compressible Euler Equation Equation of State: Ideal Gas
Spatial Discretization	2^{nd} order accuracy in space 2D Total Variation Diminishing (TVD) limiter: Continuous
Riemann Solver	Minimum Dissipation: LHS & RHS Activate pressure switch: Supersonic Activate pressure gradient switch: Aggressive
Time Integration	2^{nd} order explicit Runge-kutta Dual time stepping CFL: 1
Mesh Size	0.1 mm 532,766 triangles Topology: Unstructured
Reaction	1 step
Figure 33 – 34 (Shocktube6)	
Dimensions	0.1 x 0.02 m
Initial Conditions	Products: 200 kPa, 300 K Reactant: 101 kPa, 300 K
Boundary Conditions	Inlet: Multi-species inviscid surface tangency (Wall) Outlet: Multi-species inviscid surface tangency (Wall) Left: Multi-species inviscid surface tangency (Wall) Right: Multi-species inviscid surface tangency (Wall)
Equation Set	Compressible Euler Equation Equation of State: Ideal Gas

Spatial Discretization	2^{nd} order accuracy in space 2D Total Variation Diminishing (TVD) limiter: Continuous
Riemann Solver	Minimum Dissipation: LHS & RHS Activate pressure switch: Supersonic Activate pressure gradient switch: Normal
Time Integration	Point implicit Dual time stepping CFL: 1
Mesh Size	0.1 mm 532,766 triangles Topology: Unstructured
Reaction	2 step
Figure 35 – 36 (Shocktube8)	
Dimensions	0.1 x 0.02 m
Initial Conditions	Products: 200 kPa, 300 K Reactant: 101 kPa, 300 K
Boundary Conditions	Inlet: Multi-species inviscid surface tangency (Wall) Outlet: Multi-species inviscid surface tangency (Wall) Left: Multi-species inviscid surface tangency (Wall) Right: Multi-species inviscid surface tangency (Wall)
Equation Set	Compressible Euler Equation Equation of State: Ideal Gas
Spatial Discretization	2^{nd} order accuracy in space 2D Total Variation Diminishing (TVD) limiter: Continuous
Riemann Solver	Minimum Dissipation: LHS & RHS Activate pressure switch: Supersonic Activate pressure gradient switch: Aggressive
Time Integration	Point implicit Dual time stepping CFL: 1
Mesh Size	0.05 mm 2,113,220 triangles Topology: Unstructured
Reaction	2 step
Figure 37 – 38 (Shocktube9)	
Dimensions	0.1 x 0.02 m
Initial Conditions	Products: 200 kPa, 3,000 K Reactant: 101 kPa, 300 K
Boundary Conditions	Inlet: Multi-species inviscid surface tangency (Wall) Outlet: Multi-species inviscid surface tangency (Wall) Left: Multi-species inviscid surface tangency (Wall) Right: Multi-species inviscid surface tangency (Wall)

Equation Set	Compressible Euler Equation Equation of State: Ideal Gas
Spatial Discretization	2nd order accuracy in space 2D Total Variation Diminishing (TVD) limiter: Minmod
Riemann Solver	Minimum Dissipation: LHS & RHS Activate pressure switch: Supersonic Activate pressure gradient switch: Normal
Time Integration	Point implicit Dual time stepping CFL: 1
Mesh Size	0.05 mm 2,113,220 triangles Topology: Unstructured
Reaction	9 species 18 reactions
Figure 39 – 40 (Shocktube11)	
Dimensions	0.1 x 0.02 m
Initial Conditions	Products: 400 kPa, 3,000 K Reactant: 100 kPa, 300 K
Boundary Conditions	Inlet: Multi-species inviscid surface tangency (Wall) Outlet: Multi-species inviscid surface tangency (Wall) Left: Multi-species inviscid surface tangency (Wall) Right: Multi-species inviscid surface tangency (Wall)
Equation Set	Incompressible Euler Equation Equation of State: Ideal Gas
Spatial Discretization	2nd order accuracy in space 2D Total Variation Diminishing (TVD) limiter: Minmod
Riemann Solver	Minimum Dissipation: LHS & RHS Activate pressure switch: Supersonic Activate pressure gradient switch: Normal
Time Integration	Point implicit Dual time stepping CFL: 1
Mesh Size	0.05 mm 797,601 quadilaterals Topology: Structured
Reaction	9 species 18 reactions
Figure 41 – 42 (rde2_1)	
Dimensions	0.1 x 0.02 m
Initial Conditions	Products: 400 kPa, 3,000K Reactant: 100 kPa, 300K
Boundary Conditions	Inlet: Multi-species inviscid surface tangency (Wall) Outlet: Multi-species inviscid surface tangency (Wall)

	Left: Multi-species inviscid surface tangency (Wall) Right: Multi-species inviscid surface tangency (Wall)
Equation Set	Compressible Euler Equation Equation of State: Ideal Gas
Spatial Discretization	2^{nd} order accuracy in space 2D Total Variation Diminishing (TVD) limiter: Minmod
Riemann Solver	Minimum Dissipation: LHS only
Time Integration	4^{th} order explicit Runge-kutta CFL: 1
Mesh Size	0.05 mm 797,601 quadilaterals Topology: Structured
Reaction	9 species 18 reactions

THIS PAGE INTENTIONALLY LEFT BLANK

APPENDIX B: SIMULATION VIDEOS

The following is the list of simulation videos associated to the shocktube simulation, full RDE simulation and the novel RDE simulation. The videos can be found URL: http://edocs.nps.edu/npspubs/scholarly/theses/2010/Dec/10Dec_Lim_Eugene_tools.pdf

S/No	Title	Description
1	shocktube.avi	This video shows the pressure contour of a shocktube described in Figure 41.
2	full_rde_temperature.avi	This video shows the temperature contour of the full RDE simulation described in Chapter V Section E.
3	full_rde_pressure.avi	This video shows the pressure contour of the full RDE simulation described in Chapter V Section E.
4	novel_rde_temperature.avi	This video shows the temperature contour of the novel RDE simulation described in Chapter V Section F.
5	novel_rde_pressure.avi	This video shows the pressure contour of the novel RDE simulation described in Chapter V Section F.

THIS PAGE INTENTIONALLY LEFT BLANK

LIST OF REFERENCES

[1] F. K. Lu, "Prospects for detonation in propulsion," *Proceeding of the 9th International Symposium on Experimental and Computational Aerodynamics of Internal Flows (ISAIF9), 8–11 September 2009,* Gyeongju, Korea, Paper No IL-2, 2009.

[2] K. K. Kuo, *Principle of Combustion (2nd Edition)*. Hoboken, NJ: John Wiley & Sons, 2005.

[3] H. S. J. Lee, *The Detonation Phenomenon*. Cambridge, MA: Cambridge University Press, 2008.

[4] I. C. Ho and J. O. Sinibaldi, "Determination of practical computational cell size requirements for simulation of H2-Air detonations in pulse detonation engines," *AIAA Journal,* 2010-957, 2010.

[5] M. J. Kaneshige, "Gaseous detonation initiation and stabilization by hypervelocity projectiles," PhD thesis, California Institute of Technology, 1999.

[6] J. Y. Choi, I. S. Jeung and Y. B. Yoong, "Computational fluid dynamics algorithms for unsteady shock-induced combustion, Part 2: Comparison," *AIAA Journal*, vol. 38, no.7, 2000.

[7] B. V. Voitsekhovskii, "Stationary Detonation," *Doklady USSR, Academy of Science,* 129, 1959.

[8] S. A. Zhdan, F. A. Bykovskii, and E. F. Verdenikov, "Numerical study of a rotating detonation n gaseous H2-O2 mixture," *Pulse and Continuous Detonations*. Moscow: Torus Press Ltd, 2006.

[9] D. M. Davidenko, I. Gokalp and A. N. Kudryavtsev, "Numerical simulation of the continuous rotating wave rocket engine," *AIAA Journal*, 2008-2680, 2008.

[10] T. H. Yi, C. Turangan, J. Lou, P. Wolanski and J. Kindracki, "A Three-Dimensional Numerical Study of Rotational Detonation in an Annular Chamber," *AIAA Journal,* 2009-634, 2009.

[11] T.H. Yi, C. Turangan, J. Lou, P. Wolanski and J. Kindracki, "Effect of Nozzle Shapes on the Performance of Continuously Rotating Detonation Engine," *AIAA Journal,* 2010-152, 2010.

[12] M. Hishida, T. Fujiwara and P. Wolanski, "Fundamentals of Rotating Detonation," *Shock Waves*, vol. 19, pp. 1–10, 2009.

[13] T. Yamada, A. K. Hayashi, E. Yamada, N. Tsuboi, V. E. Tangirala and T. Fujiwara, " Numerical analysis of the threshold of limit detonation in rotating detonation engine," *AIAA Journal*, 2010-153, 2010.

[14] M. Sun, S. Liu, J. Liang, W. Liu, J. Zhou, Z. Wang and F. Zhuang, "An improved uncoupled solver for non-equilibrium reacting flow and its application to simulation of rotating detonation wave engine," *AIAA Journal*, 2010-6746, 2010.

[15] D. A. Schwer and K. Kailasanath, "Numerical investigation of rotating detonation engines," *AIAA Journal*, 2010-6880, 2010.

[16] J. A. Nicholls, R. E. Cullen and Ragland, "Feasibility studies of a rotating detonation wave rocket motor," *J. Spacecraft*, vol 3, no. 6, pp. 893 – 898, 1966.

[17] S. A. Zhdan, A. M. Mardashev and V.V. Mitrofanov, "Calculation of the flow of spin detonation in an annular chamber," *Combustion, Explosion and Shock Waves*, vol. 26, no.2, pp. 210–214, 1990.

[18] F. A. Bykovskii, V. V. Mitrofanov and F. F. Vedernikov, "Continuous detonation combustion of fuel-air mixtures," *Combustion, Explosion and Shock Waves*, vol. 33, no.3, 1997.

[19] A. Lentsch, R. Bec, L. Serre, F. Falempin, E. Daniau, D. Piton, A. Prigent, G. Canteins, R. Zitoun, D. Desbordes, F. Jouot and I. Gokslp, "Overview of current French activities on PDRE and continuous detonation wave rocket engines," *AIAA Journal*, 2005-3232, 2005.

[20] A. K. Hayashi, Y. Kimura, T. Yamada, E. Yamada, J. Kindracki, E. Dzieminska, P. Wolanski, N. Tsuboi, V. E. Tangirala and T. Fujiwara, " Sensitivity analysis of rotating detonation engine with a detail reaction model," *AIAA Journal*, 2009-0633, 2009.

[21] F. Falempin and B. L. Naour, "R&T effort on pulsed and continuous detonation wave engines," *AIAA Journal*, 2009-7248, 2009.

[22] R. C. Rogers and W. Chinitz, "Using a global hydrogen-air combustion model in turbulent reacting flow calculations," *AIAA Journal*, vol. 21, no. 4, 1982.

[23] M. C. Burrows and A. P. Kurkov, "Analytical & Experimental Study of Supersonic Combustion of Hydrogen in a Vitiated Air Stream," NASA TM X-2828, 1973.

[24] Metacomp Technologies Inc., "CFD++ User Manual," 2010.

INITIAL DISTRIBUTION LIST

1. Defense Technical Information Center
   Ft. Belvoir, Virginia

2. Dudley Knox Library
   Naval Postgraduate School
   Monterey, California

3. Prof. Jose O. Sinibaldi
   Department of Physics
   Naval Postgraduate School
   Monterey, California

4. Prof. Christopher M. Brophy
   Department of Mechanical and Aerospace Engineering
   Naval Postgraduate School
   Monterey, California

5. Prof. Knox T. Millsaps
   Department of Mechanical and Aerospace Engineering
   Naval Postgraduate School
   Monterey, California

6. CPT Lim Wei Han Eugene
   Singapore Armed Forces
   Republic of Singapore

7. Prof. Yeo Tat Soon
   Temasek Defence Systems Institute
   National University of Singapore
   Republic of Singapore

8. Ms. Tan Lai Poh
   Temasek Defence Systems Institute
   National University of Singapore
   Republic of Singapore